

Some Physical and Statistical Aspects of Clear Air Turbulence

By
Peter F. Lester

Department of Atmospheric Science
Colorado State University
Fort Collins, Colorado



**Department of
Atmospheric Science**

Paper No. 165

**SOME PHYSICAL AND STATISTICAL
ASPECTS OF CLEAR AIR TURBULENCE**

by
Peter F. Lester

**This study has been supported by the
National Science Foundation under
NSF Grants GA-12980 and GA-23175**

Principal Investigator: E. R. Reiter

Atmospheric Science Paper No. 165

**Department of Atmospheric Science
Colorado State University
Fort Collins, Colorado**

September 1970



U18401 0575879

ABSTRACT

Intermittency or patchiness is an integral characteristic of clear air turbulence (CAT). However, previous studies have frequently neglected the inhomogenities of CAT in order to simplify analyses. In the present investigation an effort is made to develop analysis techniques which take intermittency into account. The proposed techniques are tested on turbulence data derived from three cases of CAT in mountain lee waves.

Intermittency is most clearly defined as a statistical property of a record. Therefore, it is proposed that the probabilistic structure of CAT be examined for preliminary evidence of patchiness. Several quantitative indicators of intermittency are derived from an idealized statistical model. Statistical analyses of actual CAT data verify the main predictions of the model, however, the model does not account for significant skewness which was observed in some cases. It is shown that the intermittency indicators and the characteristics of energy spectra are highly sensitive to the manner in which CAT samples are selected.

In order to illuminate some of the small-scale, physical characteristics of intermittent CAT, it is proposed that the flow be divided into mean and turbulent parts with a set of numerical filters. In this way, both mean flow and turbulent flow parameters become space dependent. The concept of an "instantaneous" (filtered) mean and deviation is also applied in the computation of the turbulent kinetic energy budget. Results show that mechanisms such as the transport of turbulent energy by the mean wind can be important under intermittent conditions and that interactions between the mean flow and the turbulence may also be large.

Insight into the nature of the instabilities responsible for the statistical intermittency of the record is gained by noting the behavior of filtered, mean flow variables and the fluctuations of the terms of the instantaneous energy budget along the aircraft track.

Recommendations are given for further applications of the proposed methodology and the design experiments for the investigations of intermittent CAT.

ACKNOWLEDGEMENTS

The author expresses his sincere thanks to Professor E. R. Reiter for his guidance throughout the course of this research. The constructive criticisms of Professors G. R. Stegen and D. B. Rao are also gratefully acknowledged. Dr. T. J. Simons made several helpful suggestions concerning the use of numerical filters and Professor J. S. Williams aided in the formulation of the statistical model. Professor W. M. Gray participated with the author in several thought-provoking discussions concerning general aspects of the study. Dr. D. K. Lilly of the National Center for Atmospheric Research* (NCAR) provided the aircraft data and time on the NCAR computer for part of the reduction of that data. Dr. Lilly and Dr. D. H. Lenschow, also of NCAR, unselfishly spent many sessions with the author, discussing the complexities of aircraft data handling.

Computer programming was efficiently carried out at various stages of the study by Messrs. R. G. Derickson, J. T. Kochneff, R. Lackman and K. Hansen. Mr. R. Gobin deserves special credit for his excellent work in data reduction. The manuscript was typed by Mrs. N. Phillips, Mrs. P. Johnson and Mrs. A. Morgan.

The accomplishment of this work was made easier by the kindness and understanding of the author's wife, Daphne, and by the prayers and encouragement of his parents.

This report is based on a dissertation submitted to the Graduate Faculty of Colorado State University in partial fulfillment of the requirements for the degree of Doctor of Philosophy. The work was sponsored by the National Science Foundation (NSF) under Grants GA 12980 and GA 23175.

* Sponsored by the National Science Foundation

TABLE OF CONTENTS

<u>Chapter</u>	<u>Page</u>
I. Introduction.	1
II. Intermittency	7
III. A Statistical-Physical Approach to the Problem of Intermittent CAT.	19
IV. The Application of the Proposed Approach to CAT Data. . .	40
V. Results	54
VI. Summary, Conclusions and Recommendations.	112
LITERATURE CITED	
	119
Appendix A: Computational Procedures.	126
Appendix B: Analogue and Digital Filters.	130
Appendix C: Filtering and the Reynolds Averaging Rules.	138
Appendix D: The Effects of Filtering on Statistical Analyses and Energy Budget Computations.	147

LIST OF TABLES

<u>Table</u>	<u>Page</u>
1. Description of Clear Air Turbulence cases selected for analysis. All data were acquired from the National Center for Atmospheric Research (NCAR).	44
2. Terms of equation (51) which were computed from the available data for each case study.	52
3. Summary of statistical parameters for all samples of Case 1.	62
4. Summary of statistical parameters for all samples of Case 2.	81
5. Summary of statistical parameters for all samples of Case 3.	96
6. Integrated terms of partial energy budget for Case 3. Units are $10^{-3} \text{m}^2 \text{sec}^{-3}$ (10^{-3} watts kg^{-1}). Circled numbers correspond with numbered terms in equation (51)	104
B-1 Characteristic parameters of Martin-Graham filters. . . .	134
D-1 Cutoff frequencies (f_c) and termination frequencies (f_t) for Martin-Graham high pass filters. "Original filter" denotes the filter used in the analyses presented in the main text. The "new filter" was applied in the reanalysis of the data	147

LIST OF FIGURES

<u>Figure</u>		<u>Page</u>
1	Schematic diagram of the response function of the Martin-Graham low pass filter	32
2	Schematic representation of three possible arrangements of response functions for high pass and low pass filters.	34
3	Topographical chart of geographical region in which the Rocky Mountain Lee Wave Experiment was conducted.	43
4	Sectional surface and 500 mb analyses for 1700 MST, February 19, 1968	55
5	Vertical profiles of temperature, dewpoint, wind speed, and direction. The Granby sounding was made at 1300 MST and the NCAR sounding at 1330 MST, February 19, 1968. . .	55
6	Vertical cross section oriented along the aircraft track for Case 1.	57
7	Top: Velocity component along the aircraft track for Case 1 after low pass filtering. Bottom: Velocity component along the aircraft track after high pass filtering	59
8	Energy spectrum of longitudinal velocity component for sample (a) of Case 1, plotted in logarithmic coordinates and with area proportional to energy.	60
9	Actual and normal frequency distributions of longitudinal gust velocities of Case 1	60
10	Energy spectra for subsamples from Case 1	63
11	Same as figure 9, but for subsamples of Case 1.	64
12	Top: Distribution of the kinetic energy of the longitudinal gust component along a portion of the aircraft track for Case 1. Bottom: Distribution of terms, $\textcircled{1}$, $\textcircled{5}$, and $\textcircled{9}$ (equation (51))	66
13	1100 MST surface analysis and 1700 MST 500 mb analysis for February 20, 1968	72
14	Same as figure 5 except for 0800 MST, February 20, 1968 .	72

List of Figures Continued

<u>Figure</u>		<u>Page</u>
15	Same as figure 6, but for Case 2. Original analysis by D. K. Lilly of NCAR.	73
16	Same as figure 7, but for Case 2.	75
17	Same as figure 8, but for Case 2.	76
18	Same as figure 9, but for Case 2.	76
19	Same as figure 10, but for Case 2	78
20	Same as figure 11, but for Case 2	79
21	Same as figure 12, but for Case 2	82
22	0800 MST surface analysis and 0500 MST 500 mb analysis for February 17, 1970	85
23	Kremmling (0200 MST) and Denver (0500 MST) soundings for February 17, 1970	85
24	Same as figure 6, but for Case 3. The cross section is based on a preliminary analysis by D. K. Lilly of NCAR. .	87
25	Filtered velocity components along the aircraft track for Case 3.	88
26	u, v and w energy spectra for sample (a) in figure 25 . .	90
27	Same as figure 9, but for Case 3.	92
28	Same as figure 10, but for selected subsamples from Case 3.	94
29	Same as figure 9, but for selected subsamples from Case 3.	95
30	Top: Distribution of total turbulent kinetic energy along the aircraft track for Case 3. Bottom: Distributions of terms ① + ② + ③ and ⑦ of equation (51). Time axes are identical on both diagrams.	98
31	Distributions of several terms of equation (51) for Case 3. See inset for identification of curves.	100

List of Figures Continued

<u>Figure</u>	<u>Page</u>
32	Distribution of the flux Richardson number (R_f) along the aircraft track for Case 3 102
33	Distribution of the residual of computed terms of the energy budget, not including interaction terms, for Case 3. 102
34	Distribution of the sum of the interaction terms, (18), (19), and (20) for Case 3. 103
35	Distribution of the residual of computed terms of the energy budget including interaction terms, for Case 3 . . . 103
36	Distributions of \bar{W} (a), \bar{T} (b), \bar{U} (c) and \bar{E} (d) for the period 1020 to 1022 MST for Case 3. Schematic sketches of deduced wave forms are shown at the bottom of diagrams (a) and (b). See text for further elaboration. 109
B-1	Response function for four-point, equally weighted, running averages. Averaging period is 0.125 sec. 135
B-2	Effects of averaging and aliasing on an idealized spectrum with a $-5/3$ slope in double logarithmic coordinates . . . 135
B-3	Analogue filter gain and Martin-Graham filter response for Case 3. 136
B-4	Analogue filter phase lag as a function of frequency for Case 3. 136
B-5	Response function for Martin-Graham low pass filter which was utilized in the analysis of Cases 1, 2 and 3. 137
B-6	Same as figure B-5, but for high pass filter. 137
C-1	Response functions of Martin-Graham high pass and low pass filters utilized for Test 1 141
C-2	Test 1 results for \bar{u} and \bar{u} (top) and $\overline{u^2}$ and $\overline{u^2}$ (bottom) . . . 142
C-3	Test 1 results for $\overline{u^2}$ 143
C-4	Test 1 results for $\overline{u^2}$ and $\overline{u^2}/2$ 143

List of Figures Continued

<u>Figure</u>		<u>Page</u>
C-5	Response functions of Martin-Graham low pass filter and high pass filter utilized in Test 2.	144
C-6	Test 2 results for $\overline{u'}$	145
C-7	Test 2 for $\overline{u'u}$ and $\overline{u'^2/2}$	145
C-8	Test 3 results for $\overline{u'u}$ and $\overline{u'^2/2}$	146
D-1	Cumulative frequency distributions of longitudinal gusts which have been defined by two different filters. Data are the entire CAT sample for Case 2	151
D-2	Same as figure D-1, but for the most turbulent subsample of Case 2.	151
D-3	Same as figure D-1, but for the entire sample of Case 3.	152
D-4	Same of figure D-1, but for the most turbulent sample of Case 3.	152
D-5	Distributions of u' and $\overline{u'^2/2}$ along a portion of the aircraft track for Case 2 after filtering the data with a higher cutoff frequency.	153
D-6	Terms (1) and (5) of equation (51) from Case 2 after filtering with a higher cutoff frequency.. . . .	154

DEFINITION OF SYMBOLS

English Letters

A, B, C	constants of proportionality
$A(\omega)$	Fourier coefficient
$B(\omega)$	Fourier coefficient
C_o	ratio of the mean deviation to the standard deviation
C_{ok}	generalized ratio of the mean deviation to the standard deviation
$E(f)$	energy density
$E(x)$	the mathematical expectation of x
f	an arbitrary frequency (Hz)
f_c	cutoff frequency (Hz)
f_n	Nyquist frequency (Hz)
f_s	sampling frequency (Hz)
f_t	termination frequency (Hz)
$f(x)$	the probability density function of x
g	acceleration due to gravity
K_H	heat exchange coefficient
K_M	momentum exchange coefficient
$\ln x$	logarithm of x to the base e
N	total number of weights on one side of the central weight; also sample size
N_k	Gaussian value of the generalized ratio, C_{ok}
NW	total number of weights
\overline{NW}	total number of weights necessary for less than a 1% filter error

Definition of Symbols Continued

English Letters

p	pressure
$P(x)$	lognormal probability density function
R_i	gradient Richardson number
R_f	flux Richardson number
R_{NL}	general interaction term
$R(f), R(\omega)$	response function
t	time
T	temperature; also averaging period
TAS	true air speed
u, v, w	velocity components along the x, y and z axes, respectively
u_i	tensor form of the three velocity components ($i = 1, 2, 3$)
W_n	n^{th} filter weight
W_0	central filter weight
$W(\tau)$	weighting function
x	coordinate axis oriented parallel to, and in the same direction as, the mean wind vector; also an arbitrary variable
x_i	tensor form of the three independent space variables ($i = 1, 2, 3$)
$x(t)$	an arbitrary time dependent variable
y	coordinate axis oriented 90° to the left of the mean wind vector
$y(t)$	stationary Gaussian process with zero mean and unit variance
z	vertical coordinate, positive upward
$z(t)$	a series of step functions

Definition of Symbols Continued

Greek Letters

α	coefficient of intermittency
β_2	kurtosis or flatness factor
β_{2k}	generalized kurtosis
δ	intermittency factor
δ_1	skewness
Δt	finite time increment
Δf_r	magnitude of the difference between the termination frequency and the cutoff frequency
$\Delta \omega$	finite frequency difference
ϵ	kinetic energy dissipation rate
ζ	a small time lag
θ	potential temperature
λ	wave length
μ_1	mean
μ_2	variance
ν	kinematic viscosity
ρ	density
σ	standard deviation
τ	time lag; also length of record
ϕ	phase angle
ω	circular frequency (radians sec ⁻¹)
Ω_c	cutoff frequency (radians sec ⁻¹)

Definitions of Symbols Continued

- ($\bar{\quad}$) arithmetic averaging with respect to statistical computations; also low pass filtering with respect to energy budget calculations
- (\prime) a deviation from the mean; also high pass filtering

I. INTRODUCTION

Statement of the Problem

The rapid increase in the number, speed, and operational altitudes of aircraft over the past thirty years has been paralleled by a similar growth in the interest in meso- and microscale meteorological processes. Clear air turbulence (CAT) is among the most important of these phenomena due to the severe effects that turbulence may have on aircraft operations (National Committee for Clear Air Turbulence, 1966). Interest in CAT has also arisen in areas outside the field of aviation. In the last five years, scientific evidence (Kung, 1966a, 1966b, 1967; Trout and Panofsky, 1969; Reed, 1969; Businger, 1969; Reiter, 1969) has indicated that CAT may play a significant role in the modification of the mesoscale characteristics of the atmosphere and in the dissipation of kinetic energy. The correct parameterization of such important small scale processes is a substantial factor in the successful numerical modeling of macroscale atmospheric circulations (Fleagle, 1969).

Given its original impetus by the rapid development of the aircraft industry, CAT research has continued to intensity with the realization of the broader importance of that phenomenon. As a result, many aspects of CAT have been documented (Clodman et al., 1960; Reiter, 1963, 1968, 1969; Vinnichenko et al., 1968; Pao and Goldberg, 1969; Dutton and Panofsky, 1970). Climatologies of CAT with respect to certain geographical areas, altitudes, and seasons

have been established. Synoptic and mesoscale models of atmospheric conditions favorable for CAT have been developed and a number of theoretical models of CAT mechanisms have been proposed. These models, together with a few detailed atmospheric observations and the results of laboratory experiments, lend support to the theory that much of the observed CAT is the result of instabilities of the Kelvin-Helmholtz type. Despite the progress made to date, serious deficiencies exist in the quantitative knowledge of CAT as the scale of observations decreases. For example, the physical details of the life cycle of CAT and the interactions of CAT with its environment are not well-known. The lack of insight into the causes and effects of CAT is epitomized in the fact that CAT cannot be forecasted with much accuracy.

The source of the problem lies in the nature of the phenomenon; CAT occurs at small scales and is characteristically intermittent. Because of the small scale of CAT and the inability of ordinary meteorological measurement systems (e.g., rawinsondes) to resolve it, special ground-based and airborne instrumentation has been developed for CAT research (Vinnichenko et al., 1968; Pao and Goldberg, 1969). However, intermittency, or the tendency for CAT intensity to vary along a flight path, complicates the measurements, even with the sophisticated sensors which continue to be developed.

Intermittency affects CAT observations in two general ways: first, CAT occurrences are relatively rare and hundreds of hours of flying time, spent in search of CAT patches, usually result in only a few tens of hours of actual CAT encounters (Crooks et al., 1968); second, the turbulence intensity within a given patch of CAT often

varies substantially. The second, intermittent effect has not been considered by CAT investigators until recently. Dutton (1968) has given evidence of intermittency within an individual CAT patch and has pointed out important influences of intermittency on the probabilistic structure of CAT. Specifically, intermittency in the CAT records analyzed by Dutton (1968) was characterized by non-Gaussian gust distributions. This finding is of great concern to aircraft design engineers, since the determination of aircraft response to atmospheric turbulence has been traditionally based on the Gaussian distribution of gusts.

Participants at a number of recent national and international scientific conferences¹ have stressed the importance of studying the physical causes of intermittency in order to gain a better understanding of CAT mechanisms (see also, Dutton and Lane, 1969). However, the treatment of CAT as an intermittent phenomenon cannot be accomplished by the continued application of present investigative techniques. CAT research methodology suffers from a number of shortcomings. Specifically, three problematic areas may be isolated:

(a) Methods of data collection have generally not been adequate for the complete description of the environment, the dimensions, and the behavior of a turbulent patch. The problem has been one of economy and safety. Although, as stated earlier, instrumentation has been developed which may be utilized to study CAT in detail,

¹Symposium on Clear Air Turbulence and Its Detection, Seattle, August, 1968. Colloquium on Spectra of Meteorological Variables, Stockholm, June, 1969. Global Atmospheric Research Program (GARP) Conference, Boulder, October, 1969. Symposium on Planetary Boundary Layers, Boulder, March, 1970.

ground-based devices are often restricted by their lack of mobility and the use of properly-equipped aircraft is presently limited by their small number. Also, and understandably, planners hesitate to vector more than one aircraft at a time into a given turbulent region. Furthermore, the frequent lack of supporting data such as vertical wind and temperature profiles and the lack of a sufficient number of samples collected over space and time within the same CAT region often force the investigator to make simplifying assumptions with respect to the stationarity and homogeneity of the sample. Thus, the effects of improper data collection are reflected in the final analyses and in their interpretation.

(b) Methods of data reduction have often contaminated the data by the removal of features which are important in the understanding of the nature of CAT. For example, by the arbitrary selection of homogeneous samples of CAT, the characteristic intermittency of the entire CAT record is lost.

(c) Methods of data analysis are often incomplete, a problem which leads to the loss of important, but often available, information concerning the nature of CAT. The tendency of many meteorologists has been to resort primarily to power spectrum analysis techniques in dealing with CAT data (e.g., Pinus et al., 1967). The results are that physical interpretation of the data is dependent on the spectral theories of Kolmogorov (1941), Obukhov (1941), Bolgiano (1959, 1962), Lumley (1965), Phillips (1965), and others, and that CAT is often treated as a stationary, homogeneous, and isotropic phenomenon. These assumptions are frequently unrealistic. Since CAT is actually an intermittent phenomenon with radical variations in space and time,

the use of spectrum analysis alone is insufficient to specify its characteristics. Note should be taken of the recommendations of Dutton and Lane (1969) and the few attempts to characterize intermittent CAT (Vinnichenko et al., 1968; Vinnichenko, 1969; Dutton, 1968; Dutton et al., 1969), and present analysis techniques should be suitably modified.

Assuming that adequate facilities will be available for research, judicious planning of future experiments should serve to overcome the present problems involved in data collection. However, inadequacies in data reduction and analysis can only be dealt with by modifying and extending present methods and developing new ones for the purpose of characterizing intermittent CAT.

The Purpose of the Study

The purpose of the present investigation is to extend previous CAT research methodology and to develop new techniques applicable to the study of the statistical and physical aspects of intermittent clear air turbulence.

Approach

In order to accomplish the aims of the study, the investigation is carried out in the following manner. As an initial step, the literature is reviewed in detail with emphasis on the causes and effects of intermittent turbulence and on its measurement in the laboratory, in the atmospheric boundary layer, and in the free atmosphere. A statistical model of intermittency is then proposed on the basis of this review, and statistical indicators of intermittency are

derived. It is shown that some of the physical aspects of intermittent CAT at small scales may be revealed by a modified computation of various terms of the energy budget.

The suggested methods are then applied to three case studies to demonstrate their feasibility. Since the planning and execution of a CAT data-collection program were beyond the scope of the present research, special efforts were made to select data which were not severely affected by the data-collection problems cited earlier. Finally, on the basis of the results of the case studies, the proposed approach for the determination of the statistical and physical aspects of intermittent CAT is re-evaluated in terms of its application to future experiments.

II. INTERMITTENCY

General

Since the importance of studying the intermittent nature of CAT has only recently been brought to the attention of the majority of meteorologists (see Chapter I), general knowledge of methods applicable to the investigation of that characteristic is lacking. However, intermittent turbulence in various forms has been investigated in the laboratory for many years and, more recently, has been examined in the atmospheric boundary layer. In the present chapter the various types of intermittency and the methods utilized to investigate them will be reviewed as background to the problem of intermittent CAT and the recent literature which deals directly with intermittent CAT will be summarized.

Observations

According to Dutton and Lane (1969):

. . . [A] record exhibits intermittent characteristics if the sample variance is distributed in a distinctly nonuniform manner, so that a relatively large fraction of the total variance comes from a relatively small fraction of the total record. An associated characteristic of many atmospheric records is that important and intermittent events occur randomly and apparently independently.

It is important to note that intermittency is not defined with respect to any particular physical mechanism or scale of motion and is therefore quite general. It is shown below that intermittency in turbulent flow occurs over a wide range of scales and for a variety of reasons.

In the laboratory, intermittency has been observed during transition from laminar to turbulent flow at low Reynolds numbers. Under these conditions the turbulence occurs in patches which have characteristic shapes, velocities, and dimensions. Coles (1961) has summarized studies of the intermittency of transition in pipe flows, circular coette flows, and boundary layer flows.

Another type of intermittency, which has been documented in laboratory experiments at high Reynolds numbers, occurs in wakes, jets, and boundary layers. In these cases, a sharp boundary exists between the turbulent flow and the nearby laminar flow. A probe placed near the interface will alternately sense laminar and fully turbulent flow due to random convolutions in the boundary. Intermittency of this type has been studied extensively (e.g., Corrsin, 1943; Townsend, 1948, 1949; Corrsin and Kistler, 1955; Sandborn, 1959; Coles, 1961; Kibens and Kovasznay, 1969).

Intermittency of a third type occurs in all turbulent flows at small scales and high Reynolds numbers and differs radically from the two types discussed thus far. Batchelor (1953) has suggested that the observed behavior of the higher statistical moments of the derivatives of turbulent velocities at small scales is due to the tendency for turbulent energy at high wave numbers to be found in isolated regions of space. Kolmogorov (1962), in modifying his classic universal equilibrium theory (Kolmogorov, 1941), has viewed the tendency for intermittency of this type to occur within the turbulent flow in terms of ϵ , the kinetic energy dissipation. That is, with an increase in the ratio between the characteristic scale of the energy-containing eddies and the scale at which dissipation occurs, the variation of ϵ

should increase without limit. Studies of intermittency of this type have been carried out in the atmospheric boundary layer by Gurvitch and Zubkovski (1963, 1965), Sheih (1969), Stewart et al. (1970), Gibson et al. (1970), and others.

Prior to discussing the observations of intermittent CAT, it is important to differentiate between the phenomenon of CAT and that of classical turbulence. Sutton (1949) defines the latter as a state of fluid flow "in which the instantaneous velocities exhibit irregular and apparently random fluctuations. . . ." CAT has been defined by the National Committee for Clear Air Turbulence (1966) as:

all turbulence in the free atmosphere of interest in aerospace operations that is not in or adjacent to visible convective activity (this includes turbulence found in cirrus clouds not in or adjacent to visible convective activity).

Dutton and Panofsky (1970) have defined CAT as:

. . . turbulence occurring several kilometers above the earth's surface in air that is free of clouds and strong convective currents. It generally implies turbulence severe enough to produce noticeable motions of aircraft flying through it.

Perhaps the most general and concise definition of CAT is "bumpiness in flight through clear air" (Reiter, 1962).

These statements stress an important point concerning the nature of CAT. It is defined with respect to the aerospace vehicles which encounter it and therefore covers a much wider range of motion scales than were considered in the intermittency types discussed thus far. As opposed to the concept of classical turbulence, CAT may be composed of undulance (organized, laminar wave motions) and/or classical turbulence.

The intermittency of CAT is reflected in its rare occurrences (Clodman et al., 1960; Colson, 1963, 1969; Endlich et al., 1966) and in studies of the decrease of the frequency of occurrence of CAT with height above the ground (Vinnichenko et al., 1968; Vinnichenko, 1969). Dutton (1968) and Dutton et al. (1969) have produced statistical evidence of intermittency from investigations of detailed CAT records. Also, turbulence samples collected during project HICAT (Crooks et al., 1968) graphically illustrate both the intermittency of CAT and its apparent wave-turbulence character.

The hybrid nature of CAT suggests that intermittency may arise because of waves or localized instabilities. In these cases, the mesoscale variations in atmospheric parameters such as lateral and vertical wind shears and static stability become important in the physical understanding of intermittent CAT. The fact that CAT is also a function of aircraft design adds to the complexity of the study of its intermittency. For example, a very fast aircraft which intersects a finite region of short waves may experience bumpiness for a brief period while a slower-flying vehicle on the same track may not, unless the waves destabilize and break down. In another case, an aircraft may intersect a disturbed laminar-turbulent interface and encounter true classical turbulence, but only briefly. Whereas the turbulence record from such a flight would display an intermittent character (i.e., a "burst"), intermittency within the burst may also be occurring, but on a smaller scale. Intermittent CAT is therefore an entirely different phenomenon from the intermittent turbulence encountered in the laboratory and the atmospheric boundary layer.

Measurements

The measurement of intermittency in the laboratory has been based on a relatively simple question: What fraction (γ) of the flow field is turbulent? There are basically two methods by which an answer to this question may be found. Townsend (1948), in studying the turbulence in the wake of a cylinder, has suggested that the kurtosis, β_2 , of the first derivative of the velocity, u , be used to determine γ , the intermittency factor. The kurtosis is given by

$$\beta_2 = \left(\frac{\partial u}{\partial x} \right)^4 / \overline{\left(\frac{\partial u}{\partial x} \right)^2}^2 \quad (1).$$

Turbulent intermittency, of course, is reflected in the velocities themselves. However, the velocity derivatives (or velocity differences) show an even greater sensitivity to intermittency since they will exhibit relatively large values in the vicinity of a burst of turbulence and small values outside the burst.

Assuming a model of intermittent turbulence such that the boundaries between regions of laminar and turbulent motion are sharp and distinct and the turbulence is isotropic within each turbulent region, Townsend (1948) shows that

$$\gamma = \frac{\beta_2'}{\beta_2} \quad (2),$$

where β_2' is the kurtosis within the turbulent region ($\beta_2' = 3$ for a Gaussian distribution) and β_2 is the kurtosis of the mixed regime.

The kurtosis² or flatness factor, by virtue of its large, even exponent, emphasizes both the very small and the extreme values which the variable in question assumes. Its relation to the fraction of time the flow is turbulent (γ) is based on the critical assumptions that the particular variable being considered takes on the value zero in the non-turbulent flow and that it is homogeneous in the turbulent regions. Under these conditions, the probability density function of the variable has a central peak of infinite height which encloses a finite area equal to $(1-\gamma)$ (i.e., the fraction of time the flow is non-turbulent). As indicated by Batchelor (1953), such an idealization is rarely found in practice and, at best, γ computed by equation (2) is only a qualitative estimate of the fraction of time the flow is turbulent.

The second method to determine the intermittency factor was also introduced by Townsend (1949). An electronic signal is generated during turbulent periods (based on some threshold). The integral of the signal, $\overline{I(t)}$, is then related to γ as

$$\gamma = \frac{\overline{I(t)}}{\tau} \quad (3),$$

where τ is the total period of the record.

In subsequent investigations of intermittency near an interface, γ has been measured almost exclusively via equation (3) with some modifications with respect to instrumentation and the particular

²A related quantity is the coefficient of excess defined as $(\beta_2 - 3)$.

parameter selected to differentiate between turbulent and laminar flow (e.g., Corrsin and Kistler, 1955; Kibens and Kovasznay, 1969).

Finn and Sandborn (1964) have carried out comparative laboratory measurements of the intermittency factor computed both by the kurtosis method and by measuring γ directly, in the turbulent wake of a disc. They found agreement between the two measurements within about 10 per cent. One problem with the first method, which was cited by these investigators, is that periodic fluctuations in turbulence levels may lead to a kurtosis less than the Gaussian value of 3 and thus $\gamma > 1.0$ (e.g., $\beta_2 = 1.5$ for a sine wave).

The usefulness of the universal equilibrium theory (Kolmogorov, 1941, 1962; Obukhov, 1941, 1962) in dealing with problems of small scale turbulence (e.g., see Batchelor, 1961) has focused the attention of scientists on the verification of the predictions of the theory and the determination of its associated constants. Therefore, the intermittent behavior of ϵ has been studied by a number of investigators. Indications of the intermittency of energy dissipation have been predicted theoretically by Novikov and Stewart (1964), and Gurvitch and Yaglom (1967). Specifically, these studies predict that the probability density function of ϵ should be log-normal. If x is distributed log-normally, then the probability density function, $P(x)$, is given by

$$P(x) = \frac{1}{\sigma x \sqrt{2\pi}} \exp\left(-\frac{(\ln x - m)^2}{2\sigma^2}\right) \quad (4),$$

where $m = \overline{\ln x}$ and $\sigma^2 = \overline{(\ln x)^2} - (\overline{\ln x})^2$.

The log-normal distribution of a given variable corresponds to large probabilities of very small or extreme values of the variable (of the order of the root-mean-square value or larger), but to relatively small probabilities of intermediate values (Gurvitch and Yaglom, 1967; Brooks and Carruthers, 1953). This property of the log-normal distribution thus corresponds with the large values of kurtosis, as discussed earlier.

In laboratory investigations, the practical size of the wind tunnel places an upper limit on the size of the energy-containing eddies. Therefore, it is difficult to obtain Reynolds numbers which are large enough to yield an extensive inertial subrange (Batchelor, 1961; Sheih, 1969) and a few investigators have turned to the atmospheric boundary layer for measurements of the intermittency of ϵ (e.g., Gurvitch and Zubkovski, 1963, 1965; Sheih, 1969; Stewart et al., 1970; Gibson et al., 1970). Measurements in this region are not made without great difficulty. Because ϵ cannot usually be determined directly, certain related quantities are measured at small scales, such as the velocity structure function or the squared streamwise derivative of the velocity. The character of the probability distributions of these variables is thought to reflect the characteristics of the distribution of ϵ . The results of these studies indicate that the intermittency of ϵ is proportional to the ratio of the size of the energy-containing eddies to the size of the eddies at which dissipation occurs, as predicted by Kolmogorov (1962). Also, the probability density function of ϵ is approximately log-normal.

The measurement of the intermittency characteristics of CAT has been carried out in only a few cases. Vinnichenko et al. (1968) and

Vinnichenko (1969) have reported on measurements of a quantity similar to γ in the lowest few kilometers of the atmosphere. Defining α , the coefficient of intermittency, as the ratio of flight time with "bumpiness" to the total flight time, the investigators have shown that α characteristically decreases to near zero within two kilometers of the surface. The rate of decrease is a function of the static stability of the atmosphere. Analyses of this type can only be taken as qualitative indicators of the intermittency of CAT because α is a function of pilot, aircraft, and/or instrument response. Pilot response depends largely on factors such as pilot experience, the suddenness of the onset of the turbulence, etc., and will generally vary from pilot to pilot. Aircraft response depends on the size, design, and speed of the aircraft. Although instrument response may be dictated more objectively in design, the selection of some turbulence threshold is often arbitrary. Stewart (1959), in considering classical turbulence, explains that the selection of an arbitrary lower threshold often leads to the erroneous classification of regions as non-turbulent where low intensity turbulence is occurring.

The intermittency of CAT in the free atmosphere (i.e., above the boundary layer) has been considered in the recent investigations carried out by Dutton (1968), Dutton et al. (1969), and Dutton and Deaven (1969). The approach utilized by these investigators is primarily statistical in that the intermittency was characterized in terms of probability density functions and exceedence statistics. Dutton (1968) has derived a statistical model of intermittency which is based on the occurrence of turbulence in Gaussian "bursts" separated

by non-turbulent regions. The model is successful in predicting some of the observed non-Gaussian aspects of CAT records.

Dutton and Lane (1969) have proposed another method for the investigation of intermittency. Since intermittency, as a reflection of non-linear processes, affects both the amplitude and phase of the variable being considered, both of these properties should have a characteristic behavior under intermittent conditions. The influences in the amplitude domain have already been discussed in terms of probability density functions and the higher statistical moments. Dutton and Lane (1969) have illustrated the effects of intermittency on phase in the following manner. A single delta function is given as the prototype of the intermittent record. The Fourier transformation of the record is given by

$$\int \delta(x-x_0) e^{i\omega x} dx = e^{i\omega x_0} \quad (5),$$

where x is the intermittent variable with a single spike at x_0 , ω is frequency, and $i = \sqrt{-1}$. The phase angle difference ($\Delta\phi$) between two frequencies of difference $\Delta\omega$ is then

$$\phi(\omega+\Delta\omega) - \phi(\omega) = x_0 \Delta\omega \quad (6).$$

In this ideal case, the spectrum is one of white noise, however, phase differences are a function of frequency only. Dutton and Lane (1969) recommend that intermittency effects on phase should be investigated by determining phase angle as a function of frequency. The application of this analysis to real data is presently being attempted by

Dutton (1970), however, no indications of its feasibility have appeared in the literature.

In summary, the brief review presented above has shown that several types of intermittency may be found in turbulence as it is generated artificially in the laboratory and as it occurs naturally in the atmosphere. Despite the wide differences of the intermittency types (in terms of their causes), methods of characterizing them are generally similar. By far, the most common approach to the investigation of intermittency has been to specify its statistical effects in terms of the probabilistic structure of the variable in question.

Other techniques include the direct measurement of the fraction of time the flow is turbulent and the determination of the effects of intermittency on phase-frequency relations. Although the former method has been successful in the laboratory, it may only be used in a qualitative manner in the study of CAT. The inadequacy of the direct method is due to the difficulties in specifying a lower threshold for CAT and to the fact that CAT and classical turbulence are not necessarily synonymous. The analysis of phase-frequency relationships, as proposed by Dutton and Lane (1969), may yield more insight into the effects of intermittency, however, practical techniques utilizing this method have not yet been developed.

One must conclude that only progress in the study of intermittent CAT has been made in the specification of the statistical effects of intermittency in the amplitude domain. The physical mechanisms which cause the observed statistical intermittency are not clearly understood. This is due, in part, to the fact that a relatively small number of investigations have been concerned directly with

the difficulties involved in the study of intermittent CAT. In the next chapter, a methodology is proposed which is designed to specify the degree of intermittency in terms of its statistical effects and to isolate some of the physical causes of the statistical intermittency.

III. A STATISTICAL-PHYSICAL APPROACH TO THE PROBLEM OF INTERMITTENT CAT

General

It was emphasized in Chapter I that further progress in the study of CAT can only be made by treating that phenomenon as intermittent. Therefore, CAT research methodology must be revised and extended. In the present chapter, a combination of statistical and physical analyses are proposed for the investigation of intermittent CAT. Hopefully, this methodology will serve as a basis for the design and execution of further CAT experiments.

The Statistical Approach

In Chapter II, rather heuristic arguments were presented to explain why investigators chose certain statistical parameters to characterize intermittency. In the following paragraphs, a simple model of intermittency is presented and quantitative indicators of intermittency are derived on a more rigorous basis. The model is a generalization of the one proposed by Dutton (1968).

Consider stationary record possessing the following characteristics. Let $x(t)$ be an arbitrary, time-dependent variable such that

$$x(t) = y(t)z(t) \quad (7),$$

where $y(t)$ is a stationary Gaussian process with a zero mean and unit variance, approaching Gaussian white noise. That is, the autocorrelation function, $\rho(\tau)$, approaches zero for all $|\tau| > \zeta$, where τ is the

lag and ζ is a small value. $z(t)$ is a series of step functions with jumps which occur at the onset and conclusion of a burst of activity; $y(t)$ and $z(t)$ are stochastically independent variables. In other words, it is assumed that the record is composed of turbulent bursts or patches such that $x(t)$ is distributed normally within each burst, but the intensity (the variance) varies from burst to burst. In the following development, the functional notation which indicates the dependence of x , y , and z on t will be eliminated for brevity.

The mean, μ_1 , of x is given by

$$\mu_1 = E(x) \tag{8},$$

where, in general, the operator (the expectation), $E(\)$, for the continuous variable, x , is given by

$$E(\) = \int_{-\infty}^{\infty} (\) f(x) dx \tag{9}.$$

In the discrete case, (9) becomes

$$E(\) = \sum (\) f(x) \tag{10},$$

where $f(x)$ is the probability density function of x . With (7) and by virtue of the independence of y and z , (8) can be written as

$$\mu_1 = E(yz) = E(y)E(z) \tag{11}.$$

Noting that $E(y)$ in the preceding equation is the mean value of y which is equivalent to zero by definition, the mean of x is then

$$\mu_1 = 0 \tag{12}.$$

Similarly, the variance of x is given by

$$\mu_2 = E(x^2) = E(y^2 z^2) = E(y^2)E(z^2) \quad (13),$$

where, again, advantage has been taken of the independence of y and z (see also, Hogg and Craig, 1959). By definition, the variance of y , $E(y^2)$, is one; therefore,

$$\mu_2 = E(z^2) = \int_{-\infty}^{\infty} z^2 f(z) dz \quad (14).$$

Although $f(z)$ has been specified as a series of step functions, its behavior is arbitrary. It can only be stated, on the basis of (14), that μ_2 is a weighted average of the variances of all the bursts where the weighting is given by $f(z)$.

γ_1 , the skewness of the distribution of x , can be written as

$$\gamma_1 = \frac{E(x^3)}{[E(x^2)]^{3/2}} = \frac{E(y^3)E(z^3)}{[E(y^2)]^{3/2}[E(z^2)]^{3/2}} \quad (15).$$

Since y is normally distributed, it can be shown that

$$E(y^3) = \int_{-\infty}^{\infty} y^3 f(y) dy = 0 \quad (16),$$

where

$$f(y) = \frac{1}{\sqrt{2\pi}} \exp\left\{-\frac{y^2}{2}\right\} \quad (17).$$

It follows that

$$\gamma_1 = 0 \quad (18).$$

β_2 , the kurtosis (or flatness factor) of the intermittent record, is given by

$$\beta_2 = \frac{E(x^4)}{[E(x^2)]^2} = \frac{E(y^4)E(z^4)}{[E(y^2)]^2[E(z^2)]^2} \quad (19).$$

With equation (17), it can be shown that

$$\frac{E(y^4)}{[E(y^2)]^2} = \int_{-\infty}^{\infty} y^4 f(y) dy = 3 \quad (20).$$

Therefore, equation (19) becomes

$$\beta_2 = 3 \left(\frac{E(z^4)}{[E(z^2)]^2} \right) \quad (21).$$

With Schwartz's inequality (e.g., see Courant, 1937),

$$E(z^4) \geq [E(z^2)]^2 \quad (22),$$

and, therefore,

$$\beta_2 \geq 3 \quad (23).$$

The argument for the behavior of β_2 under the assumed conditions can be repeated for a generalized ratio, β_{2k} . It is found that

$$\beta_{2k} = \frac{E(|x|^{2k})}{[E(|x|^k)]^2} \geq R_k \quad (24),$$

where k is an integer ($k \geq 1$), $|x|$ indicates the absolute value of x , and R_k is the corresponding normal ratio. In a similar manner, we may examine C_o , the ratio of the mean deviation to the standard deviation, i.e.,

$$C_o = \frac{E(|x|)}{[E(x^2)]^{1/2}} = \frac{E(|y|)E(|z|)}{[E(y^2)]^{1/2}[E(z^2)]^{1/2}} \quad (25).$$

Since

$$E(y^2) = 1,$$

and, with (17),

$$E(|y|) = \int_{-\infty}^{\infty} |y| f(y) dy = \left(\frac{2}{\pi} \right)^{1/2} \quad (26),$$

then (25) may be rewritten as

$$C_o = \left(\frac{2}{\pi} \right)^{1/2} \left(\frac{E(|z|)}{[E(z^2)]^{1/2}} \right) \quad (27).$$

With Schwartz's inequality,

$$E(z^2)^{1/2} \geq E(|z|) \quad (28)$$

and it follows that

$$C_o \leq \left(\frac{2}{\pi} \right)^{1/2} \quad (29).$$

The preceding expression can also be generalized by repeating the argument for the variable, $|x|^k$, to yield

$$C_{ok} = \frac{E(|x|^k)}{[E(|x|^{2k})]^{1/2}} \leq N_k \quad (30),$$

where C_{ok} is the generalized ratio and N_k is the corresponding normal ratio.

The statistical model of intermittency yields a large number of indicators of statistical intermittency. The frequency distribution has a characteristic shape (leptokurtic), and the generalized ratios β_{2k} and C_{ok} (equations (24) and (30), respectively) behave in a characteristic manner. For example, a turbulence record, which is intermittent in the sense of the proposed model, will have a frequency distribution which is symmetric about the mean, but will exceed the Gaussian distribution at the origin and in the tails. Also, the ratio of the mean deviation to the standard deviation will be less than $\left(\frac{2}{\pi}\right)^{1/2}$. The deviation of the actual distribution from normal is a function of the degree of intermittency, i.e., the distribution of the variances of the turbulent bursts.

The prediction of the idealized model of intermittency with respect to the behavior of the frequency distribution is found to be in agreement with the results of previous statistical studies of actual CAT data (e.g., see Dutton, 1968). Lester (1970) has shown that C_o is useful in the quantitative description of the statistical intermittency of velocity differences computed from CAT data. He also gave evidence that the intermittency of velocity differences (in terms of C_o) decreases with increasing differencing interval.

In the present study, the statistical effects of intermittency will be illustrated with the frequency distributions of gust components and with the kurtosis, β_2 . The effects of the intermittency of CAT records on the representativeness of one-dimensional velocity spectra will also be considered. Details of data selection and computational procedures are given in Chapter IV.

The Physical Approach

The compilation of CAT statistics in terms of frequency of occurrence, favored environments, etc., has provided the meteorologist with insight into the general nature of CAT. Power spectrum analysis techniques have been used successfully to characterize the distribution of CAT energy in frequency space and the statistical analyses which have been carried out by Dutton (1969) and others have yielded evidence of intermittency in CAT records. However, the treatment of CAT data in a purely statistical manner has given little information concerning the detailed physical mechanisms of that phenomenon. Realistic models of the life cycle of intermittent CAT and the interaction of CAT with its environment can only be derived on the basis of detailed observations of those processes. The rapid increase in the quality of aircraft instrumentation over the last few years now allows the desired observations to be made (e.g., see Dutton, 1969). In the following paragraphs, an analysis technique is developed for the purpose of illuminating some of the small scale, physical characteristics of CAT.

With the Boussinesq approximation, the turbulent energy equation may be expressed in tensor notation as

$$\begin{aligned} \frac{\partial \bar{E}}{\partial t} + \bar{u}_j \frac{\partial \bar{E}}{\partial x_j} + \overline{u_i' u_j' \frac{\partial \bar{u}_i}{\partial x_j}} + \overline{u_i' u_j' \frac{\partial u_i'}{\partial x_j}} = \\ = - \frac{1}{\rho} \overline{u_i' \frac{\partial p'}{\partial x_i}} + \frac{g}{T} \overline{u_3'} + \overline{v u_i' \frac{\partial^2 u_i'}{\partial x_j^2}} \end{aligned} \quad (31),$$

where $E = \frac{u_i'^2}{2} = \frac{(u'^2 + v'^2 + w'^2)}{2}$, \bar{u}_i = the mean component of the wind, u_i' = the turbulent component ($u_3' = w'$), ν is the kinematic viscosity, all other terms have their usual meaning, and standard tensor notation has been used; a repeated index implies summation (Lumley and

Panofsky, 1964). Since each term of equation (31) may be interpreted physically (i.e., the local change of kinetic energy, advection of kinetic energy by the mean flow, etc.), the computation of various terms from detailed data collected within a CAT region would allow the evaluation of the importance of various mechanisms which may contribute to the occurrence and intermittency of CAT.

In the computation of the turbulent energy budget, it is frequently assumed that the mean velocity, \bar{u} , may be defined as

$$\bar{u} = \frac{1}{T} \int_{-T/2}^{T/2} u(t) dt \quad (32),$$

where T is the averaging interval. The deviations (prime terms in equation (31)) are then

$$u'(t) = u(t) - \bar{u} \quad (33).$$

This method of separating the mean and turbulent flows simplifies the derivation of equation (31) because

$$\begin{aligned} \overline{(\bar{u} + u')} &= \bar{u} \quad , \quad \overline{\bar{u}} = \bar{u} \quad , \quad \overline{u'} = 0 \\ \overline{(u + u')^2} &= \bar{u}^2 + \overline{u'^2} \quad , \quad \overline{u^2} = \bar{u}^2 \quad , \quad \overline{2uu'} = 0 \end{aligned} \quad (34)$$

Dutton (1969), Myrup (1969), and Lenschow (1970) have demonstrated the feasibility of computing a number of terms of the turbulent energy budget from aircraft data. In Dutton's (1969) study, deviations were determined by the removal of linear trends from gust data which were previously subjected to a high pass filter (scales greater than about 2 km were eliminated). Covariances were computed in the usual manner, that is, an overbar in equation (31) was defined

as in equation (32). By making T (the averaging time)³ equivalent to the time it takes the sampling aircraft to traverse a long stretch of CAT, the assumptions of lateral homogeneity and $\bar{w} = 0$ could be rationalized. An indication of the validity of this approach is reflected in the results of Dutton's (1969) study; his budget balanced within about 8 per cent of the total rate of the shear production of energy. This method, however, does not lend itself to the study of the energetics of intermittent CAT.

The burst character of CAT records suggests that radical changes in turbulent energy often occur in short distances along the aircraft track. This, in turn, implies that energy production, dissipation, etc. should also show rapid changes in space. The inadequacy of the energy budget approach taken by Dutton for the study of the nature of localized turbulent bursts is revealed in earlier studies (Dutton, 1968; Dutton et al., 1969) of the statistical characteristics of the same case considered for energy budget calculations (Dutton, 1969). These investigations show that, statistically, the record in question is highly intermittent. In spite of this fact, the calculated energy budget gives little, if any, information about the physics of the intermittency.

It is clear that the energy budget must be computed in a different manner if it is to yield information about the bursts of CAT. An apparently simple way to do this would be to divide the length of the turbulent record into a number of smaller records of equal length and

³For aircraft observations, the common assumption is that $x = \overline{TAS}\Delta t$, where x is distance along the aircraft track, Δt is a given time interval and \overline{TAS} is the mean true air speed of the aircraft.

to compute individual budgets over each of the subsections. In the limit, this is equivalent to computing equally-weighted running averages, i.e.,

$$\bar{u}(t) = \frac{1}{T} \int_{-T/2}^{T/2} u(t+\tau) d\tau \quad (35),$$

so that the mean becomes a function of time (or space). It is well known (e.g., see Holloway, 1958) that such an averaging process results in the damping of amplitudes in frequency space according to

$$R(f) \approx \frac{\sin \pi f T}{\pi f T} \quad (36),$$

where $R(f)$ is the response function at frequency f (Hz) and T is the averaging interval (for an example, see Appendix B). Also, the Reynolds averaging rules (equation (34)) are only satisfied by (35) if u is a constant or a linear function of time. This is not usually the case, especially in regions of CAT. It is obvious that for equation (31) to hold, the Reynolds averaging rules must be satisfied and, therefore, the simple approach suggested by equation (35) is invalid. The problem to be dealt with is then a realistic separation of scales which will satisfy the Reynolds averaging rules.

The Separation of Scales

Isakson,⁴ in a classical work, has devised an idealized scheme for the separation of scales and the satisfaction of the Reynolds averaging rules (see also, Charnock, 1957). Briefly, his approach is the following:

Let the total motion be represented by a mean and a deviation, i.e.,

$$u(t) = \bar{u}(t) + u'(t) \quad (37),$$

where

$$\bar{u}(t) \equiv \int_{-\infty}^{\infty} w(\tau) u(t+\tau) d\tau \quad (38).$$

$w(\tau)$ is a weighting function which may be written as a Fourier integral,

$$w(\tau) = \frac{1}{\pi} \int_0^{\infty} R(\omega) \cos \omega \tau d\omega \quad (39),$$

where ω is frequency (radians per unit time), and $R(\omega)$, the response function, is given by

$$R(\omega) = 2 \int_0^{\infty} w(\tau) \cos \omega \tau d\tau \quad (40).$$

The total motion may also be expressed in terms of Fourier integrals, i.e.,

$$u(t) = \int_0^{\infty} [A(\omega) \cos \omega t + B(\omega) \sin \omega t] d\omega \quad (41).$$

⁴A summary of Isakson's work is given by J. M. Burgers in Das Turbulenzproblem, C. W. Oseen (1930). The development presented above is based on an unpublished manuscript by T. J. Simons (1967).

The mean flow may be found by substituting (41) into (38). With the realization that $w(\tau)$ as defined by (39) is an even function,

$$\bar{u}(t) = \int_0^{\infty} R(\omega) [A(\omega) \cos \omega t + B(\omega) \sin \omega t] d\omega \quad (42),$$

where $R(\omega)$ is given by (40). This procedure may be repeated to yield

$$\begin{aligned} \overline{\overline{u}}(t) &= \int_0^{\infty} R^2(\omega) [A(\omega) \cos \omega t + \\ &\quad + B(\omega) \sin \omega t] d\omega \end{aligned} \quad (43).$$

The rule $\overline{\overline{u}}(t) = \overline{\overline{u}}(t)$ is only satisfied if $R(\omega)$ is either 0 or 1.

Defining

$$\begin{aligned} \text{and} \quad R(\omega) &\equiv 1, & 0 < \omega < \Omega_c \\ R(\omega) &\equiv 0, & \omega > \Omega_c \end{aligned} \quad (44),$$

where Ω_c is the cutoff frequency, the mean flow is defined as

$$\bar{u}(t) = \int_0^{\Omega_c} [A(\omega) \cos \omega t + B(\omega) \sin \omega t] d\omega \quad (45),$$

and the deviations are given by subtracting the mean from the original flow field. The rule, $\overline{u'} = 0$, is automatically satisfied by (44) and (45). Isakson has shown that the ideal scheme satisfies $\overline{uu'} = 0$ only if a gap of width $(3\frac{\Omega_c}{2} - \frac{\Omega_c}{2})$, which is centered on Ω_c , exists in the velocity spectrum. Further, in order for $\overline{u^2} = \overline{u}^2$, energy in the mean flow components should be absent at frequencies higher than $\frac{\Omega_c}{2}$ (see also, Charnock, 1957).

The Modified Computation of the Energy Budget

Isakson has demonstrated that, ideally, it is possible to separate scales of motion in such a manner that the Reynolds averaging rules can be satisfied. As applied to the energy budget, the mean value of a given variable would be given by an equation of the form of (38) and the deviation from the mean would be the difference between the original record and the mean. In this manner an "instantaneous" mean and deviation can be specified at each sampling point. The practical application of this procedure is not without problems. The most important of these are discussed below.

(a) Isakson's filter was derived on the basis of infinite integrals, whereas most CAT data are discrete and all CAT records are finite.

The fact that $W(\tau)$ and $R(\omega)$ are Fourier transforms of each other has facilitated the design of numerical filters for application to finite records (Holloway, 1958). One of these is the Martin-Graham (M-G) filter (Martin, 1962; Graham, 1963), which is characterized by its excellent response and flexibility. For these reasons and because it has been used extensively in recent CAT investigations (Crooks et al., 1968), this filter has been chosen as the averaging procedure to be applied in the present study of CAT energetics.

The M-G low pass filter has a response function as shown schematically in figure 1, where f_c is the cutoff frequency (Hz), f_t is the termination frequency, and $\Delta f_r = (f_t - f_c)$ is the rolloff interval. The weights for discrete points ($n = \pm 1, \pm 2, \dots, \pm N$) are given by

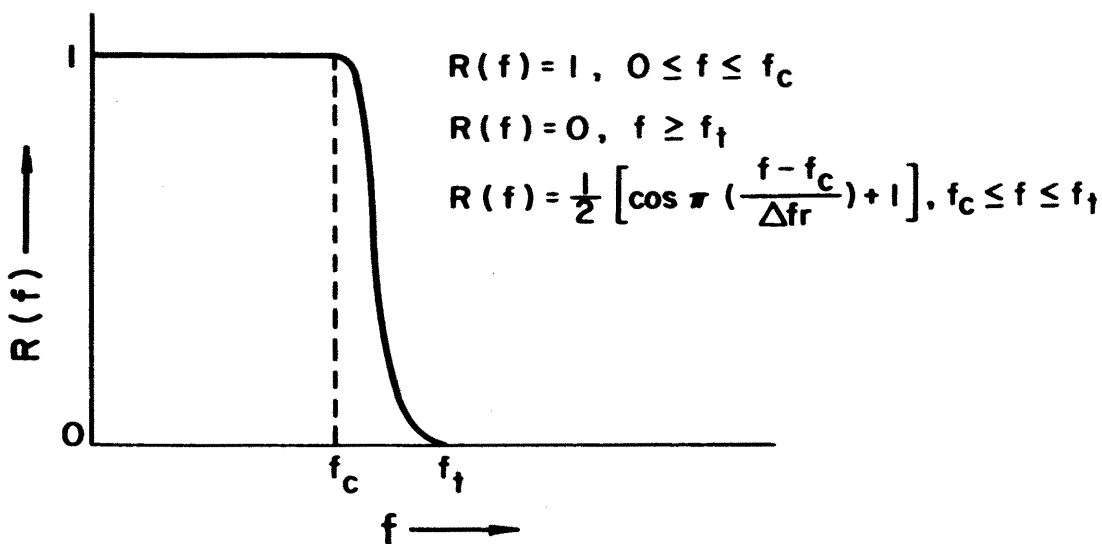


FIGURE 1. Schematic diagram of the response function, $R(f)$, of the Martin-Graham low pass filter. General response characteristics are given on the right hand side of the diagram. See text for further explanation.

$$W_n = \frac{\sin(2\pi n f_c \Delta t) + \sin(2\pi n f_t \Delta t)}{2\pi n [1 - 4n^2 \Delta f_r^2 \Delta t^2]} \quad (46),$$

where the total number of weights, NW , is $2N+1$, $\Delta t = 1/f_s$, and f_s is the sampling rate. The central weight, W_0 , is given by

$$W_0 = (f_c + f_t) \Delta t \quad (47).$$

Since (46) has a singularity at $n_s = (2\Delta f_r \Delta t)^{-1}$, the weight at that point (when it occurs) is given by

$$W_{n_s} = \frac{(f_c \Delta t) \cos(2\pi n f_c \Delta t) + (f_t \Delta t) \cos(2\pi n f_t \Delta t)}{1 - 12n^2 \Delta f_r^2 \Delta t^2} \quad (48),$$

where use has been made of l'Hospital's rule. The weights W_n are normalized by their sum to ensure that the response function is unity

at $f = 0$. The associated high pass filter is given by the difference between the low pass filter and the all pass filter (central weight = 1, all other weights = 0). The filter is completely determined by the specification of the cutoff frequency, f_c , the termination frequency, f_t , and the number of weights, NW . Graham (1963) has found from experimentation that for less than 1 per cent error in the response function on either side of the rolloff interval, the optimum number of weights, \overline{NW} , is given by

$$\overline{NW} = \frac{4f_s}{\Delta f_r} + 1 \quad (49).$$

As would be expected, as the rolloff interval, Δf_r , is decreased and the cutoff approaches the ideal, the required number of weights increases rapidly.

(b) The cutoff frequency for the ideal filter is replaced by a finite interval for the numerical filter, that is, a finite region where the response function decreases from 1 to 0.

This problem is illustrated in figure 1 by the rolloff interval, Δf_r , and causes new problems in the satisfaction of the Reynolds averaging rules. For example, consider the three schematic diagrams in figure 2. The response function for the mean (low pass filter) is given by the solid line while the dashed line represents the response function for the deviation (high pass filter). In diagram (a), low pass filtering of the raw data admits all frequencies less than f_2 with negligible amplitude damping. The high pass filter performs

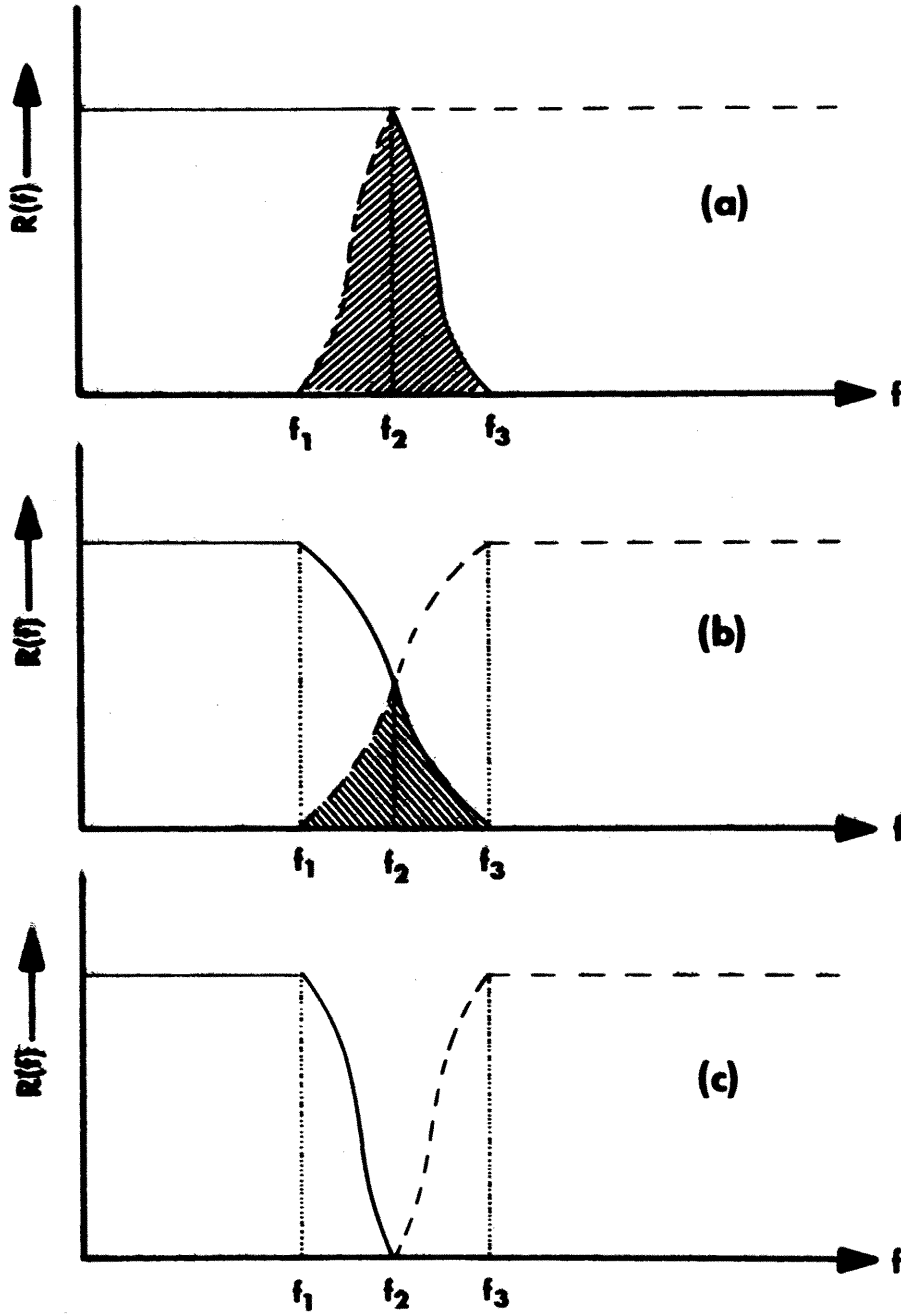


FIGURE 2. Schematic representation of three possible arrangements of response functions for high pass (dashed line) and low pass (solid line) filters. Regions of filter overlap are shaded.

similarly on the raw data for all frequencies above f_2 . However, the two filters share a common frequency band (shaded area) because of the finite interval over which the cutoff is accomplished. The result is that $u \neq \bar{u} + u'$ and $\overline{u'} \neq 0$, and therefore, the advantage gained by insuring that frequencies above and below f_2 may be passed with undamped amplitudes by one filter or the other is offset by the fact that two important Reynolds axioms are violated.

Diagram (b) insures $u = \bar{u} + u'$ because the high pass filter is the complement of the low pass filter. However, the region of overlap again does not allow $\overline{u'} = 0$. Although diagram (c) overcomes the latter problem by not permitting the filters to overlap, the problem of $u \neq \bar{u} + u'$ again occurs because of the induced gap centered at frequency f_2 .

The effects of the different arrangements of filters (diagrams (b) and (c) in particular) on the Reynolds averaging rules were tested on real data (Appendix C). On the basis of the tests it was decided to use the arrangement shown in diagram (c) in the present study, but in so doing, to keep the interval $(f_3 - f_1)$ as small as practical (for example, for the data which are presented in Chapter V, with a cutoff frequency near 0.1 Hz or about 1 km, $(f_3 - f_1) = 0.03$ Hz or about 400 m). In this way, $\overline{u'} = 0$, and the fraction of total energy lost from the mean and from the deviation is kept to a minimum, i.e., it is assumed $u \approx \bar{u} + u'$.

(c) A gap of width $(\frac{f_c}{2} - \frac{f_c}{2})$ centered at the cutoff frequency, f_c , must be present in the energy spectrum for the satisfaction of the Reynolds averaging rule, $\overline{u'u} = 0$.

The presence of a spectral gap implies the atmosphere has naturally separated itself into mean and turbulent components of flow and, further, the mean and turbulent flows are uncoupled in the sense of suppressed interactions. If the spectral gap does not exist, then interactions become large and $\overline{u'u}$, which is a manifestation of such interactions, may be of the same order of magnitude as $\frac{\overline{u'^2}}{2}$ (equation (34)).

The existence of a spectral gap at scales of 1-10 km has been discussed widely among meteorologists for a number of years (e.g., Lumley and Panofsky, 1964; Panofsky, 1969; Bretherton, 1969). Recent evidence (Vinnichenko, 1969; Vinnichenko and Dutton, 1969) indicates that such a gap may actually exist in the case of CAT because a primary cause of that phenomenon is likely to be local, small scale instabilities rather than a cascade of energy down the spectrum from the largest scales. However, no conclusive observational evidence concerning the gap is available. Until just recently, airborne instrumentation was not capable of sensing the mesoscale region where the gap may be. The development of the airborne inertial platform (Axford, 1968; Crooks et al., 1967) for purposes of meteorological research now allows measurements in the desired frequency range.

For the purposes of discussion, a gap is defined as follows: It is a spectral region where the slope of the spectrum (in double logarithmic coordinates) decreases to zero and subsequently changes sign at higher frequencies. On the low frequency side of the gap the spectral slope is characteristically steeper than $-5/3$ while on the high frequency side the slope is positive. At still higher frequencies, the slope reverts to approximately $-5/3$. The spectral energy in the gap

is at least an order of magnitude less than the spectral energies at nearby higher and lower frequencies and the gap extends from $\frac{f_c}{2}$ to $\frac{3f_c}{2}$ where f_c , the cutoff frequency, is centered in the region of lower energy. The location of the gap may be between a few tens and a few hundreds of meters.

Ideally, then, the proposed energy analysis would be carried out in the following manner. First the data would be spectrum analyzed. Next the spectrum would be scrutinized for a gap (as defined above) in the mesoscale; and finally, on the basis of the location of the gap, the data would be separated (filtered) into a mean and a deviation, both of which are functions of time (or space). Energy budget terms would then be computed with the realization that the overbar in equation (31) henceforth implies low pass filtering of the particular quantity in question and the prime represents high pass filtering. For example, $\overline{u'^2}$ would be calculated by first high pass filtering to determine u' , squaring to yield u'^2 , and finally, low pass filtering to determine $\overline{u'^2}$.

Practically speaking, however, the placement of the cutoff frequency in a gap is not always possible. Bretherton (1969) has discussed a number of the problems involved in the specification of the gap from atmospheric data. In the present study it will be shown that the position of the depression of the spectral energy (when it exists) is often ill-defined. Furthermore, the apparent gap may shift its position in frequency space, as a function of the size of the sample analyzed and the spatial position of the sample with respect to the turbulent burst or bursts.

The existence of a spectral gap, although desirable, is not an absolute necessity in the proposed analysis. However, in the absence of a gap, interactions between the mean and turbulent components of the flow become important. In Appendix C and in Case 3 (Chapter V), experimental evidence is given in support of this fact. In order to take this behavior into account in a formal manner, the total energy budget must be rederived with the inclusion of terms of the form of $\overline{uu'}$. For the present, it will suffice to rewrite equation (31) as

$$\begin{aligned} \frac{\partial \overline{E}}{\partial t} + \overline{u_j \frac{\partial E}{\partial x_j}} + \overline{u'_i u'_j \frac{\partial u_i}{\partial x_j}} + \overline{u'_i u'_j \frac{\partial u'_i}{\partial x_j}} = \\ = - \frac{1}{\rho} \overline{u'_i \frac{\partial p'}{\partial x_i}} + \frac{g}{T} \overline{u'_j u'_j} + \overline{v u'_i \frac{\partial^2 u_i}{\partial x_j^2}} + R_{NL} \quad (50). \end{aligned}$$

The term R_{NL} represents interactions between the mean and turbulent flows and includes many terms which may be large in comparison to those written explicitly in the above equation. Some of these will be considered in greater detail in the next chapter.

The Combined Approach

In the preceding sections, a statistical model has been utilized to derive several quantitative indicators of statistical intermittency. In order to investigate the physical aspects of the intermittent turbulence, a modified computation of terms of the energy budget has been proposed. Specifically, the application of a set of numerical filters has been recommended for the definition of mean and turbulent variables. The advantage of the suggested approach is that an "instantaneous" mean (or turbulent) value may be obtained as a function of

space or time. A balanced energy budget (the computation of all terms in the proposed manner) is not feasible with presently available CAT data. However, such a balance is not necessary for the success of the technique. The reason is that each term of the energy budget may be interpreted in relation to a given physical process. The ability to examine the variations of some of the more important terms of the energy budget at scales commensurate with CAT should allow a better understanding of the associated physical processes which lead to the occurrence, disappearance, and, therefore, the intermittency of CAT.

IV. THE APPLICATION OF THE PROPOSED APPROACH TO CAT DATA

General

In order to examine the feasibility of the methods which were proposed in the last chapter, a series of three CAT occurrences has been analyzed. The present chapter deals with the procedures of data selection, data reduction, and data analysis.

Background for Data Selection

Ideally, the investigation of a turbulent patch should be carried out by several flights of a number of instrumented aircraft through the same turbulent patch. In this way, the time and space variations of the turbulence can be isolated and the true physical and statistical characteristics of CAT can be determined.

It was noted in Chapter I that the utilization of proper methods of data acquisition are critical for the success of CAT research. Shortcomings in past data collection programs have been realized by most CAT researchers (e.g., see Dutton, 1969) and will likely be overcome in the planning of future experiments. However, they remain a problem in the present study because facilities were not available to carry out an experiment strictly for the purposes of this investigation. Therefore, in order to test the methodology proposed in the last chapter, data had to be selected from past CAT programs or within the framework of research projects planned for other purposes. Most available CAT data have usually been gathered by single aircraft

(e.g., Reiter and Burns, 1966; Mather, 1969; Loving, 1969), often without the benefit of detailed supporting data (e.g., simultaneous rawinsonde observations). It follows that for a meaningful interpretation of analyses of these data, certain assumptions must be made about the physical characteristics which have not been specified by the incomplete observations. In many past studies, such assumptions have been made rather arbitrarily and the results of these investigations, especially with respect to the physics of turbulence, must be interpreted with some caution.

In the present study an effort was made to select CAT records from cases in which some aspects of the CAT-producing mechanisms were known. In this way, the insufficiencies of the aircraft observations may be offset, as least partially, and the validity of various assumptions can be evaluated in a semi-quantitative manner. For the analysis of CAT measurements made during a single flight through a patch of turbulence, it is desirable to have information concerning the stationarity and geometry of the patch and its orientation with respect to the aircraft track. A priori knowledge of the turbulence mechanism may arise either from (a) previous observations of the phenomenon or (b) from indications of detailed supporting data.

One turbulence mechanism for which information of type (a) is available is the rotor which is associated with mountain lee wave systems. As opposed to other types of turbulence-producing mechanisms in the free atmosphere, the rotor has been studied in detail for many years (Kuettner, 1939a, 1939b, 1959; Holmboe and Klieforth, 1954; Harrison, 1957; Scorer and Klieforth, 1959). This is partially due to the proximity of the rotor phenomenon to the surface of the earth and

to the fact that the rotor is frequently visible because of a well-defined roll cloud. The previously-mentioned studies have outlined the general characteristics of the rotor. It is extremely turbulent, quasi-stationary, roughly symmetric with respect to an axis oriented parallel to, and downstream of, the mountain ridge which is disturbing the flow, and it has dimensions of a few kilometers in radius and many kilometers in length.

A turbulence record collected during a flight through a rotor is especially useful for the illustration of the effects of intermittency from the statistical point of view because of the obvious burst-like character of the record. Furthermore, the tendency for the rotor to be quasi-stationary with respect to the ground, and two-dimensional, allows a number of valid simplifications to be made in the analysis of its physical aspects. Two cases of downwind flights through rotors were selected for analysis in the present investigation.

Type (b) information (detailed supporting data) is available for the rotor cases and for the third case selected for analysis. The latter CAT occurrence was experienced during an upwind flight through a layer of strong vertical wind shear, also under mountain lee wave conditions. More specific information with respect to the data for each case is given in the next section.

Data

During the 1968 and 1970 phases of the Rocky Mountain Lee Wave Experiment (Kuettner and Lilly, 1968; Lilly and Toutenhoofd, 1969), mountain lee wave systems which were generated in air flow over the Colorado Rocky Mountains were examined in detail. The geographical

area of the investigation (figure 3) offers almost ideal topographical conditions for the study of lee waves. It is characterized by a rapid increase in elevation from the longitude of Boulder to the Continental Divide. The Continental Divide is oriented approximately north-south for a distance of 40 km and maintains a nearly constant elevation of about 3800 m above mean sea level in the location of the study (Vergeiner and Lilly, 1970). Turbulence data which were collected on a number of lee wave flights were made available together with supporting mesoscale data and analyses by the National Center for Atmospheric Research (NCAR). The three cases which were selected for analysis are listed in table 1. The aircraft flight paths which correspond with the case studies are shown in figure 3.

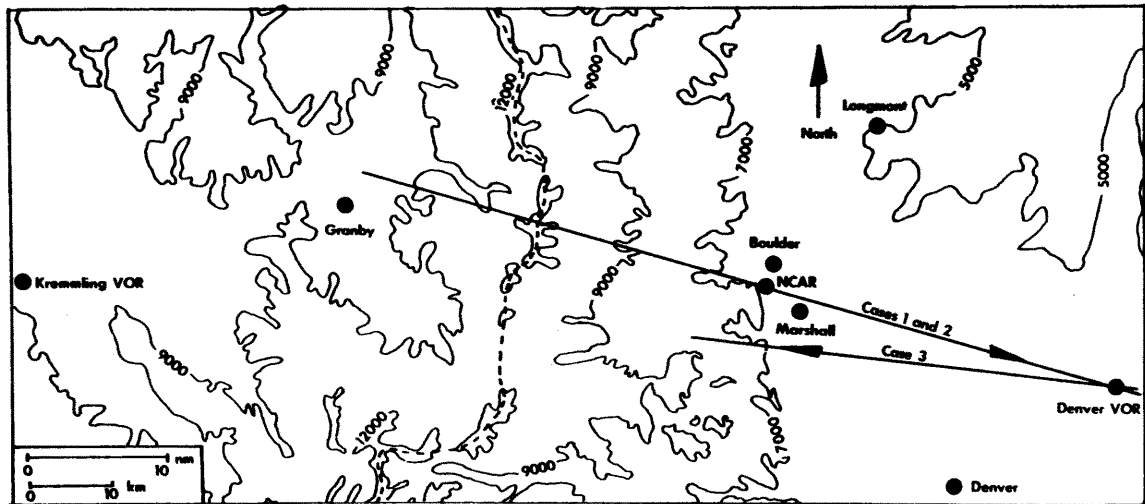


FIGURE 3. Topographical chart of geographical region in which the Rocky Mountain Lee Wave Experiment was conducted. Contours are labeled in feet (MSL). Heavy solid lines denote flight paths of aircraft for Cases 1, 2, and 3. The Continental Divide is indicated with the dashed line.

Case	Date	Aircraft	$\overline{\text{TAS}}$ (mps)	Flight Level (km)	Sample (minutes)	Data	Conditions
1	2/19/68	Beechcraft Queen Air A80	85	5.2	10	u	Severe CAT in rotor flow
2	2/20/68	Beechcraft Queen Air A80	85	5.2	10	u	Moderate CAT in rotor flow
3	2/17/70	de Havilland Buffalo	100	4.0	15	u,v,w,T	Moderate to severe CAT in a layer of strong vertical shear

TABLE 1. Description of Clear Air Turbulence cases selected for analysis. All data were acquired from the National Center for Atmospheric Research (NCAR).

The u-component information was derived from the true air speed (TAS) and Doppler data for Cases 1 and 2. For Case 3, u, v, and w information was obtained from the inertial platform system carried by the Buffalo. Instrumentation aboard the Queen Air (Cases 1 and 2) has been described by Kuettner and Lilly (1968) and Lilly and Toutenhoofd (1969). General aspects of the derivation of turbulence information from the inertial platform (Case 3) have been described by Lenschow (1967), Crooks et al. (1967), and Axford (1968). More specific information with respect to the vane sensors carried by both aircraft is given by Lenschow (1970).

The primary purpose of the Rocky Mountain Lee Wave Experiment was to observe lee wave systems in detail; therefore, for each case, several aircraft were flown on parallel tracks, vertically stacked at altitudes ranging from the low troposphere through the lower stratosphere (Kuettner and Lilly, 1968). Also, during the period of the aircraft flights, rawinsondes were launched from stations located upstream and downstream of the Continental Divide to obtain profiles of wind, temperature, and moisture. The data from the approximately simultaneous aircraft and balloon soundings provide much of the desired supplemental information for the mesoscale analysis of the environment in which the intermittent CAT was observed.

Synoptic and Mesoscale Analyses

The synoptic and mesoscale aspects of the turbulence environment are presented as background to the small scale characteristics of CAT. For each case, analyses include sectional surface and 500 millibar charts at the standard observation times closest to the period of the

aircraft flights. Time differences were less than six hours in all cases. The charts were derived from analyses prepared by the National Weather Analysis Center (NAWAC). In order to further document the nature of the CAT environment, profiles of wind, temperature, and moisture from local soundings are presented in addition to cross sections of the potential temperature field along the aircraft track.

Reduction of CAT Data

The Queen Air data (Cases 1 and 2) were recorded digitally at a rate of 32 samples sec^{-1} . Prior to the acquisition of the data for use in the present study, data were calibrated and subjected to arithmetic averaging in groups of four points to produce information at 0.125 second intervals. The effects of the preliminary averaging do not greatly affect the low frequency, lee wave aspects of the data, but they may be important in the high frequency, CAT characteristics. This problem is discussed in more detail in Appendix B.

The Buffalo data (Case 3) were subjected to analogue filtering during on-board recording. The filter gain (see Appendix B for details) decreased from unity near 6 Hz to 0.1 near 16 Hz. The original data were calibrated and placed on magnetic tape at 0.0625 second intervals. Subsequent processing included low pass filtering with the Martin-Graham filter ($f_c = 4$ Hz, $f_t = 5$ Hz, $NW = 65$) to suppress aliasing effects, and the selection of every other data sample to yield the final data set at 8 samples sec^{-1} .

All data were scrutinized for obviously "wild" points which were subsequently removed. The spike removal procedure consisted of setting upper limits for the changes of a given variable over the

sampling interval. If a change exceeded the selected threshold, the data were listed, inspected, and spikes were removed by linear interpolation. The number of points eliminated by this method was less than 1 per cent of the total sample for each case.

Sample Selection

The initial selection of the CAT samples was based on pilot and observer reports of turbulence in straight and level flight. Vertical acceleration records were then inspected for frequent excursions of ± 0.15 g or greater for periods in excess of one minute. Since the accelerometer for the Queen Air (Cases 1 and 2) was not stabilized during the flights, the TAS record from a segment of smooth flight was statistically analyzed (after high pass filtering) to determine a lower threshold for the turbulent region (i.e., $3\sigma = 0.42$ mps).

Care was taken to ensure that a sufficient portion of the record selected for analysis extended up and downstream of the turbulence region. This step was necessary because of the loss of end points in the filtering processes described earlier. The data sampling rate and the aircraft speeds demanded that the added non-turbulent sections be of the order of 2-1/2 minutes on each end of the record. This requirement could not be met fully with Case 3 because the aircraft turned and descended immediately after encountering the turbulence of the greatest intensity. Statistical analyses were accomplished on the turbulent portion of the record (after high pass filtering), while the energy budget analyses were performed on the larger samples which included the non-turbulent portions on each end.

A number of smaller samples were selected for the investigation of the variation of statistical properties of the turbulence throughout each large sample. The subsamples were chosen with respect to the location of the region of highest turbulence intensity for a given record. Cases 1 and 2 were ideal for this approach because the flights through the rotor produced one major burst. Records were chosen up and downstream and within the rotor. Minimum subsample sizes were one minute and thirty seconds (721 data points) for Case 1 and one minute and fifteen seconds (601 data points) for Case 2. Case 3 differed from the first two cases in that the turbulence increased in intensity throughout the flight rather than appearing as an isolated burst. Therefore, it was difficult to choose subsamples on the basis of the location of the primary turbulent patch. For this reason, the large record was divided into 6 adjacent two-minute records (960 data points each).

It is recognized that the relatively small samples decrease the reliability of the statistical estimates, especially with respect both to the power spectral densities at the lowest frequencies and to the probabilistic structure of the velocity differences. However, as will be seen in the next chapter, the final choice of samples was a compromise between a desire for statistical reliability and an attempt to characterize the non-homogeneous structure of the turbulent patch.

Statistical Analyses

Power spectrum analysis was carried out on the relevant variables for each turbulent sample and subsample. The "Fast Fourier Transform" (FFT) (Brigham and Morrow, 1967; Cochran et al., 1967) was utilized in

the determination of the spectrum. Raw data were first detrended by fitting the points with a linear function by the least squares method. The first and last ten per cent of each detrended sample was then bell-tapered (Enochson and Otnes, 1968), and subjected to the FFT. Energy densities were determined from one-half the sum of the squares of the real and complex parts of the transformed values. Energy density estimates were subsequently scaled for the proper units and corrected for the loss of variance due to bell tapering. For all three cases, raw estimates were averaged over eleven points to yield a smoothed spectrum. Due to the large sample in Case 3, the spectrum for the entire sample was determined by adding and averaging the spectral estimates for each subsample. This was done in a cumulative manner beginning in the region of lightest turbulence and proceeding upstream to the final subsample where the most intense turbulence occurred. In this way, the effect of the non-homogeneous nature of the turbulence on the final average spectrum could be investigated.

An attempt was made to objectively select the cutoff frequency (f_c) for the purposes of filtering on the basis of the location of a spectral gap, as discussed in the last chapter. Spectra plotted in logarithmic coordinates and with area proportional to energy were inspected for this purpose. As will be seen, the ideal criteria which were specified in Chapter III were difficult to satisfy. More than one gap frequently occurred in the high frequency portion of the spectrum and characteristically shifted position or disappeared entirely from sample to sample within a given turbulent patch. No gap was of sufficient width, and rarely did the energy at the frequency of the gap reach an order of magnitude less than energies at nearby

frequencies. The ambiguity in the definition of the gap in the present cases led to the decision that all data would be assigned a cutoff frequency near 0.1 Hz (~ 850 m for Cases 1 and 2 and ~ 1 km for Case 3). As a test of the effect of the frequency cutoff on the proposed methodology, energy budget and statistical analyses were repeated for Case 2 for $f_c = 0.2$ Hz (~ 425 m). Also the statistical analyses were repeated for $f_t = 0.06$ Hz (~ 1.67 km) for Case 3. The results of these tests are presented in Appendix D.

The remainder of the statistical analyses were performed on the data after high pass filtering. Normal and actual frequency histograms were determined for all samples. The mean variance, skewness, and kurtosis were also computed. The purpose of these analyses was to investigate statistical intermittency as a function of turbulence intensity. A description of computational procedures and computational formulae are found in Appendix A.

The Energy Budget

Since the turbulence data from the three cases were collected along flight tracks which were approximately parallel to the mean wind vector, the coordinate system for the computation of terms of the energy budget has been established as follows: the positive x direction is taken in the direction of the mean wind vector, the positive y direction is to the left, looking downwind, and z is positive upward. The energy equation may be simplified by assuming that the lee wave environment in which the data were collected is stationary and two dimensional (i.e., $\frac{\partial \overline{(\quad)}}{\partial t} = 0$, $\frac{\partial \overline{(\quad)}}{\partial y} = 0$, $\overline{v} = 0$). With the further assumption of three dimensional nondivergence equation (50) becomes

$$\begin{aligned}
 \frac{\partial \bar{E}}{\partial t} = 0 = & - \frac{\bar{u}}{2} \frac{\partial \bar{u}'^2}{\partial x} - \frac{\bar{u}}{2} \frac{\partial \bar{v}'^2}{\partial x} - \frac{\bar{u}}{2} \frac{\partial \bar{w}'^2}{\partial x} - \bar{w} \frac{\partial \bar{E}}{\partial z} \\
 & \textcircled{1} \quad \textcircled{2} \quad \textcircled{3} \quad \textcircled{4} \\
 & - \bar{u}'^2 \frac{\partial \bar{u}}{\partial x} - \bar{u}'\bar{w}' \frac{\partial \bar{w}}{\partial x} - \bar{u}'\bar{w}' \frac{\partial \bar{u}}{\partial z} - \bar{w}'^2 \frac{\partial \bar{w}}{\partial z} \\
 & \textcircled{5} \quad \textcircled{6} \quad \textcircled{7} \quad \textcircled{8} \\
 & - \frac{1}{2} \frac{\partial \overline{u'u'^2}}{\partial x} - \frac{1}{2} \frac{\partial \overline{u'v'^2}}{\partial x} - \frac{1}{2} \frac{\partial \overline{u'w'^2}}{\partial x} \\
 & \textcircled{9} \quad \textcircled{10} \quad \textcircled{11} \\
 & - \frac{\partial \bar{w}'E}{\partial z} - \frac{\bar{u}'}{\bar{\rho}} \frac{\partial \bar{p}'}{\partial x} - \frac{\bar{v}'}{\bar{\rho}} \frac{\partial \bar{p}'}{\partial y} - \frac{\bar{w}'}{\bar{\rho}} \frac{\partial \bar{p}'}{\partial z} \\
 & \textcircled{12} \quad \textcircled{13} \quad \textcircled{14} \quad \textcircled{15} \\
 & + \frac{g}{T} \overline{T'w'} - \epsilon + R_{NL} \quad \textcircled{16} \quad \textcircled{17} \quad (51).
 \end{aligned}$$

It was noted in Chapter IV that R_{NL} , the general interaction term, may be large in the absence of a spectral gap (see also Appendix C). It can be shown that a rederivation of the energy equation for the total flow, with the stipulation that terms of the form $\overline{u'u}$ are non-zero, will yield a number of mean flow and interaction terms. Three of the latter have been chosen for consideration in the present analyses and are listed in (52).

$$\begin{aligned}
 - \overline{u'u} \frac{\partial \bar{u}}{\partial x}, \quad - \overline{u'w} \frac{\partial \bar{u}}{\partial z}, \quad - \overline{uw'} \frac{\partial \bar{w}}{\partial x} \quad (52). \\
 \textcircled{18} \quad \textcircled{19} \quad \textcircled{20}
 \end{aligned}$$

Terms of the energy equation which were computed for each case are listed in table 2.

Case	Terms Computed
1	(1), (5), (9)
2	(1), (5), (9)
3	((1) + (2) + (3)), (5), (6), (7), ((9) + (10) + (11)), (16), ((18) + (19) + (20))

TABLE 2. Terms of equation (51) which were computed from the available data for each case study.

It is apparent from table 2 that, despite the simplified form of (51), many terms cannot be computed because of the lack of sufficient data. However, as mentioned earlier, a balanced energy budget is not the primary intent of the present study. Rather, the purpose is to consider the behavior of physically meaningful terms of the energy equation along the aircraft track at scales comparable with the dimensions of CAT.

It should be reiterated that for the computation of terms (1), (5), and (9) in Cases 1 and 2, the mean u component along the aircraft path was derived from the Doppler navigation system while the turbulent u component was based on the true air speed ($u' = -TAS'$ for a downwind flight). This step was necessary because at low frequencies (e.g., scales of about 1-5 km for the Queen Air) TAS fluctuations are contaminated by the uncontrollable phugoid oscillation of the aircraft (Etkin, 1959; Lenschow, 1970). Also, at low frequencies, ground speed

fluctuations become of the same order of magnitude or larger than TAS fluctuations. The Doppler system, however, is capable of resolving the lower frequencies (e.g., see Pinus, 1963; Fujita, 1966). The compatibility of the Doppler u component and TAS over the intermediate scales of 1-5 km was checked by spectrum analyzing both variables for Case 2. Slopes and magnitudes of the spectrum showed excellent agreement over the range in question.

Although ϵ (term (17) in equation (51)) is not directly computable, it can be estimated with the assumption that the $-5/3$ slope in the high frequency portion of the spectrum extends into the inertial subrange. This was done for Case 3 and the results are compared to the integrated energy budget over the entire turbulent sample.

The calculation of term (7) for Case 3 required an estimate of the mean vertical shears. This was accomplished by performing an isotach analysis of smoothed u component data derived from aircraft traverses immediately above and below, and including, the flight path in the region of the CAT encounter. Shears were tabulated at one minute intervals along the flight path and linear interpolation was performed to derive an array of values which were in the same form as the other turbulence data for computer calculations.

Further computations for Case 3 included the flux Richardson number in the form

$$R_f = \frac{\frac{g}{T} \overline{T'w'}}{\overline{u'w'} \frac{\partial \overline{u}}{\partial z}}, \quad \frac{\partial \overline{v}}{\partial z} \approx 0 \quad (53).$$

V. RESULTS

General

The results of the analysis of three cases of CAT are described in the present chapter. As noted in Chapter IV, the records of Cases 1 and 2 possess a high degree of non-homogeneity (one major burst in each record) and, also, certain aspects are known about the physical mechanisms which produced the non-homogeneity (rotors). The purpose of the presentation of extreme cases is to show, clearly, the statistical effects of intermittency and to demonstrate the application of the proposed energy budget analysis.

In contrast, Case 3 is presented as an example of the analysis of a CAT record which bears a greater similarity to records more commonly encountered in CAT research flights (Crooks et al., 1968; Mather, 1969). Data for Case 3 were gathered during a flight through a layer of strong vertical shear. As opposed to the rotor cases, CAT occurred over a much wider region and the records appear more homogeneous. Also, more data were available for Case 3 and, therefore, more terms of the energy budget could be computed. Because of the added data, the turbulence occurrence for the last case will be considered in greater detail, especially with respect to the results of energy budget computations.

Case 1

Synoptic conditions for February 19, 1968 (1700 MST) are shown in figure 4. The large scale pressure and flow patterns on this day are

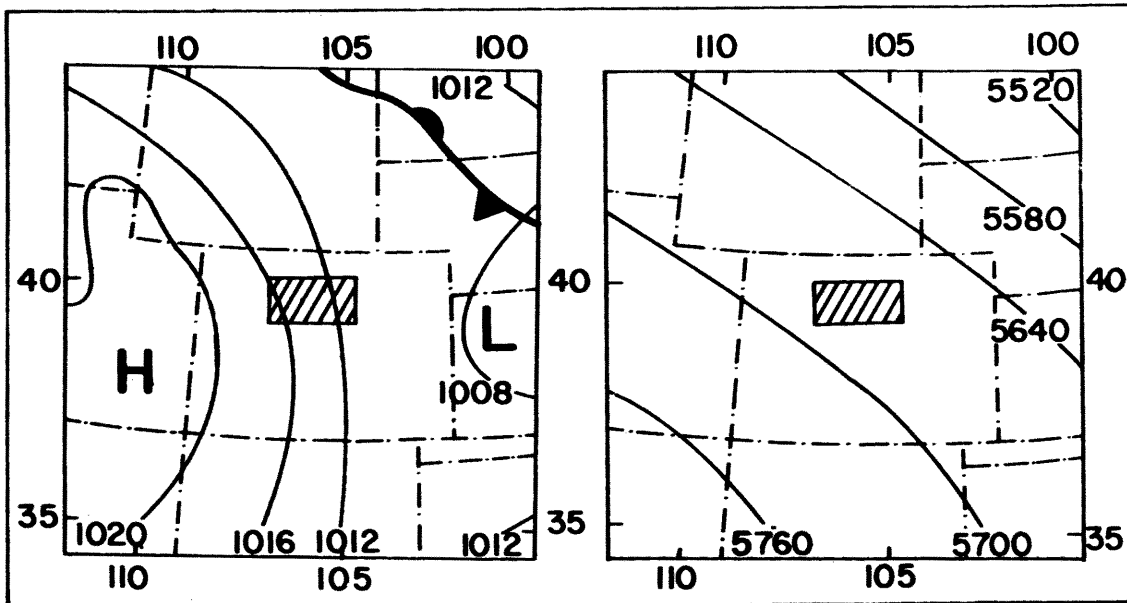


FIGURE 4. Sectional surface (left) and 500 mb (right) analyses for 1700 MST, February 19, 1968. Isobars of the surface analysis are labeled in millibars and contours of the 500 mb analysis are labeled in meters. The general geographical location of the study area is shaded.

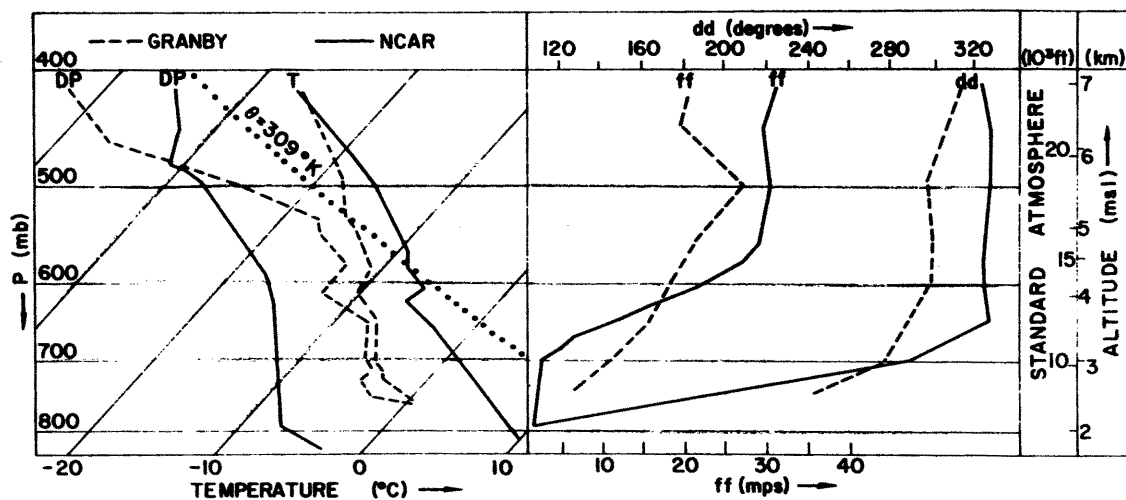


FIGURE 5. Vertical profiles of temperature (T), dewpoint (DP), wind speed (ff) and direction (dd). The Granby sounding was made at 1300 MST and the NCAR sounding at 1330 MST, February 19, 1968. Both diagrams are plotted with the same vertical scale. The temperature and dewpoint profiles are plotted on a skew-T, log P diagram. See Figure 3 for the location of sounding stations.

close to optimum for the occurrence of waves in the lee of the Continental Divide (Harrison, 1957). At the surface, a west-east pressure gradient exists across the mountains while at 500 mb, moderate northwesterly flow is present.

The aircraft flight during which the turbulence was encountered was flown between 1523 and 1531 MST. The flight path is shown in figure 3. The flight leg was the last (and lowest) of a series of four flown by the NCAR Queen Air 80 on that date. After descending to 17,000 ft MSL (~5.2 km) at the west end of track, the aircraft was flown on a straight and level track toward the Denver VOR (figure 3). The flight was smooth until a point about 12 miles (~20 km) east of the Continental Divide where severe turbulence was encountered. At this point, both the pilot and observer made visual observations of the roll cloud typically associated with rotor flow (e.g., see Kuettner, 1959). Further information derived from the flight log placed the aircraft track in the upper part of the rotor and indicated that the severe turbulence region was about 6 miles (~10 km) in length.

Temperature, wind, and moisture soundings taken up- and downstream of the Continental Divide are shown in figure 5. In addition, a vertical cross section of the potential temperature field along the aircraft track appears in figure 6. The latter analysis is based on data from four flight legs flown between 17,000 and 23,000 ft (~5.2 and 7 km) during the period 1340 to 1540 MST. The primary features on the mesoscale flow pattern are the downward motion of air over the Continental Divide (assuming that the isentropes and mean streamlines coincide) and the rotor immediately to the east. Lee waves of about 20 km in length are apparent in upper levels in the lee of the mountains. In lower levels,

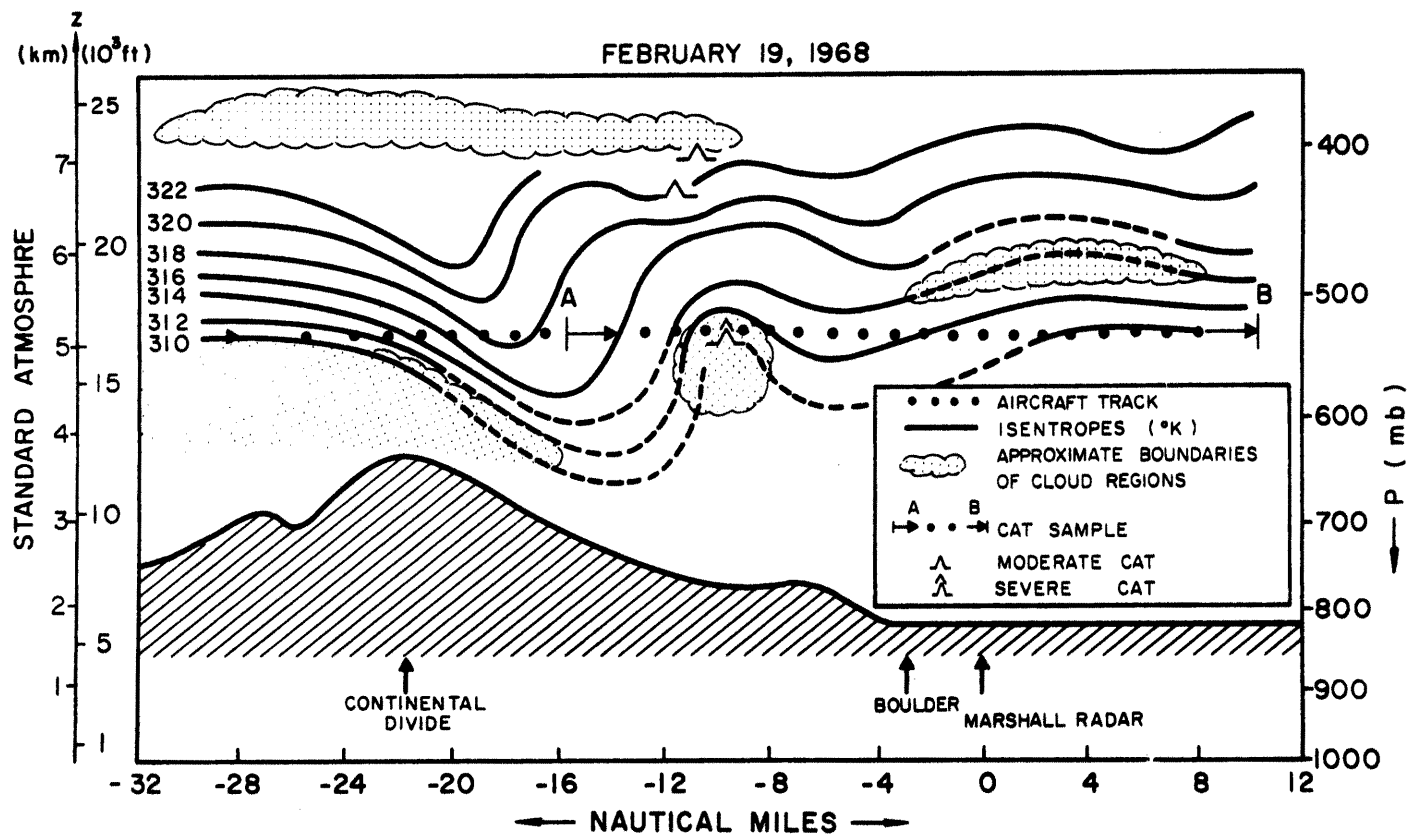


FIGURE 6. Vertical cross section oriented along the aircraft track for Case 1. Isentropes are dashed in regions where data did not show vertical consistency or where data were not available. The mean terrain profile is shaded on the lower portion of the diagram.

the rotor was clearly indicated from the aircraft data, however, the analysis downstream was more difficult, as is indicated by the dashed lines near 6 km in figure 6. Evidently, time changes had occurred in this region between flight legs. Use was made of the pilot and observer logs in the placement of the roll cloud and lenticular clouds in figure 6.

Figure 7 shows the results of scale separation. The variation of the mean wind component (\bar{u}) along the aircraft track verifies the larger scale wave environment in which the turbulence is embedded. The longitudinal gust component (u') is dominated by a strong burst at the location of the rotor (1524.25 MST). The turbulence near the rotor was of such great intensity that the Doppler navigation system was in "memory" (inoperative) for one minute and fifteen seconds. The term "memory" implies that ground speed and drift angle remain constant at their last measured value until the system begins operating again. The period in which this problem occurred is indicated in figure 7. In the case of constant ground speed and drift angle, changes in the mean wind component along the aircraft track will reflect only changes in the mean TAS.

The portion of the flight selected for analysis extends from point A to point B in figure 6. The primary sample, (a), and subsamples, (b) - (e), which were subjected to the statistical analyses are indicated in figure 7. The overall, statistical view of the CAT record is shown in figures 8 and 9. It should be noted that the longitudinal velocity spectrum presented in figure 8 is based on the TAS record alone because the Doppler winds were contaminated by the loss of ground speed and drift angle information in the vicinity of the rotor. Therefore, the spectral estimates beyond frequencies of about 0.10 to 0.033 Hz (scales of 850 m

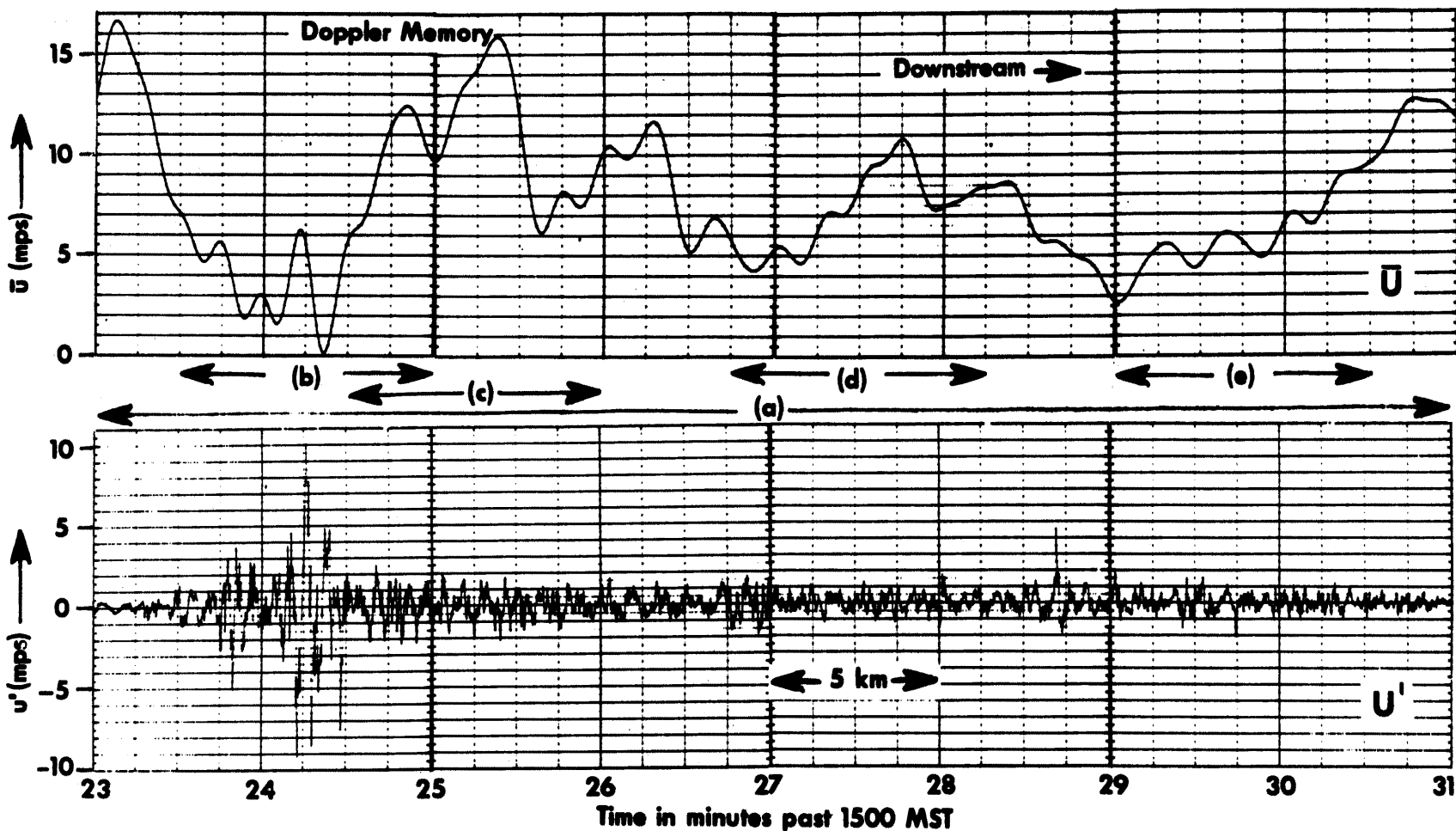


FIGURE 7. Top: Velocity component along the aircraft track for Case 1 after low pass filtering. Bottom: Velocity component along the aircraft track after high pass filtering. Bad point near 1528.7 was removed prior to statistical and energy budget analyses. Time axes of the diagrams are identical. See text for further explanation.

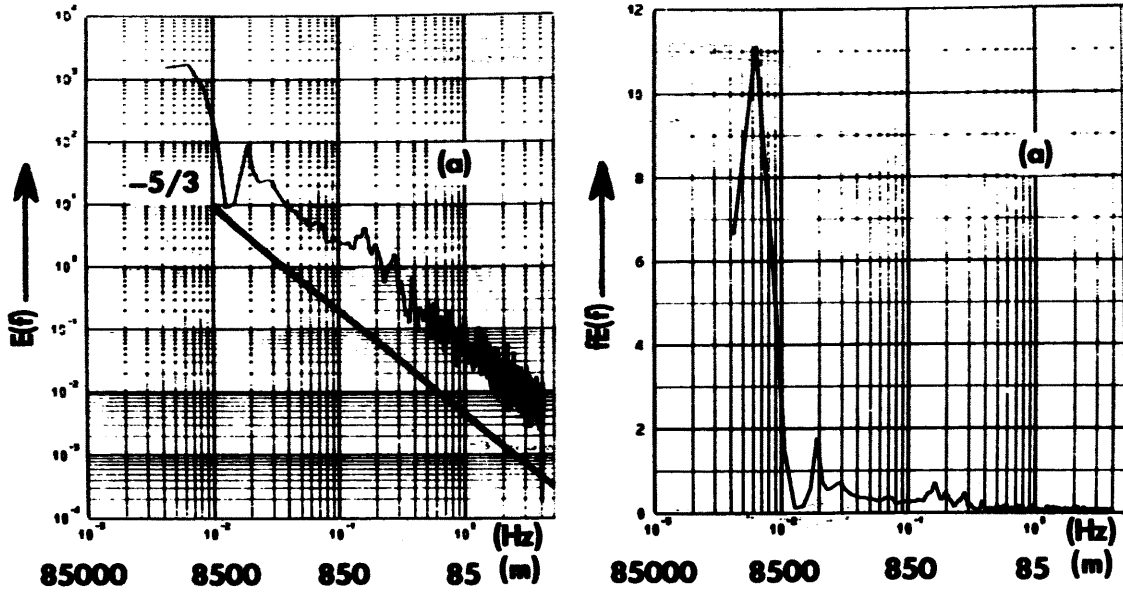


FIGURE 8. Energy spectrum of longitudinal velocity component for sample (a) of Case 1, plotted in logarithmic coordinates (left) and with area proportional to energy (right). $E(f)$ has units of $m^2sec^{-2} (Hz)^{-1}$, $fE(f)$ has units of m^2sec^{-2} .

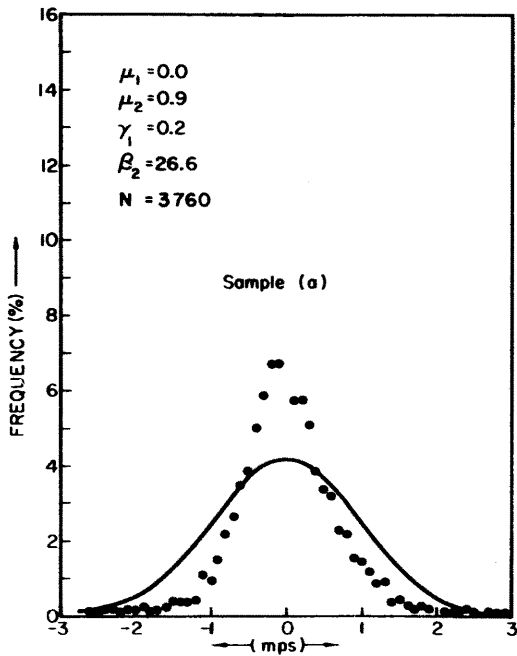


FIGURE 9. Actual (dots) and normal (solid line) frequency distribution of longitudinal gust velocities of Case 1. The mean (μ_1 , mps), variance (μ_2 , m^2sec^{-2}), skewness (γ_1), kurtosis (β_2), and sample size (N) are given in the upper left hand corner of the diagram. The class interval is 0.1 mps.

to 2550 m) cannot be interpreted with much confidence. In the higher frequencies, the energy spectrum is not unlike those derived from past studies (e.g., see Pinus et al., 1967; Crooks et al., 1968; Vinnichenko, 1969). The spectrum in the double logarithmic plot (figure 8) is fairly flat near scales of 850 m. At about 500 m, a slight hump occurs in the spectral curve. Proceeding toward smaller scales, the mean spectral slope steepens to about -2 to near 200 m beyond which it assumes a slope near -5/3. The plot of the spectrum with area proportional to energy (figure 8) emphasizes the spectral hump near 500 m. The component of velocity along the aircraft path was separated into mean and turbulent portions by selecting the cutoff frequency immediately to the left of that feature, at 0.1 Hz (~ 850 m).

The intermittent aspects of sample (a) are illustrated with the plot of the actual and normal frequency distributions (figure 9). The actual distribution greatly exceeds the normal distribution for very small values while the reverse is true between about one and three standard deviations ($\sigma = 0.95$ mps). The extremely non-Gaussian shape of the frequency distribution is reflected in the kurtosis value of 26.6 as compared to a Gaussian value of three. The statistical intermittency of the entire CAT sample (a) is not unexpected. The record is composed of an isolated burst within which the variance increases by nearly an order of magnitude. In fact, the behavior of the variance closely approximates a step function which was utilized in the derivation of the statistical model of intermittency presented in Chapter III.

The radical variation of turbulent intensities within the CAT region suggests that the record should be broken up into sections to determine the statistical characteristics of more homogeneous collectives. This

procedure is fairly simple in the present case because the record is composed of one major turbulent burst. Statistical analyses of subsamples (b) - (e) are presented in figures 10 and 11. The primary features of these analyses are:

- (a) In figure 10 there is a marked decrease in the magnitudes of the energy densities as one proceeds downstream from the rotor (sample (b)).
- (b) There is a lack of a well-defined $-5/3$ range in the high frequency portion of the spectrum of sample (b) (the rotor) as compared with the downstream samples.
- (c) The position of what might be called a spectral gap varies from subsample (b) near 85 m to subsample (d) near 425 m.
- (d) In figure 11 there is a large decrease in the value of β_2 from the larger sample (a) to the subsamples, as a result of the selection of more homogeneous portions of the record.
- (e) There is a tendency for sample (b) (the rotor) to deviate more radically from the Gaussian distribution than the downstream subsamples.

A summary of the first four statistical moments for each of the samples of Case 1 is presented in table 3.

Sample	Sample Size N	Mean μ_1	Variance μ_2	Skewness γ_1	Kurtosis β_2
(a)	3760	$-2.43 \cdot 10^{-3}$	$9.21 \cdot 10^{-1}$	$2.18 \cdot 10^{-1}$	26.60
(b)	721	$1.30 \cdot 10^{-2}$	3.87	$6.04 \cdot 10^{-2}$	7.91
(c)	721	$-3.34 \cdot 10^{-3}$	$5.24 \cdot 10^{-1}$	$-3.93 \cdot 10^{-2}$	3.36
(d)	721	$-1.31 \cdot 10^{-3}$	$2.37 \cdot 10^{-1}$	$-2.63 \cdot 10^{-2}$	3.80
(e)	721	$1.98 \cdot 10^{-3}$	$2.00 \cdot 10^{-1}$	$-8.17 \cdot 10^{-2}$	4.63

TABLE 3. Summary of statistical parameters for all samples of Case 1.

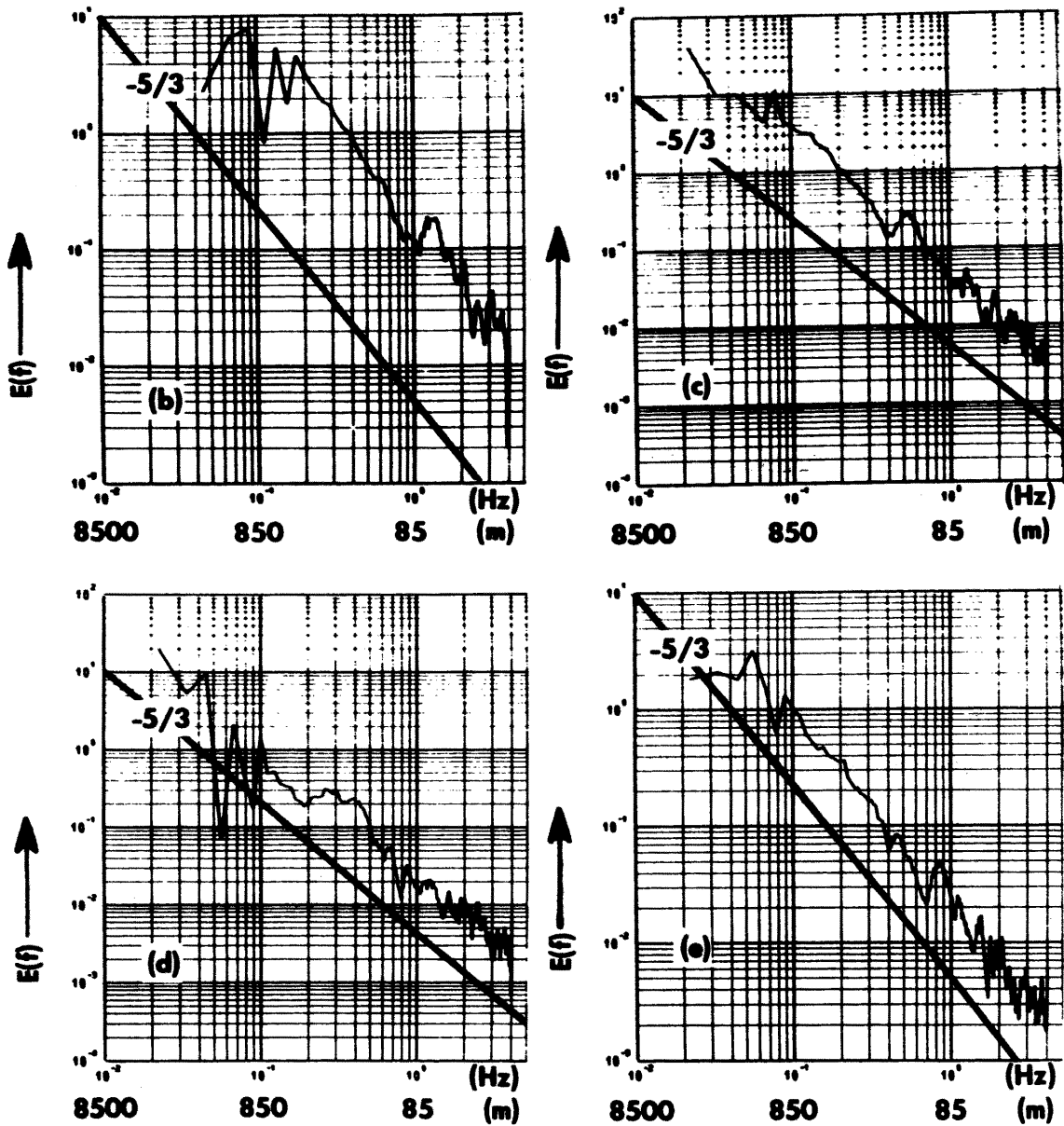


FIGURE 10. Energy spectra for subsamples from Case 1. The line with the $-5/3$ slope is in the same position relative to the logarithmic coordinates on each diagram. $E(f)$ has units of $m^2 \text{ sec}^{-2} (\text{HZ})$, $fE(f)$ has units of $m^2 \text{ sec}^{-2}$.

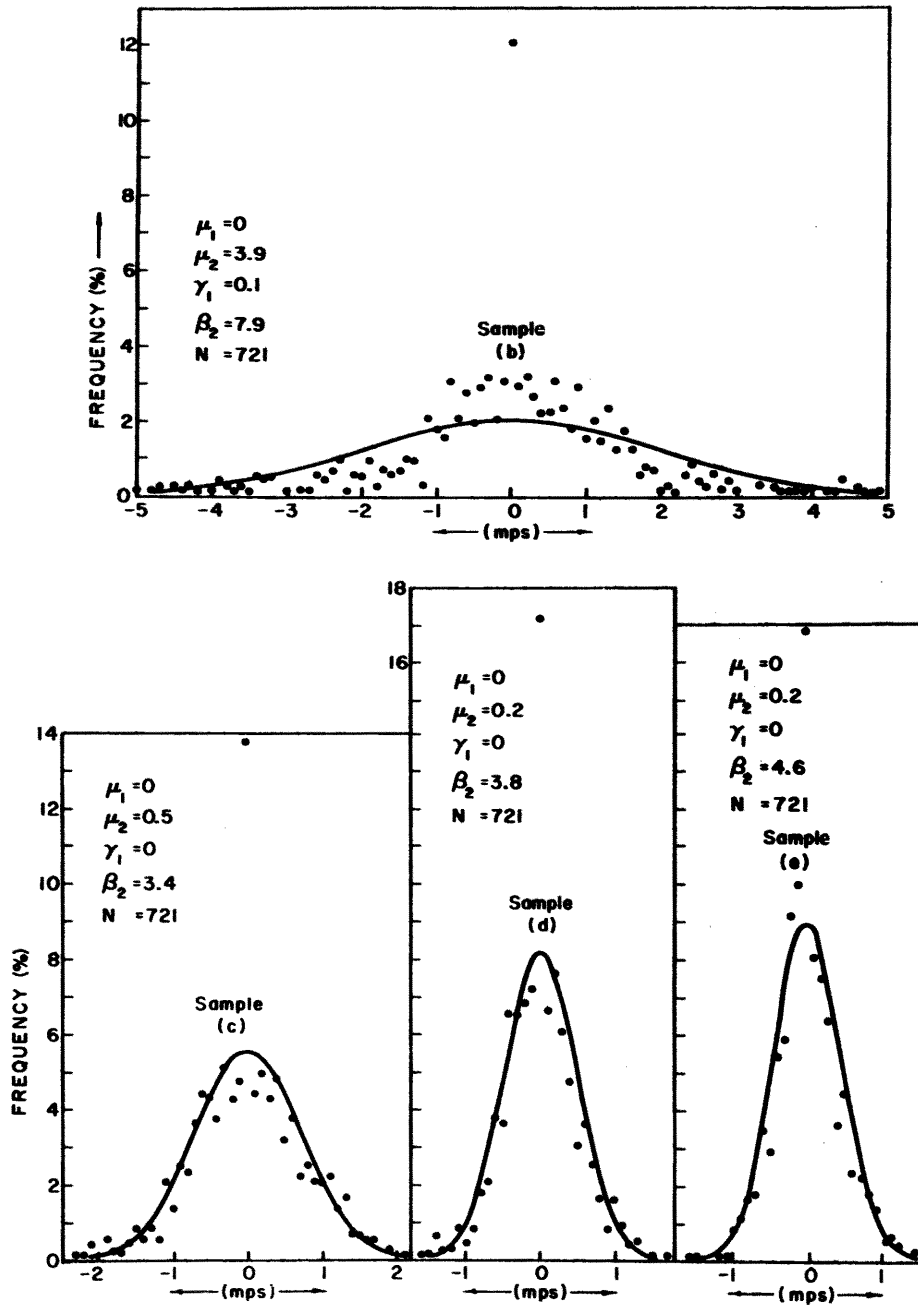


FIGURE 11. Same as Figure 9, but for subsamples of Case 1.

As was noted earlier, the record which has been subjected to statistical analysis was known to be intermittent from the visual inspection of the turbulence record (figure 7). The selection of data which obviously possess this quality has been especially useful in the demonstration of the statistical effects of intermittency. Thus, the results of the statistical analyses have quantitatively verified the strongly intermittent character of the record of Case 1.

The data were also chosen with knowledge of physical mechanism which caused the statistical intermittency. Although the detailed aircraft data for Case 1 are limited (i.e., only the longitudinal velocity component is considered), it is known that the primary turbulence encounter was associated with a rotor. Therefore, an interpretation of some of the physical aspects of the burst is possible with the computation of a few terms of the energy budget.

The upper portion of figure 12 shows the mean kinetic energy of the longitudinal gust component $\left(\frac{u'^2}{2} \right)$. The intermittent nature of the CAT record is apparent in the large isolated peak which is found in the same region as the rotor in figure 7. The portion of the record beyond 1027 MST is not included, since energy in that region remains less than $0.5 \text{ m}^2\text{sec}^{-2}$ (about 4 per cent of maximum value near the rotor). The small regions of negative mean energy are the result of minor filter errors (discussed in Appendix B).

Insight into the causes of the intermittency may be gained by considering the three terms of the energy budget (equation (51)) which could be calculated from the available data. The terms are plotted in the lower portion of figure 12 and show a general symmetry with respect to the energy spike associated with the rotor. Because the magnitudes of

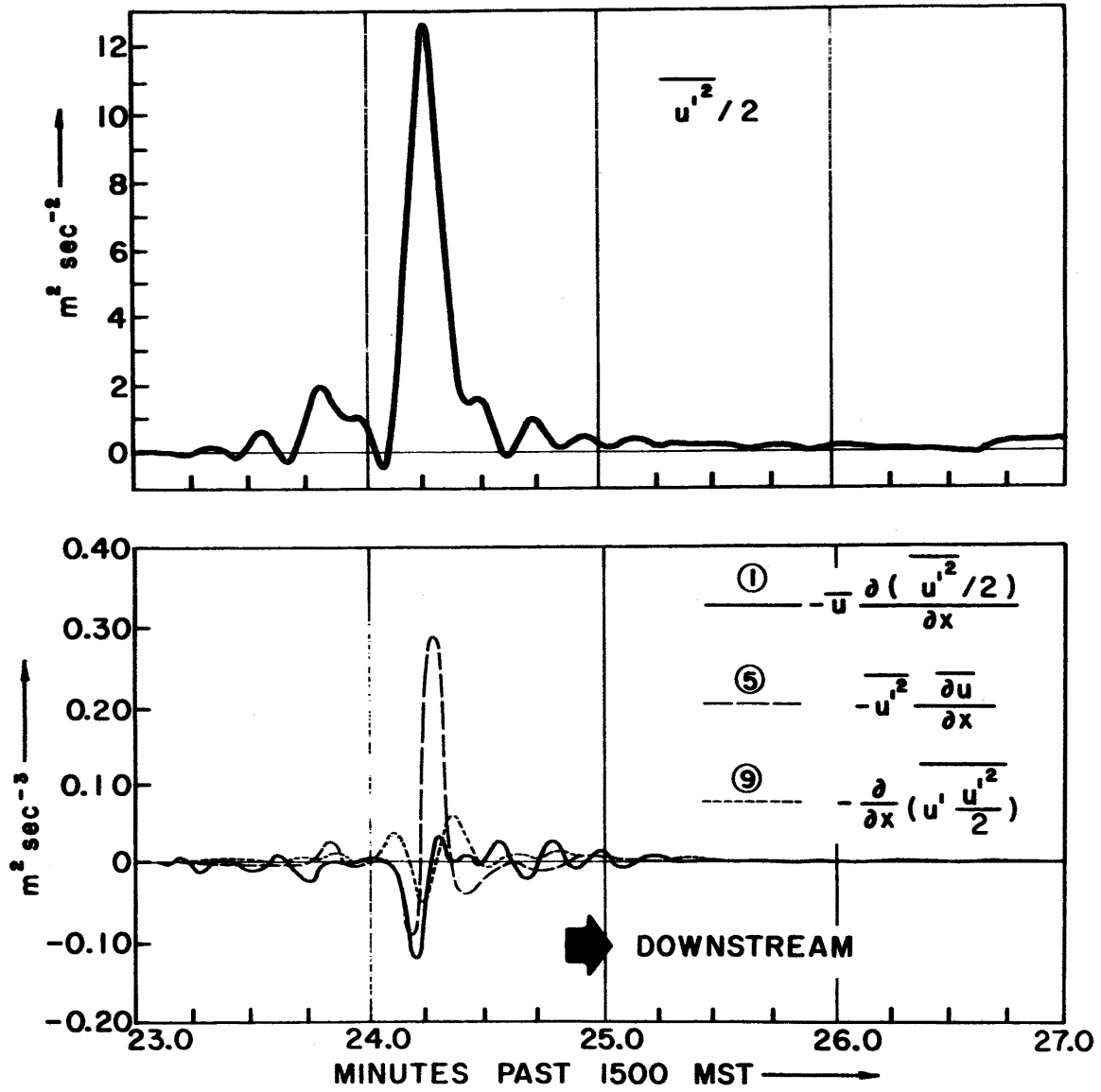


FIGURE 12. Top: Distribution of the kinetic energy of the longitudinal gust component along a portion of the aircraft track for Case 1. Bottom: Distribution of terms (1), (5), and (9) (equation (51)). Time axes are identical on both diagrams.

all terms are nearly zero beyond 1027 MST, the diagram has been truncated at that point.

Term (1) is the advection of the kinetic energy of the longitudinal gust component by the mean wind along the aircraft path. It reflects a loss of kinetic energy on the upwind side of the turbulent burst due to the advection of less turbulent air into the region. If the rotor was symmetric, one would expect the upwind energy loss by advection to be reflected in a downwind gain of the same magnitude. The expected behavior does not occur. Although the value of term (1) downwind of the maximum energy peak is positive, it is an order of magnitude smaller than the upwind value. The cause of this behavior is shown in figure 7. The mean u component reaches a secondary maximum upwind of the maximum turbulence and decreases to near zero immediately downwind. Although the turbulence intensity decreases rapidly downstream of the primary burst, the advection is small because the mean wind component parallel to the aircraft track is small. It appears, in fact, that the aircraft penetrated the rotor very close to its center ($\bar{u}=0$) and that the maximum turbulent burst occurred immediately upstream of that point.

Term (5) (figure 12) may be interpreted as an energy redistribution term due to the convergence (or divergence) of the mean wind along the aircraft track. A local energy loss occurs upwind of the maximum turbulence while an energy gain occurs downwind. The cause of this pattern is again found in figure 7. Proceeding downwind, the mean wind component increases rapidly (divergence) then falls abruptly (convergence) in the vicinity of the kinetic energy maximum.

Term (9) is the flux convergence of the turbulent energy of the u component. The shaded region in the lower portion of figure 12 indicates

that computations have been locally contaminated due to the small region of negative energy. The effect of the erroneous energy value is particularly apparent in the values of term (9) in the same area. In the uncontaminated region of the kinetic energy peak, there is an energy loss on the upstream side of the peak and a gain on the downwind side, due to the flux divergence and convergence, respectively.

The terms presented in figure 12 are frequently neglected in the usual method of computing the turbulent kinetic energy budget (e.g., see Lumley and Panofsky, 1964; Dutton, 1969). The assumption of longitudinal homogeneity on the scale of the entire CAT sample ((a) in figure 7) would probably be verified in the present case. That is, the integration of terms (1), (5), and (9) over the entire patch of CAT would lead to compensation of positive and negative values and the inclusion of many values very close to zero. The result would be a very small average value. The instantaneous values of these terms, however, show that, near the major burst, they may be quite important.

The assessment of the relative local importance of terms (1), (5), and (9) would normally be made by comparing them to other terms of the energy budget. This procedure is not possible in the present case since terms such as the energy feeding due to a mean vertical wind shear ((7) in equation (51)) could not be computed from the available data. Therefore, the establishment of a reference must be accomplished indirectly. This may be done by drawing upon the information available from the mesoscale analyses (figure 6). The turbulence is embedded in a large amplitude, standing wave. Under such conditions the mean streamlines execute a large vertical oscillation. Therefore, as one passes through the region of strongest turbulence (the rotor) it would be expected that

the direction of maximum shear would vary radically. For this reason, the shear of the mean vertical velocity along the flight path should approach the same magnitude as the vertical shear of the longitudinal wind component. Thus, upon intersecting the rotor, it would be expected that the shear feeding of energy would alternately be accomplished by the terms

$$- \overline{u'w'} \frac{\partial \bar{w}}{\partial x} \text{ and } - \overline{u'w'} \frac{\partial \bar{u}}{\partial z} .$$

Assuming that u' and w' are of the same order of magnitude and that $\left(\frac{\bar{w}}{\bar{u}}\right)$ is a constant which is of the order unity on the flanks of the rotor, then it can be shown that

$$A \left| \overline{u'w'} \frac{\partial \bar{u}}{\partial z} \right| = B \left| \overline{u'w'} \frac{\partial \bar{w}}{\partial x} \right| = C \left| \overline{u'^2} \frac{\partial \bar{u}}{\partial x} \right| \quad (54),$$

where A, B, and C are constants of order unity and the vertical lines indicate the absolute value. The assumptions on which equation (54) is based take advantage of the large amplitude and extreme turbulence found in the rotor. The equality signs imply that the terms may attain similar magnitudes within the rotor environment, although not necessarily at the same location.

The argument presented above states that term (5) (figure 12) may at times be as large as the energy feeding due to vertical shears. Since the latter term is normally considered one of the more important terms of the energy budget (Lumley and Panofsky, 1964; Dutton, 1969), it is concluded that term (5) is also important in the present case, at least locally. Utilizing term (5) as reference in figure 12, it becomes apparent that the advection (term (1)) is also locally important, but that flux divergence (term (9)) is only of secondary importance.

Although an energy balance cannot be considered on the basis of the few terms presented in figure 12, certain qualitative conjectures can be made about other terms which could not be computed. The relative stability of the environment outside the rotor suggests that in that region, damping due to buoyancy effects is very large. Further, as shown in figure 5, the NCAR sounding shows only small vertical shear near flight level, downstream of the rotor. Assuming that the sounding is representative of the mean flow implies that in that region the energy fed from the mean flow due to vertical shear is small. On the upstream side of the rotor, the shear is larger (Granby sounding in figure 5) but the static stability is also larger west of the Continental Divide. In the immediate vicinity of the rotor, static stability decreases rapidly as is evidenced by the variation of potential temperature along the aircraft track in figure 6. This feature suggests that strong mixing is occurring in that region due to the overturning of the air within the rotor. Thus, the buoyancy term ((16) in equation (51)) would be expected to be zero or to act in the same direction as the mean vertical shear in the center of the rotor, that is, to contribute positively to the turbulent energy.

The previous discussion of the magnitude of term (5) implies that a major part of the shear production of energy in the rotor is accomplished alternately by the horizontal and vertical shears of the \bar{w} and \bar{u} components, respectively. This suggestion emphasizes the fact that the meso-scale wave structure is included in the mean flow. Therefore, the turbulent air is being carried away from the rotor along a mean streamline which passes through the flight level.

The causes of the statistical intermittency of the record are now apparent. The aircraft penetrated a locally, unstable region during

horizontal flight through a generally stable environment disturbed by mesoscale waves. Because turbulent eddies which left the rotor were being swept downstream through the flight level, there was a large element of surprise (i.e., a high degree of statistical intermittency).

Case 2

Synoptic conditions for February 20, 1968 are presented in figure 13. Only small changes occurred in the synoptic pattern in the 18 hours which elapsed between Case 1 and Case 2. The west-east sea level pressure gradient intensified due to the movement of a surface frontal system into northeastern Colorado, while at 500 mb wind speeds remained moderate (15-20 mps) but with a slight shift to a more westerly direction.

The Queen Air 80 encountered light to moderate turbulence at a flight level of 5.2 km in the lee of the Continental Divide during the period 0949 to 0957 MST. The mean heading and flight path were the same as on the preceding day (figure 3). Mesoscale meteorological conditions are shown in figures 14 and 15. The descent of the air as it passed over the mountains is evidenced in the intense inversion near 550 mb in the NCAR sounding (figure 14).

The vertical cross section showing the potential temperature field along the aircraft path appears in figure 15. As indicated by the schematic cloud regions, the path of the aircraft crossed over two roll clouds and intersected a third. Light turbulence was reported near the second rotor and moderate turbulence was reported in connection with the third. Some difficulty was encountered in the analysis of the region indicated by dashed lines in figure 15. Discussions with the aircraft observer and reference to the flight log suggest that the secondary

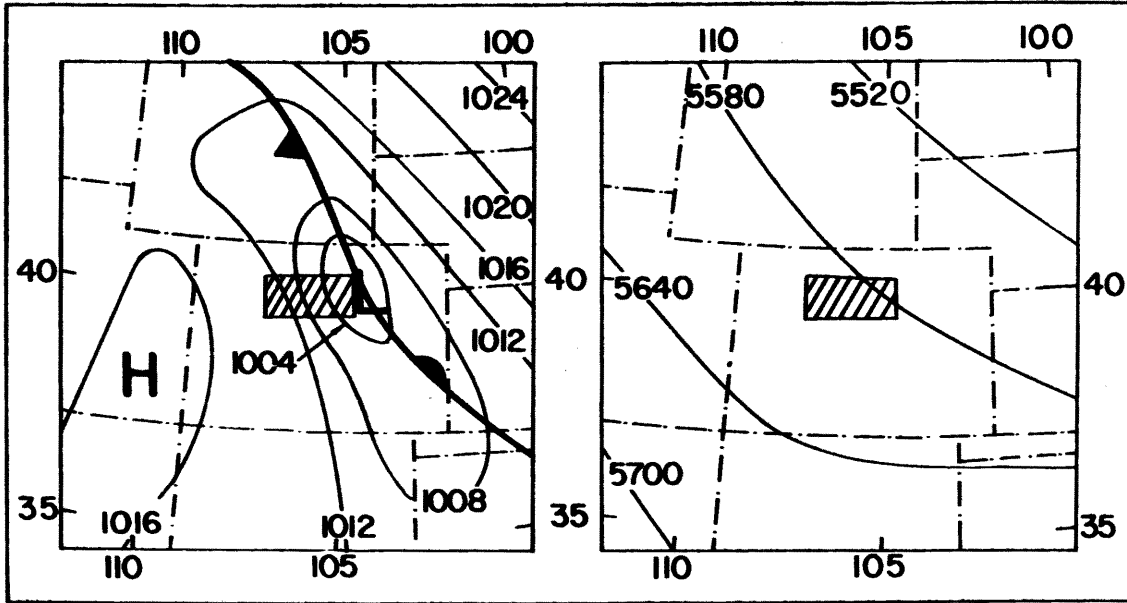


FIGURE 13. 1100 MST surface analysis (left) and 1700 MST 500 mb analysis (right) for February 20, 1968.

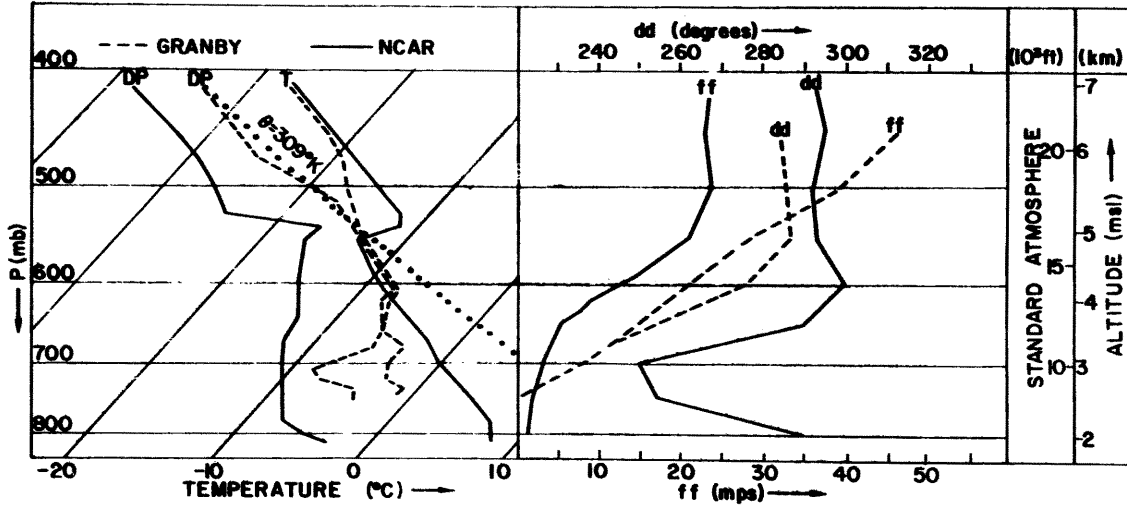


FIGURE 14. Same as figure 5 except for 0800 MST, February 20, 1968.

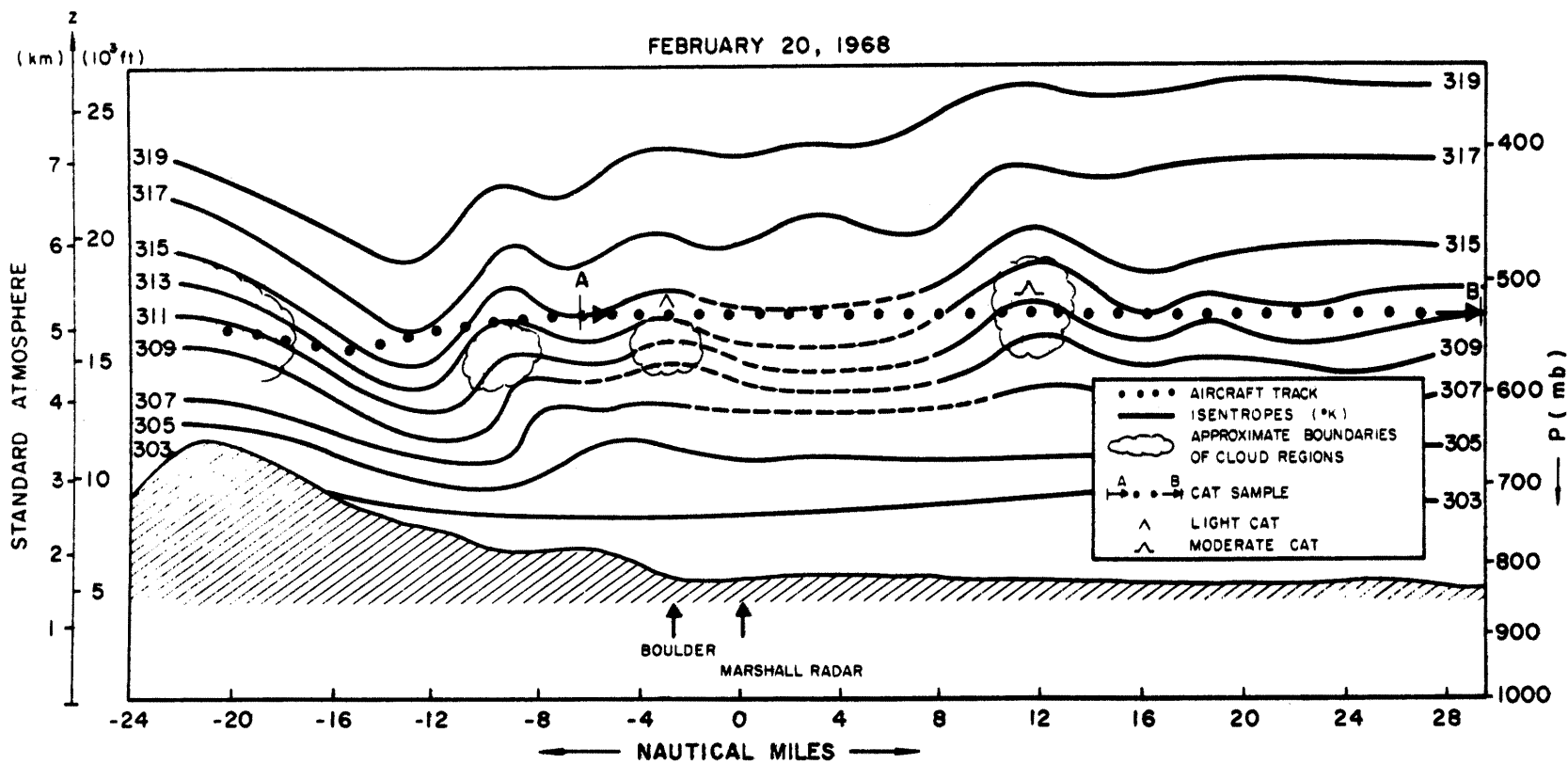


FIGURE 15. Same as figure 6, but for Case 2. Original analysis by Dr. D. K. Lilly of NCAR.

rotors were transitory phenomena, that is, that time changes were occurring during the time it took to traverse the previous flight leg and return over the same track at a lower level.

The filtered mean and turbulent portions of the wind component along the aircraft track are shown in figure 16. The segment of the flight selected for analysis lies between points A and B in figure 15. The large sample and subsamples subjected to statistical analysis are indicated by the letters (a) through (e) in figure 16.

The undulating nature of the mean component (\bar{u}) verifies the existence of the mesoscale lee waves. The turbulent record (u') shows that the magnitudes of the maximum gusts are about one-half those which were encountered in Case 1. The well-defined, sinusoidal character of the record of u' near 0956 MST indicates that some sort of wave motion may be present. It is also noted that there are two brief periods where the longitudinal gust fluctuations are somewhat less than the threshold defined in Chapter IV. These portions of the record are found near 0950.5 MST and 0955 MST. It can be concluded from the observations discussed above that the CAT record to be analyzed from both the physical and statistical points of view is less intense, but slightly more complex than in Case 1.

Since the Doppler winds were available throughout the flight it was possible to obtain an energy spectrum analysis of the longitudinal component of the wind from scales of about 20 m to about 4 km by combining low frequency Doppler information and high frequency TAS information. The combined spectrum for the entire sample (a) appears in figure 17. The spectrum is characterized by an approximately -2 slope in the logarithmic plot from scales of four kilometers to about 850 meters. To the

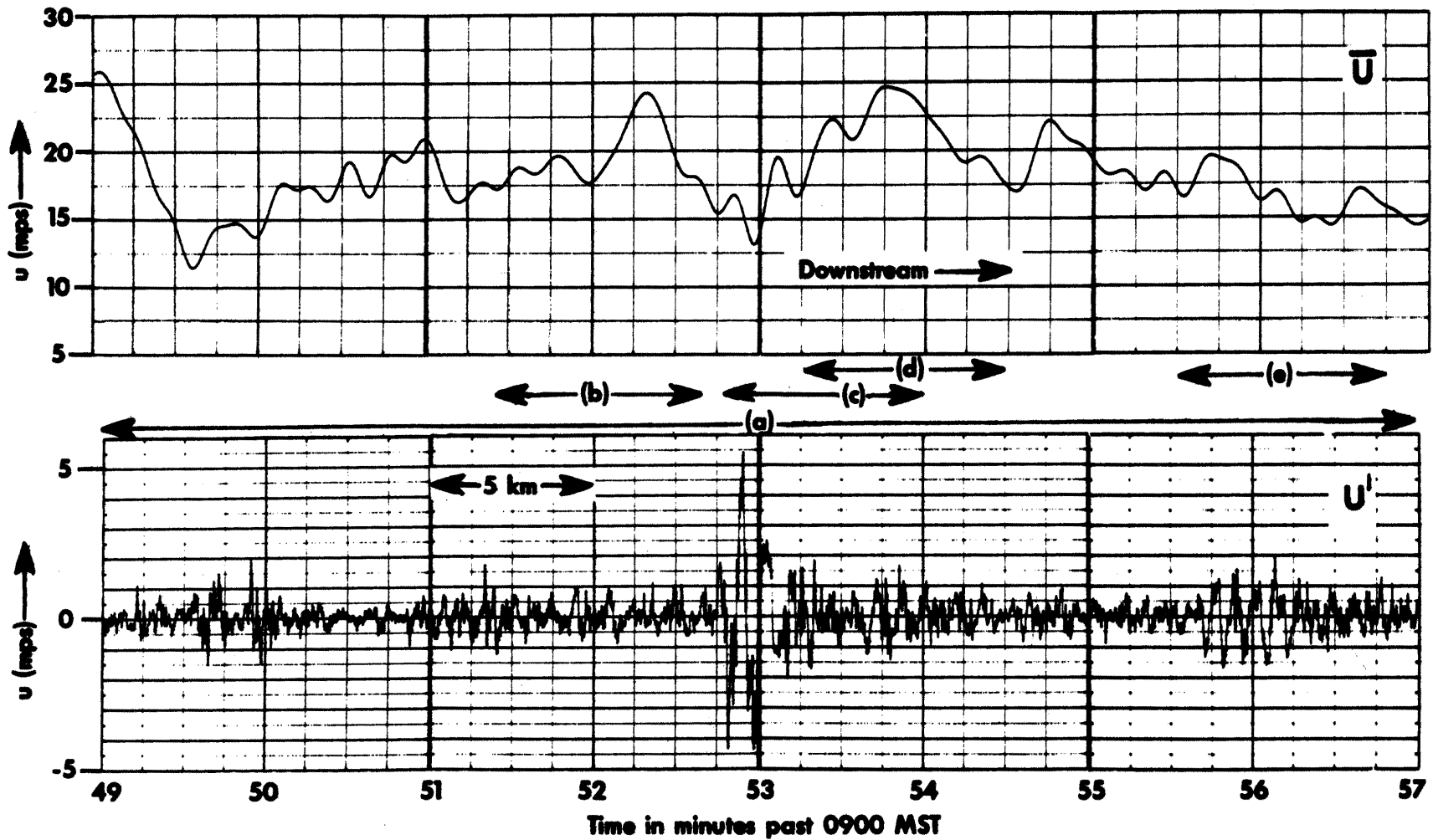


FIGURE 16. Same as figure 7, but for Case 2.

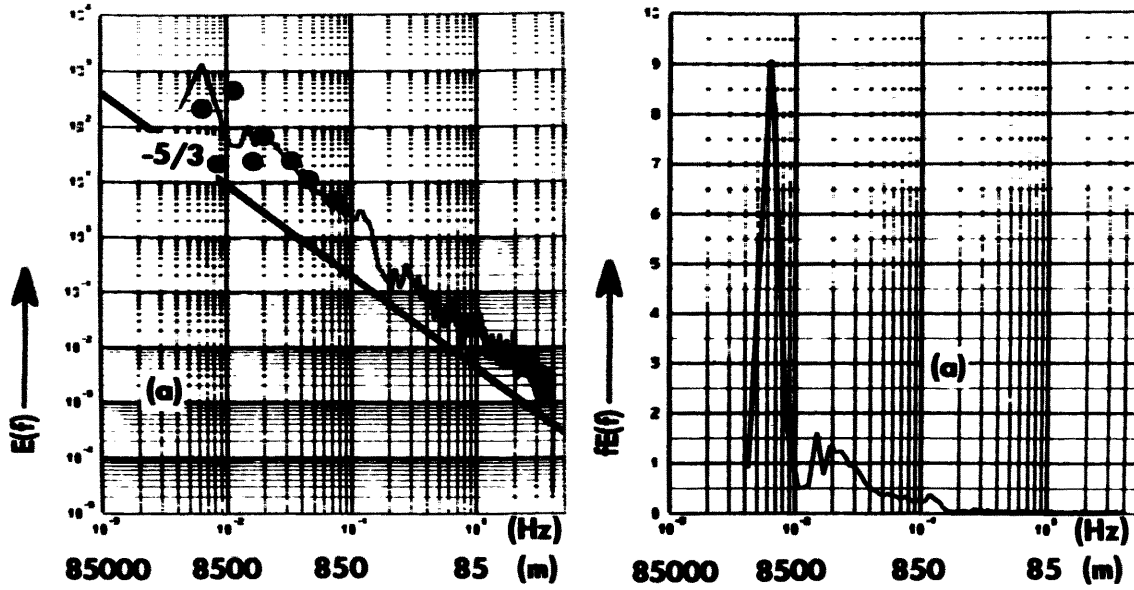


FIGURE 17. Same as figure 8, but for Case 2. Also, dots indicate spectral estimates based on longitudinal component of doppler winds.

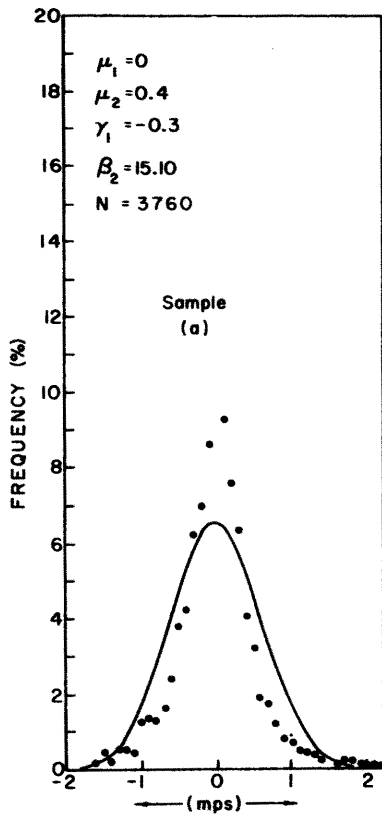


FIGURE 18. Same as figure 9, but for Case 2.

right of the latter point a slight hump occurs, beyond which the energy densities fall off rapidly. The spectrum subsequently flattens out in the 400-200 m range and then follows an approximately $-5/3$ slope from 200 m to the smallest resolvable scales. The separation of the mean and turbulent portions of the record was accomplished by placing the cutoff frequency at 0.1 Hz (850 m). The plot of the spectrum with area proportional to energy (figure 17) indicates a slight plateau in the energy level near that point. Since the energy density decreases so rapidly between about 700 m and 425 m and because of the interest in the effects of varying the cutoff frequency on the statistical and energy budget computations, the analysis of Case 2 was repeated with a cutoff frequency near 0.2 Hz (425 m). The results are presented in Appendix D. The present discussion is based on a cutoff frequency of 0.1 Hz (850 m).

The normal and actual frequency distributions for the entire sample (a) are shown in figure 18. The actual distribution deviates from normal in that it is negatively skewed and more peaked. The kurtosis, β_2 , as a measure of the intermittency of the record, is less than the kurtosis for the entire record in Case 1 (15.1 versus 26.6). The decrease in the overall intermittency (although still large) is due to a number of factors. Primarily, the intensity of the largest burst (figure 16) is closer in magnitude to the intensity of "background" turbulence. Put in terms of the statistical model, the step function variation in the variance of the record is smaller in Case 2 than in Case 1.

The statistical analyses of the subsamples indicated in figure 16 are presented in figures 19 and 20. The energy spectrum analyses (figure 19) are based on the TAS record alone. The primary features of interest are:

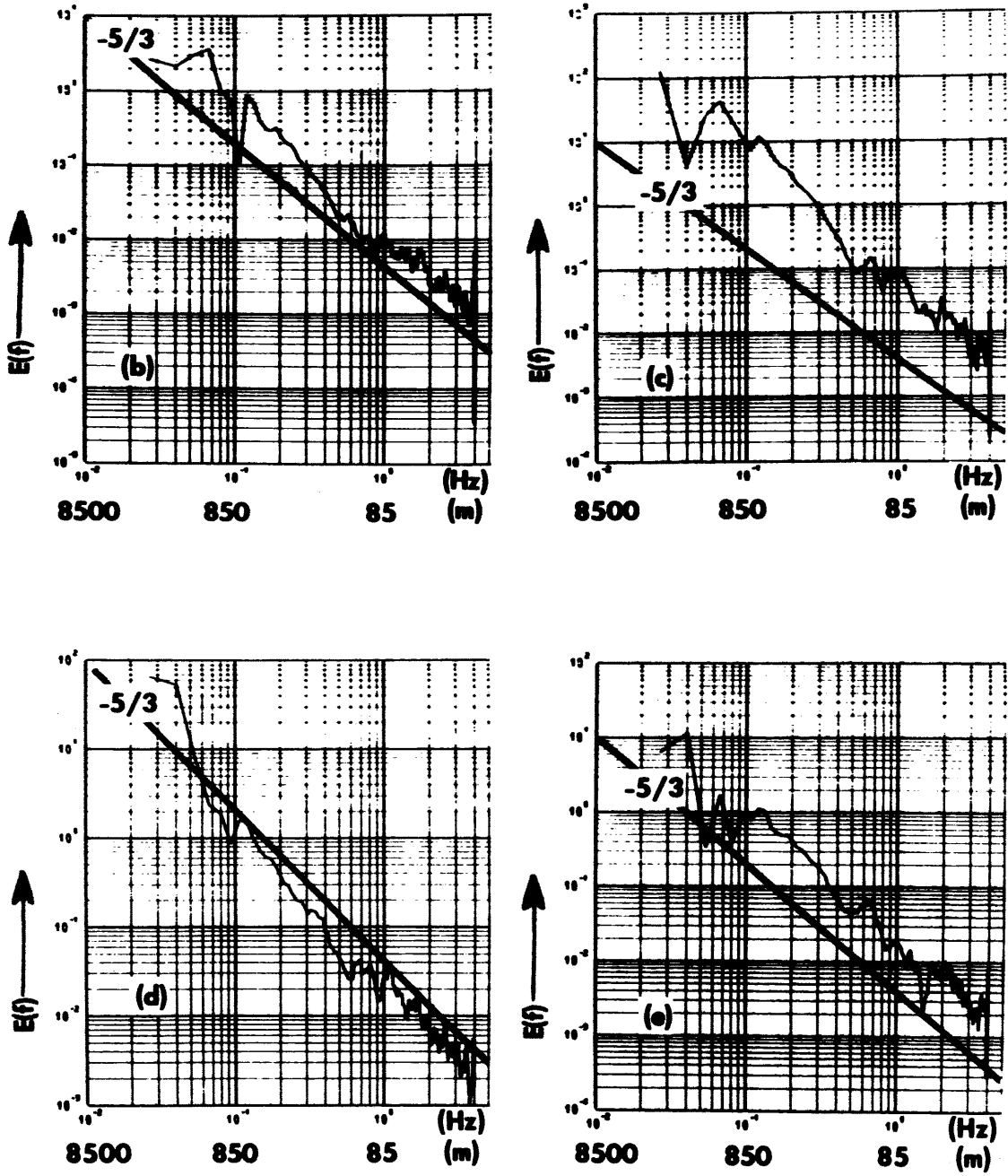


FIGURE 19. Same as figure 10, but for Case 2.

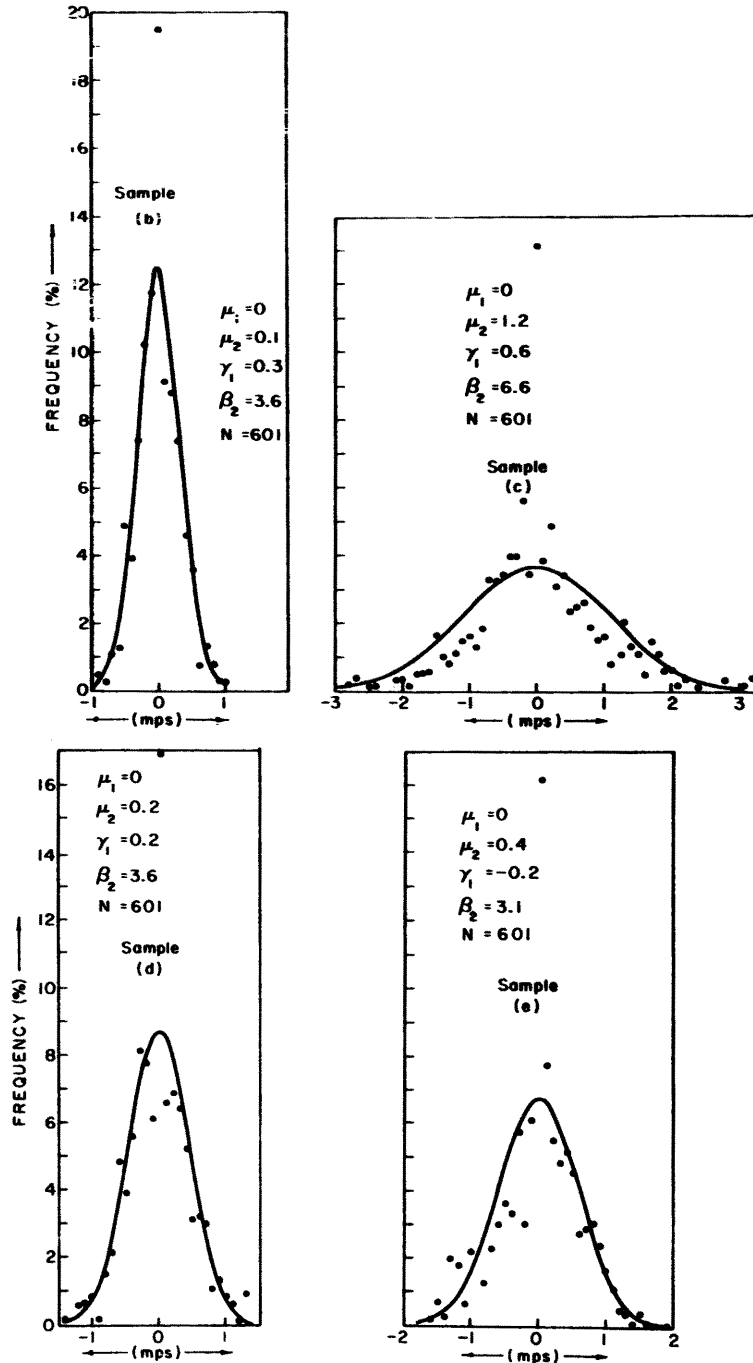


FIGURE 20. Same as figure 11, but for Case 2.

(a) In figure 19 there is a remarkable similarity in the shapes of the energy spectra at scales less than 850 m despite the large changes in total variance from sample to sample. The rotor corresponds with sample (c). All spectra show a hump near scales of 700 m and decrease sharply to scales of 150 to 200 m. A slope of $-5/3$ is realized approximately at scales smaller than 85 m. This behavior is contrary to that of the entire sample (figure 17). The average slope of the latter spectrum remains approximately $-5/3$ to scales greater than 200 m.

(b) In figure 20 there is a marked decrease in the degree of intermittency (in terms of β_2) when individual samples are selected. Both up- and downstream of the rotor, β_2 approaches the Gaussian value of three. The sample which includes the rotor (sample (c)) has the greatest deviation from normal. Similar behavior was observed in Case 1 (figure 11).

(c) There is a tendency for the actual frequency distributions in samples (d) and (e) to fluctuate radically about the normal distribution curve. For example, sample (d) tends to have two secondary peaks near ± 0.2 mps and a large probability of smaller magnitudes. The cause of this behavior is not known.

(d) As opposed to Case 1, there is a tendency for significant skewness to be present in all subsamples. The statistical model of intermittency does not account for this behavior, although it has been observed at smaller scales (Gibson et al., 1970; Stewart et al., 1970).

Table 4 contains tabulations of the pertinent statistical parameters for the longitudinal gust velocities for each sample of Case 2.

Sample	Sample Size N	Mean μ_1	Variance μ_2	Skewness γ_1	Kurtosis β_2
(a)	3760	$6.84 \cdot 10^{-4}$	$3.72 \cdot 10^{-1}$	$3.02 \cdot 10^{-1}$	15.07
(b)	601	$-7.97 \cdot 10^{-3}$	$1.02 \cdot 10^{-1}$	$2.83 \cdot 10^{-1}$	3.60
(c)	601	$5.45 \cdot 10^{-2}$	1.21	$6.03 \cdot 10^{-1}$	6.61
(d)	601	$1.04 \cdot 10^{-3}$	$2.09 \cdot 10^{-1}$	$2.23 \cdot 10^{-1}$	3.57
(e)	601	$3.02 \cdot 10^{-5}$	$3.56 \cdot 10^{-1}$	$-2.12 \cdot 10^{-1}$	3.13

TABLE 4. Summary of statistical parameters for all samples of Case 2.

The instantaneous mean kinetic energy of the longitudinal gust component $\left(\frac{u'^2}{2}\right)$ is shown in figure 21. The energy at the central peak (a rotor) exceeds that of the rest of CAT record by an order of magnitude or more. Minor energy peaks occur near 0949.75 MST and near 0956 MST.

Terms (1), (5), and (9) of equation (51) were the only terms which could be computed for Case 2. They are shown in the lower portion of figure 21. The behavior of the terms along the aircraft track bears a general resemblance to Case 1 (figure 12), however, there are important exceptions.

Term (1), the advection of the energy of the longitudinal gust component by the mean wind, displays a large sinusoidal fluctuation in the vicinity of the maximum energy peak (a rotor), and smaller oscillations near the less intense bursts. The loss of energy due to the advection of less turbulent air into the rotor exceeds the energy gain due to the advection out of the rotor, on the downstream side. Similar behavior was noted in Case 1 (figure 12), however, the asymmetry of the advection

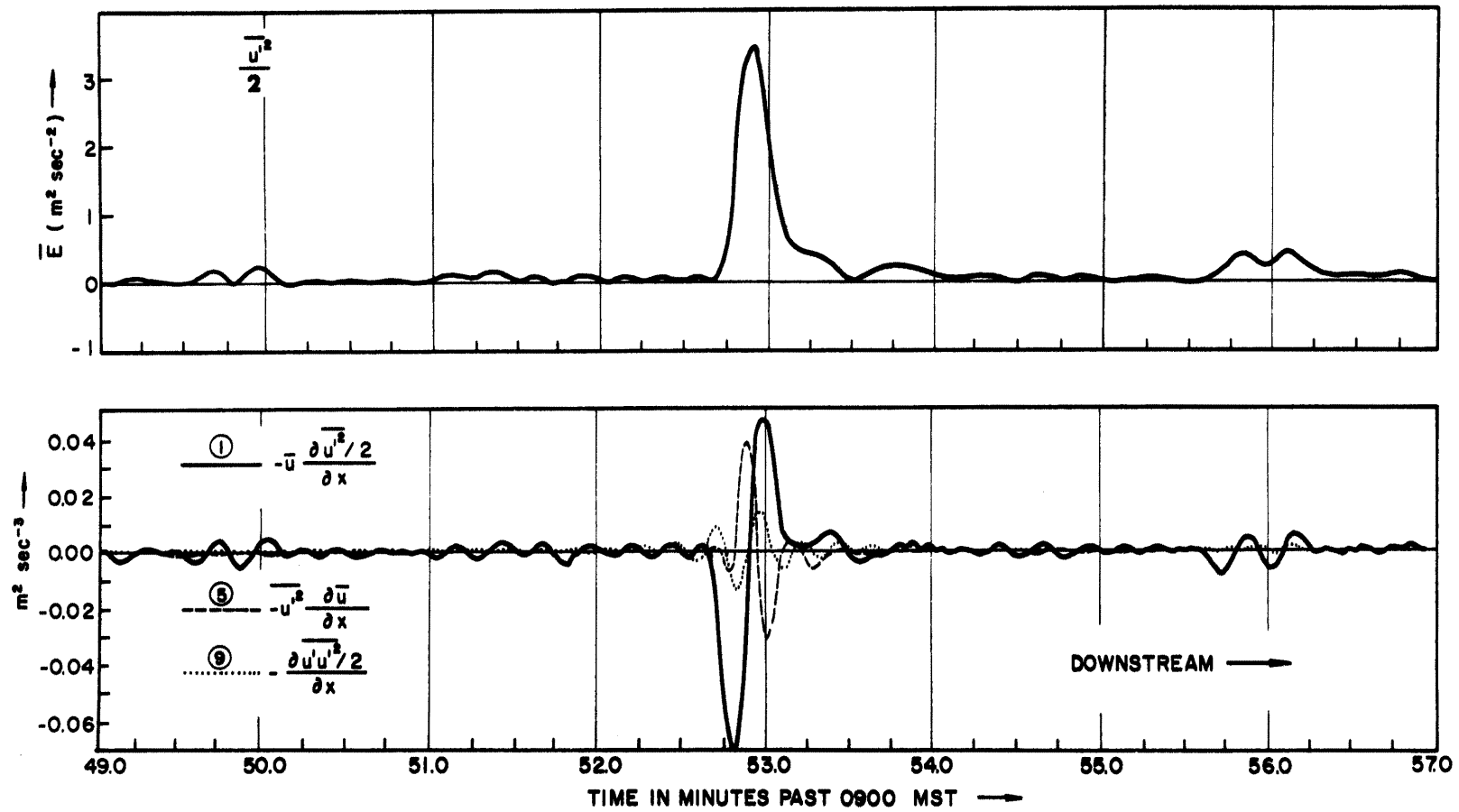


FIGURE 21. Same as figure 12, but for Case 2.

term was more pronounced. The cause of the asymmetry in the present case is found in the record of \bar{u} (figure 16) and in the streamwise variation of $\frac{\overline{u'^2}}{2}$ (figure 21) immediately downstream of the energy peak. The mean wind component reaches a minimum in that region. Furthermore, the magnitude of the energy decrease in the same area is less than the magnitude of the increase on the upwind side of the burst.

Term (5) (figure 21), which represents energy changes due to energy redistribution by convergence of the mean wind, displays maxima and minima which are slightly less than in Case 1 near the location of the largest turbulent burst. The records of \bar{u} (figure 16) and $\frac{\overline{u'^2}}{2}$ (figure 21) may also be utilized to explain the behavior of term (5). The relatively large positive maxima derives its magnitude from the presence of large turbulent kinetic energy in a region where the mean velocity along the aircraft track is decreasing downstream (convergence), while the reverse is true for the magnitude of the negative maximum. Magnitudes of the divergence of the mean u component are as large in the present case as in Case 1 ($5 \cdot 10^{-3} \text{sec}^{-1}$ and greater), however, the intensity of the turbulence is less, thus accounting for the lower magnitude of term (5).

The flux divergence, term (9), is very similar to Case 1. Inspection of figure 21 reveals confined regions of flux convergence and divergence in the immediate area of the rotor. Furthermore, as in Case 1, the maximum values attained by term (9) are smaller than the maxima of terms (1) and (5) by a factor of one-half or less.

The physical mechanisms behind the intermittency of the CAT record appear to be very similar to Case 1. Evidently the flight path in the present case intersected the upper part of a rotor in the major burst. The lower turbulence intensity, as compared with Case 1, is due to either

a smaller degree to static instability of the overturned air or to the location of the flight path in the extreme upper part of the rotor. Evidence for the latter possibility is found in figure 16. At no point does the mean velocity component along the track of the aircraft approach zero as in Case 1 (figure 7). The minor turbulence burst located upstream of the major occurrence appears to be due to flight over the top of another rotor according to pilot and observers logs, while downstream, the turbulence appears to be due to a series of short wave-like perturbations (figure 16, sample (c)).

Case 3

Synoptic conditions for Case 3 are shown in figure 22. At the surface, a west-east gradient in sea level pressure is present across the Continental Divide, while westerly winds of 15-20 mps are found at 500 mb. Soundings taken at 0200 MST at Kremmling and 0500 MST at Denver are shown in figure 23. An indication of the descent of air in the lee of the mountains appears as a difference in the temperature profiles between the two stations. A weak inversion, just below 500 mb ($\theta \approx 315^\circ \text{K}$), in the Kremmling sounding is found to be more intense and at a lower level (~630 mb) in the Denver sounding farther downstream. An outstanding feature of wind regimes (figure 23) is the narrow layer of intense winds near 650 mb at Denver. Strong vertical shears are found both above and below that level.

CAT data were gathered by the NCAR de Havilland Buffalo. The aircraft, after completing a series of flight legs through the lee wave system at higher levels, descended to approximately 4 km (MSL) near the Denver VOR. Beginning at 1014 MST, it flew straight and level on a

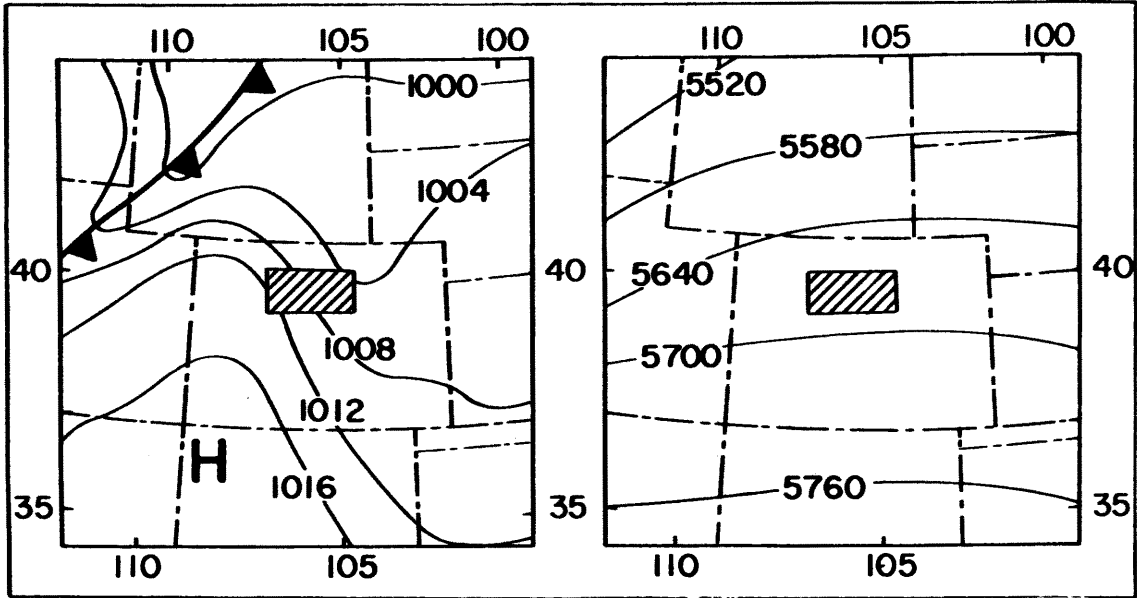


FIGURE 22. 0800 MST surface analysis (left) and 0500 MST 500 MB analysis (right) for February 17, 1970.

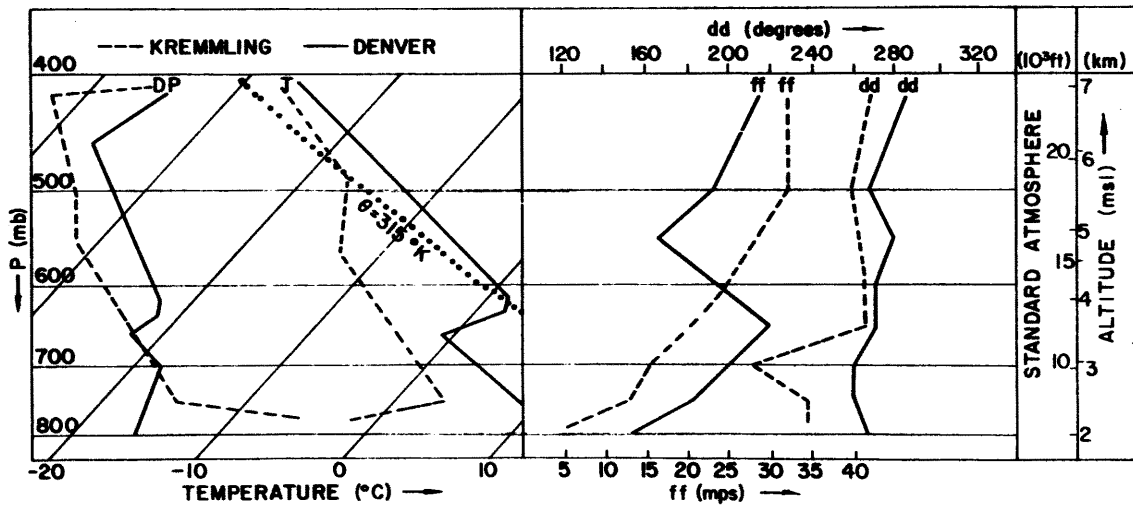


FIGURE 23. Kremmling (0200 MST) and Denver (0500 MST) soundings for February 17, 1970. See figure 3 for location of sounding stations.

westerly heading for approximately 15 minutes (figure 3). During this period, the CAT intensity, as reported by the pilot, increased from very light to severe. Just beyond the point at which the maximum gusts were experienced, the aircraft turned 180° and descended.

Figure 24 shows the flight path of the aircraft during the upwind portion of the flight and the cross section analysis of the potential temperature field. Turbulence reports collected on other flight legs are included. Recalling the previous discussion of the temperature and wind profiles (figure 23) it is apparent that the aircraft is near the top of a strong inversion where the vertical wind shear is large. The disturbed nature of the isentropes in the lee of the mountains (figure 24) suggests that one of the causes of the general increase of CAT intensity along the flight path was the penetration of the aircraft deeper into the shear layer as it proceeded westward.

The mean and turbulent wind components are shown in figure 25. The behavior of \bar{u} and \bar{w} , the mean wind component along the aircraft track, and the mean vertical component, respectively, indicates the presence of mesoscale lee waves of about 12 km in length near the western (right) half of the record. Both shorter and longer wave lengths appear and it is apparent that the cross section analysis (figure 24) of potential temperature reflects only the longest wave. In terms of the shearing layer which was discussed earlier, the general trend of \bar{u} along the flight path also suggests that the aircraft penetrated a region of strong vertical shears.

Unlike the first two cases, the turbulent components (u' , v' and w' , figure 25) show an increase in turbulence intensity throughout the flight. The largest fluctuations occur in the u' component. Visual

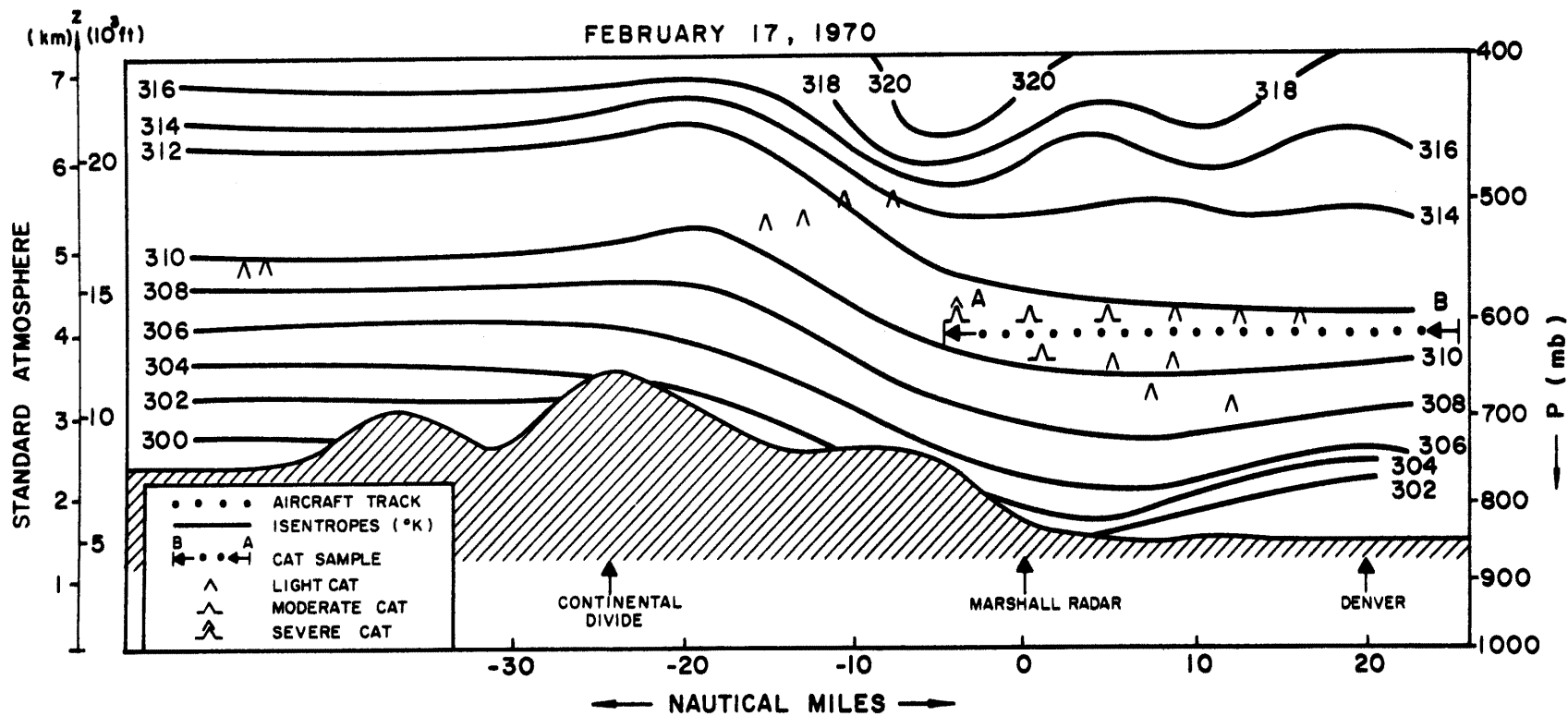


FIGURE 24. Same as figure 6, but for Case 3. The cross section is based on a preliminary analysis by D. K. Lilly of NCAR.

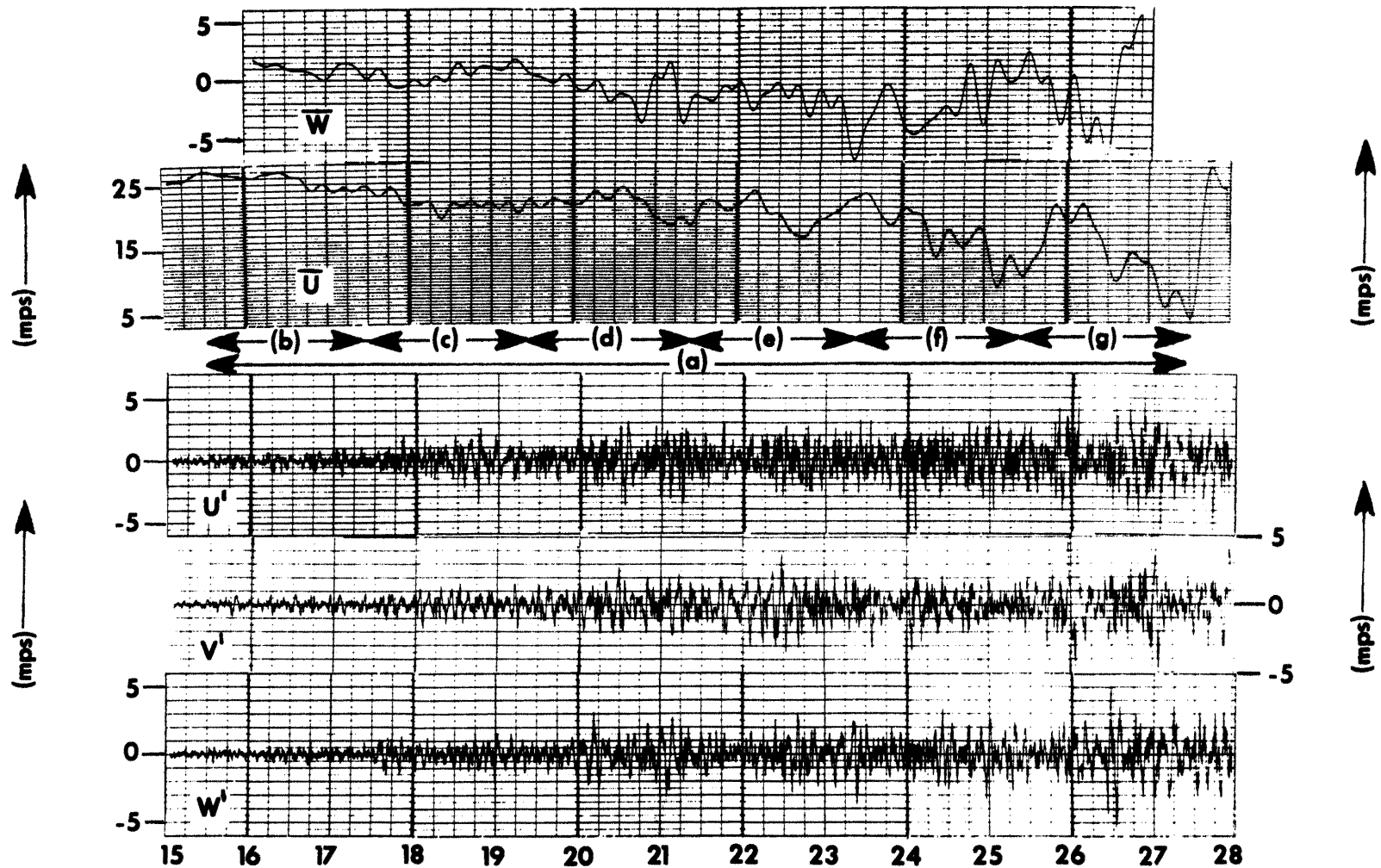


FIGURE 25. Filtered velocity components along the aircraft track for Case 3. \bar{w} record has been truncated at the first and last points at which energy budget calculations could be made. Time axes of the diagrams are identical. Abscissa is labeled in time in minutes past 1000 MST.

inspection of the figures reveals that several bursts occur in the record (e.g., near 1022.5, 1026.0, and 1027.0 MST in figure 25), however, none of these is as well defined as in the rotor cases. The total sample, (a), and subsamples, (b) - (g), are shown in figure 25.

The spectrum analyses of the velocity components for sample (a) are presented in figure 26. A feature which is immediately obvious from the spectra is that while the u-component spectrum shows only minor deviations from a slope near $-5/3$ (double logarithmic plot), the v- and w-component spectra fall off steeply at scales less than about 500 m. At the time of this writing, the specific cause of this behavior is not known, although it is suspected that boom flexing may have caused a contamination of the data. Spectrum analyses of the raw data indicated not only a continuation of the rapid decrease of spectral densities in the v and w spectra to frequencies of 2 Hz (~50 m) but also the presence of large noise spikes at 4 Hz (~25 m) and 8 Hz (~12.5 m). In order to overcome this problem, at least partially, the v and w data were subjected to low pass filtering at 2 Hz, to eliminate the large data spikes.

An estimate of the loss of energy in specific frequency bands can be made by utilizing the u-component spectrum as a reference, since it is apparently uncontaminated. It is assumed that the v and w spectra are uncontaminated at frequencies below 0.2 Hz (scales >500 m) and that energy in the frequency band 0.1 to 0.2 Hz bears the same proportion to the true energy in the band 0.2-4 Hz in the v and w spectra as in the u spectra. Integrations show that approximately 56.5 per cent of the total energy in the frequency band 0.2-4 Hz has been lost in the v and w spectra. For the band 0.1-4 Hz, the loss amounts to 31.5 per cent, which

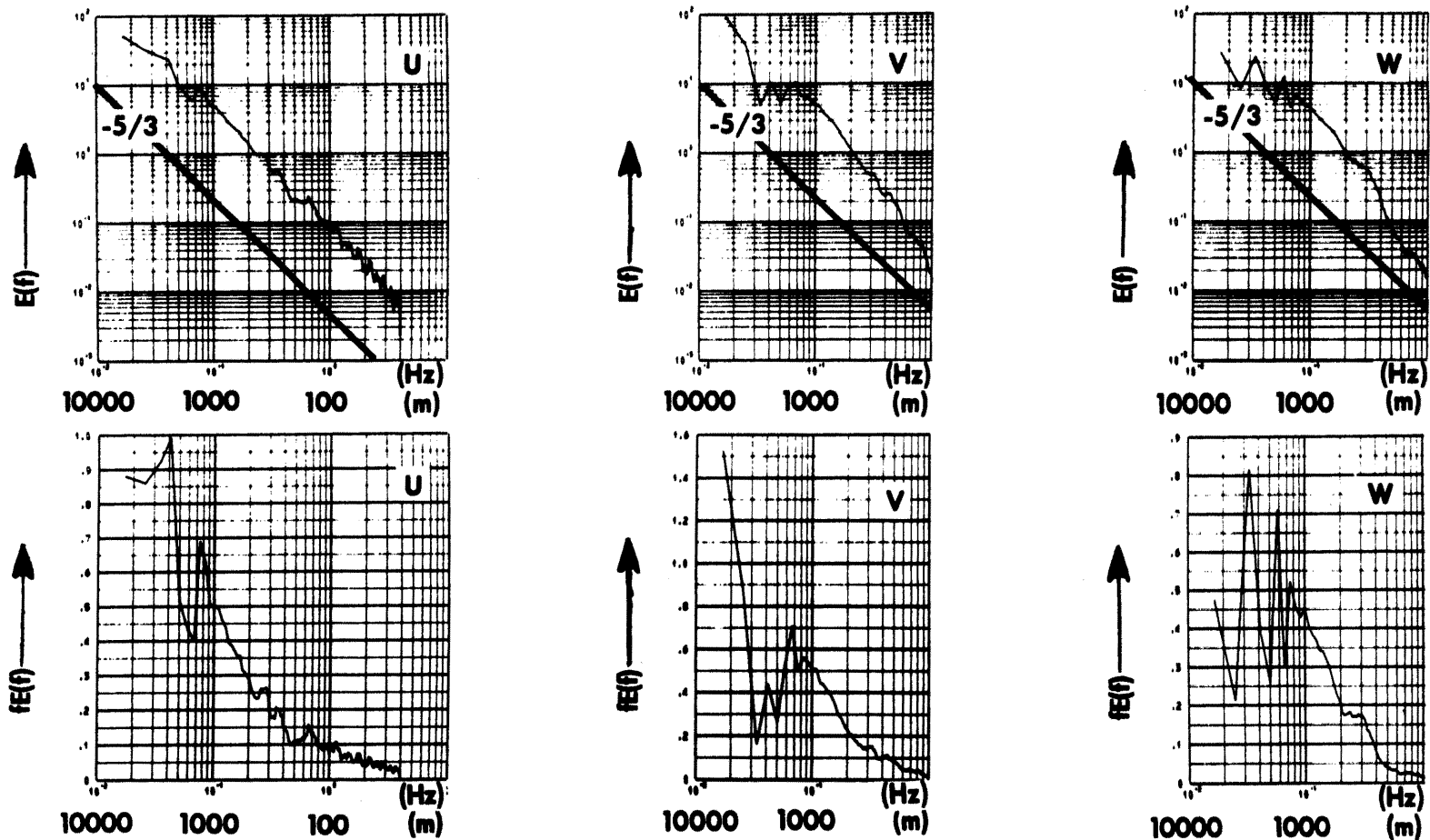


FIGURE 26. u, v and w energy spectra for sample (a) in figure 25. Spectra were determined by averaging raw estimates from 6 two-minute subsamples. The procedure is explained in Chapter IV. Upper diagrams show spectra in logarithmic plots, lower diagrams show the same spectra plotted with area proportional to energy.

is the approximate difference in variance between the u' and the v' and w' component variances (i.e., $\mu_2 = 1.1 \text{ m}^2\text{sec}^{-2}$ for u' and $0.7 \text{ m}^2\text{sec}^{-2}$ for v' and w').

Because of the problem discussed above, only the u' component will be considered in the discussion of the statistical aspects of intermittency. However, v and w components will be utilized in the computation of terms of the energy budget. The argument for their inclusion in the latter computation is that nearly half the turbulent energy lies in the uncontaminated portion of spectra, that is, from 0.1 Hz (the cutoff frequency) to 0.2 Hz, and that the partial loss is confined to higher frequencies. For the purposes of demonstrating the energy budget approach, the loss of energy is not critical. The effect of the energy deficit on various terms of the energy equation will be discussed in more detail in a later section.

Returning to the discussion of the statistical aspects of the entire sample, figure 26 shows that the u -component spectrum, averaged over the six subsamples, (b) - (g) (figure 25), has an average slope very close to $-5/3$ over the frequency range 0.08 to 4 Hz ($\sim 1250 \text{ m}$ to 25 m). The spectral plot with area proportional to energy (figure 26) reveals apparent spectral gaps near 0.06 Hz ($\sim 1.7 \text{ km}$) and near 0.5 Hz ($\sim 200 \text{ m}$). The selection of 0.1 Hz ($\sim 1 \text{ km}$) for the separation of scales was necessary for the following reasons: (a) the energy loss due to the problem described earlier occurs in the highest frequencies. Thus, the selection of a cutoff frequency near 0.5 Hz would result in v' and w' records with a much greater deficit in energy relative to the u' energy; (b) a sharp cutoff at low frequencies requires a large number of weights; the result is that more data would be lost from the end of the record where the most

intense turbulence occurs. In order to check the effects of filter cut-off frequency on the intermittency statistics of the u' component, data were filtered near 0.06 Hz, using 1001 weights; however, the filter cut-off was poor in comparison to the one utilized in the present analysis. The results of the experiment are given in Appendix D; (c) the selection of a cutoff near 0.1 Hz allows a comparison of the results of the first two studies with the present study.

A major feature of the frequency distribution for the total sample (figure 27) is the relatively small value of β_2 (5.5) for the u' component as compared to Case 1 ($\beta_2 = 26.6$) and Case 2 ($\beta_2 = 15.1$). The actual frequency distribution appears to be much closer to normal than in the rotor cases. Application of the Kolmogorov-Smirnov test (e.g., see Essenwanger, 1970) indicates that the actual distribution of u' for the entire sample is significantly different from the normal distribution at the 99 per cent level.

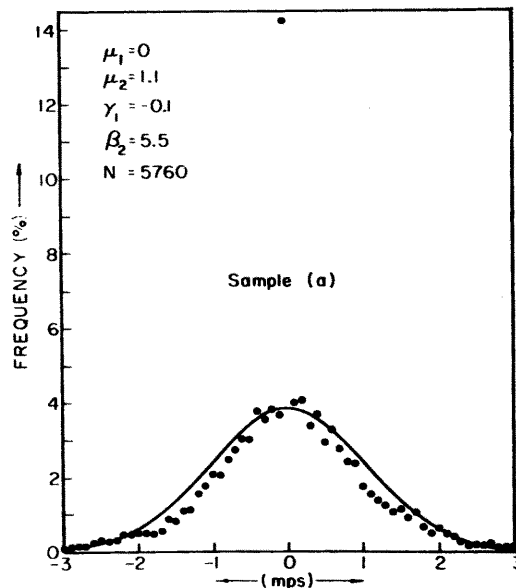


FIGURE 27. Same as figure 9, but for Case 3.

The statistical analyses of individual subsamples are shown in figures 28 and 29. Subsamples (c), (e), and (g) were selected as representative of the six original subsamples. The main features of interest are:

(a) In figure 28 there is an overall increase in spectral densities from sample (c) through (g).

(b) Energies decrease more rapidly at lower frequencies as one proceeds downstream from the region of maximum turbulence (sample (g)). This behavior is illustrated by the flat spectral slopes near 0.2 Hz (~500 m) in the spectra of sample (e). The up- and downstream spectra (samples (c) and (g), respectively) show steeper mean slopes ($\approx -5/3$) in this region.

(c) All spectra have slopes of approximately $-5/3$ in the high frequency range.

(d) In figure 29, all frequency distributions are characterized by kurtosis values near 3 (the Gaussian value). However, the histograms show a tendency for probabilities of values within ± 0.05 mps to greatly exceed the Gaussian probabilities while values slightly greater than ± 0.05 mps have a smaller-than-normal probability. Application of the Kolmogorov-Smirnov test to the most turbulent sample (g) ($\beta_2 \approx 3.9$) indicates that the sample distribution is significantly different from normal at the 99 per cent level. The maximum deviation of the actual cumulative frequency distribution from the normal is due to the large number of small values in the filtered data. The cause of this behavior is not known.

A tabular summary of statistical parameters for longitudinal gust velocities of samples (a) - (g) is presented in table 5.

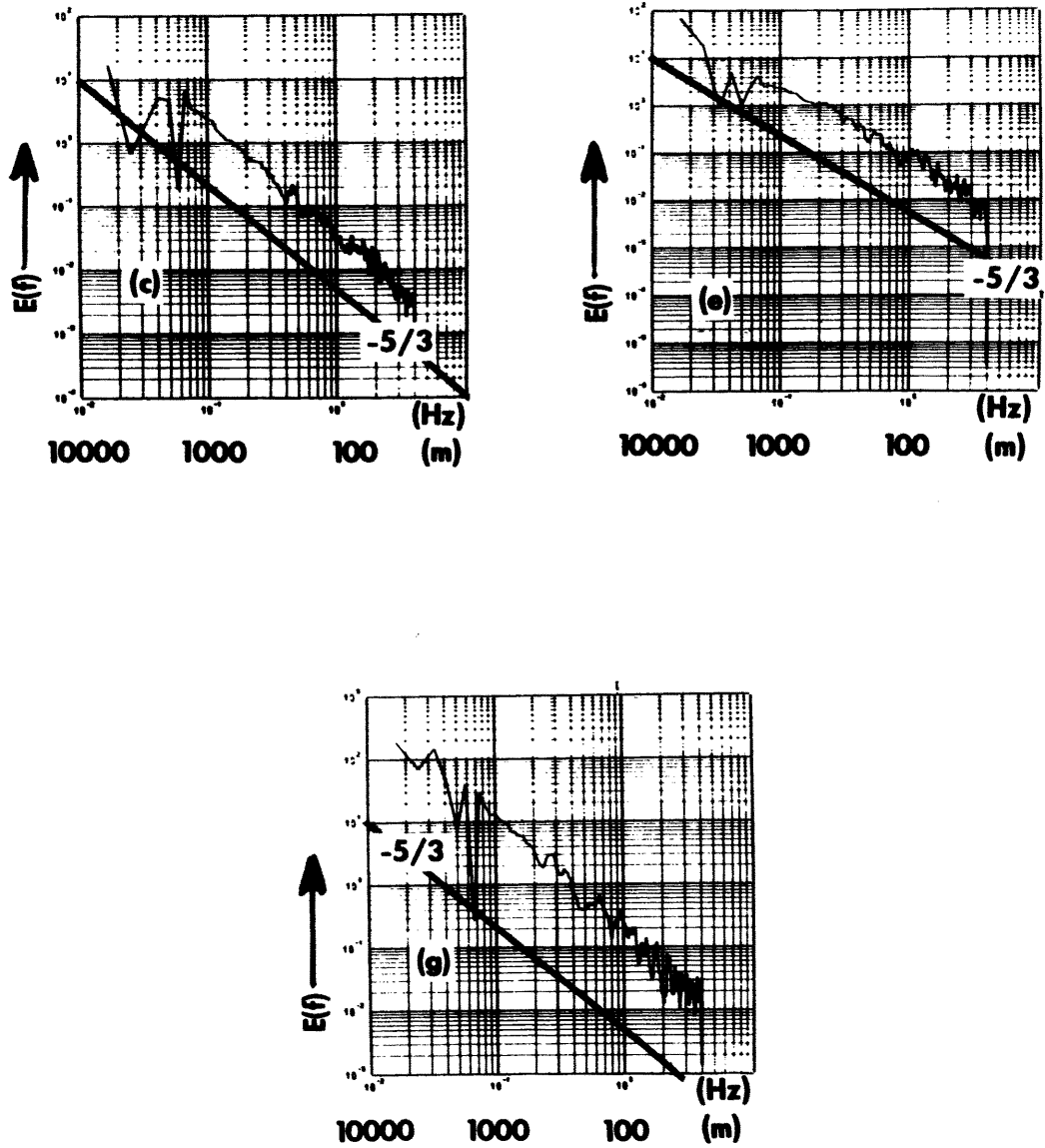


FIGURE 28. Same as figure 10, but for selected subsamples from Case 3.

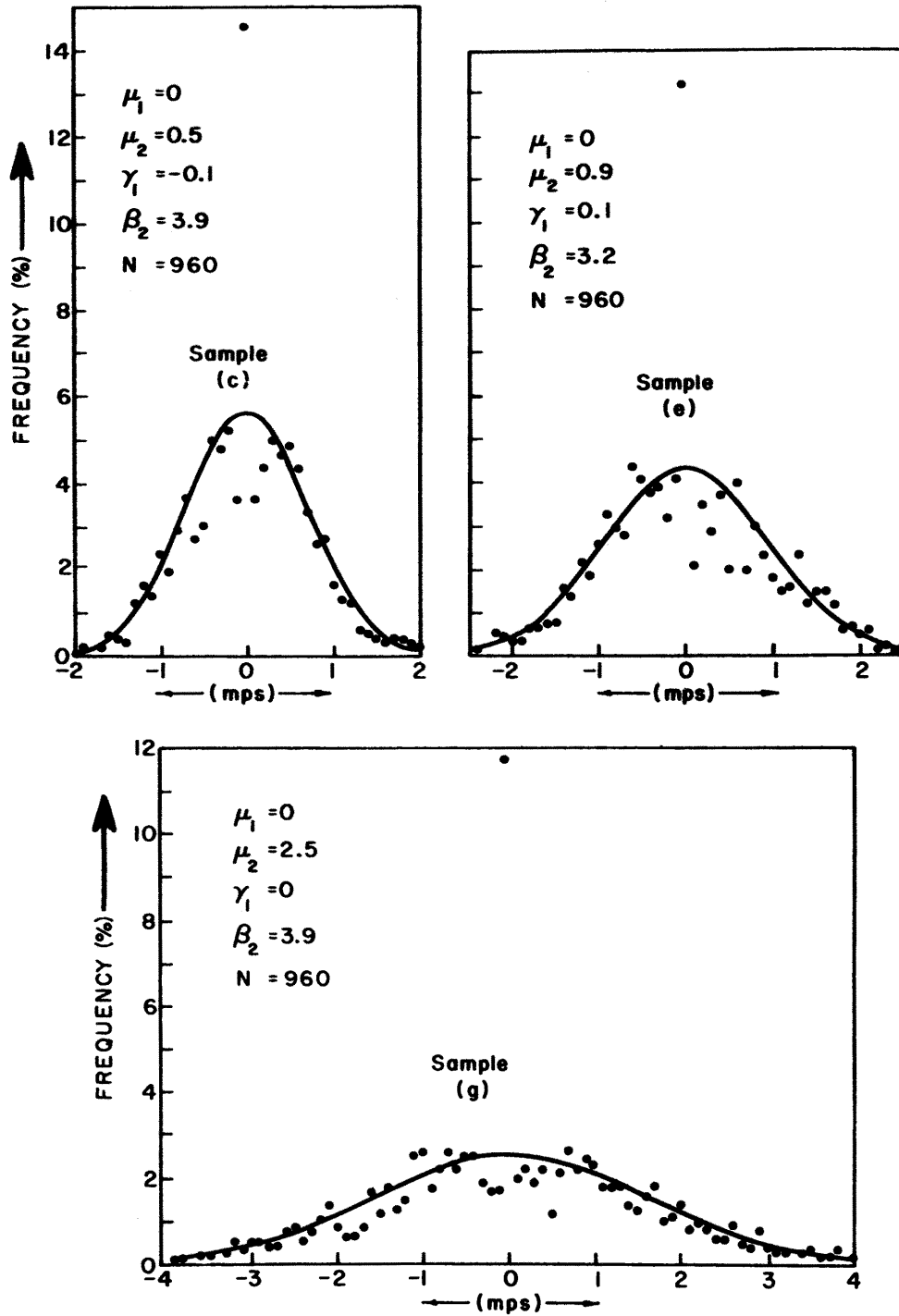


FIGURE 29. Same as figure 9, but for selected subsamples from Case 3.

Sample	Sample Size N	Mean μ_1	Variance μ_2	Skewness γ_1	Kurtosis β_2
(a)	5760	$3.25 \cdot 10^{-4}$	1.09	$-8.62 \cdot 10^{-2}$	5.51
(b)	960	$-4.03 \cdot 10^{-3}$	$8.78 \cdot 10^{-2}$	$-1.52 \cdot 10^{-1}$	4.33
(c)	960	$4.59 \cdot 10^{-3}$	$4.98 \cdot 10^{-1}$	$-8.85 \cdot 10^{-2}$	3.86
(d)	960	$1.23 \cdot 10^{-3}$	$9.42 \cdot 10^{-1}$	$-2.70 \cdot 10^{-1}$	4.10
(e)	960	$-1.26 \cdot 10^{-3}$	$8.69 \cdot 10^{-1}$	$1.41 \cdot 10^{-1}$	3.24
(f)	960	$4.90 \cdot 10^{-3}$	1.20	$-2.98 \cdot 10^{-1}$	4.04
(g)	960	$1.23 \cdot 10^{-2}$	2.52	$8.15 \cdot 10^{-3}$	3.89

TABLE 5. Summary of statistical parameters for all samples of Case 3.

At the present stage of the analysis of Case 3 the following facts are known about the turbulence encounter:

- (a) The mesoscale environment is a lee wave system.
- (b) The CAT occurs in a layer of strong vertical shear (on the order of 10^{-2}sec^{-1} when measured over a 1 km layer).
- (c) The gradient Richardson number, Ri (derived from mesoscale analysis of the aircraft data), is of the order of 0.7.
- (d) The turbulence recorded along the aircraft path increases in intensity to a maximum at the western end of the track. One cause of the increase was found in the sloping character of the shear layer, that is, the aircraft penetrated deeper into the region of strong shear as it flew westward.

Information similar to (a) - (d) has been derived from previous CAT investigations when mesoscale data were available. Turbulence in a region of strong vertical shears is not unexpected, but it is not well

understood. None of the desired information about the small scale characteristics of the turbulence can be determined from the mesoscale analyses alone.

Spectrum analysis of the entire u record (figure 26) has added two more, but still not unusual, facts about the frequency distribution of energy, i.e.,

(e) The average spectral slope in the logarithmic plot is close to $-5/3$ and

(f) A large and rather isolated energy spike (figure 26) is present at scales slightly larger than 1 km.

Fact (e) has lead many investigators to the universal equilibrium theory for a physical explanation of the turbulence mechanisms.

Fact (f) suggests that a predominant wave mode ($\lambda = 1.3$ km) is present.

At this point, the majority of CAT investigations conducted in the past have terminated. The frequent conclusion is that short, unstable waves are breaking down into isotropic turbulence. Although this statement may be true, the question remains: where and how do the instabilities occur? That the entire layer does not break down simultaneously, despite the strong mean shears, first becomes apparent in the frequency distribution of the turbulent gusts (figure 27). The non-Gaussian character suggests that the variance of the gusts is not uniform along the flight path. By breaking the record up into sections, the non-homogeneity is emphasized in the tendency for the smaller samples to approach normal distributions, but with different variances (figure 29). Distributions of energy with frequency (figure 28) also reflect the inhomogenities of the

record in the variations of energy densities among the subsample spectra. Thus, the inclusion of only a few more statistical analyses has revealed additional information about the turbulence encounter, i.e.,

(g) The record has been shown, quantitatively, to be statistically intermittent (e.g., for u' , $\beta_2 = 5.5$)

It is emphasized that this is only a statistical suggestion and one must turn to other aspects (e.g., the energetics) of the data to isolate the physics of the intermittent CAT. The distribution of the mean kinetic energy (total of the three components) is shown in figure 30. The inhomogenieties of the record are better defined by the mean kinetic energy distribution rather than the individual gust records (figure 25). Whereas the

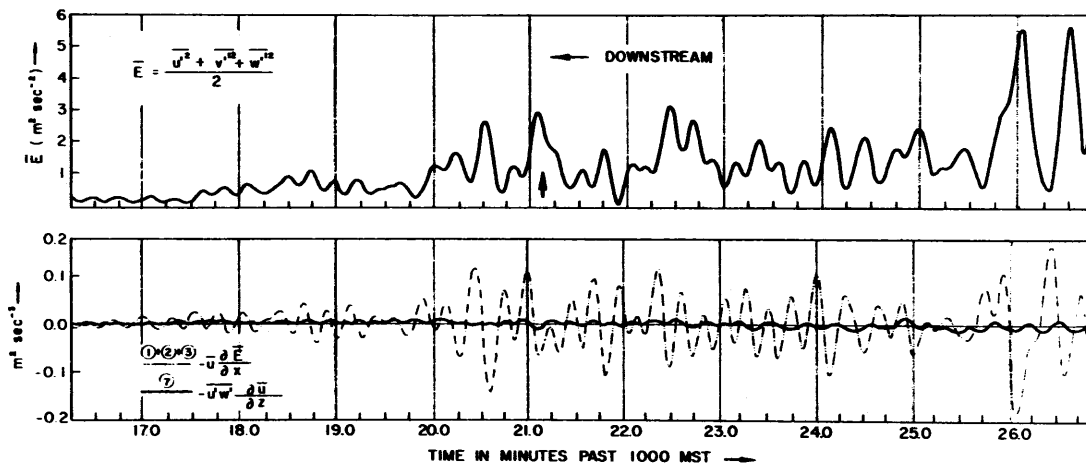


FIGURE 30. Top: distribution of total turbulent kinetic energy along the aircraft track for Case 3. Bottom: distributions of terms $\textcircled{1} + \textcircled{2} + \textcircled{3}$ and $\textcircled{7}$ of equation (51). Time axes are identical on both diagrams.

pilot and observer logs gave the impression of gradually increasing turbulence intensity along the flight path, figure 30 shows that the major turbulence occurred in bursts which were distributed irregularly along the track. The vertical-pointing arrow near 1021 MST in figure 30 indicates a portion of the record which will be discussed in greater detail later in the paper.

The lower portion of figure 30 illustrates the distributions of the advection term $(\textcircled{1}) + (\textcircled{2}) + (\textcircled{3})$ in equation (51)) and the shear production term $(\textcircled{7})$ along the track of the aircraft. Because the horizontal advection of turbulent energy by the mean wind has maxima and minima which are nearly an order of magnitude larger than the extreme values of the remaining terms, the latter are presented on an expanded scale in figure 31. Identification of each term is provided in the legends of figures 30 and 31.

The oscillating nature of the distributions of the terms reflects the intermittent nature of the turbulence. Relatively speaking, apart from the dominance of the horizontal advection, the feeding of energy due to turbulence in the presence of vertical shears (term $(\textcircled{7})$) and the redistribution of energy due to convergence of the mean wind along the flight path (term $(\textcircled{5})$) appear to be important. Term $(\textcircled{9}) + (\textcircled{10}) + (\textcircled{11})$, the flux divergence of turbulent energy, reaches magnitudes commensurate with terms $(\textcircled{5})$ and $(\textcircled{7})$ only near the upstream end of the track where the turbulence reaches its greatest intensity. The feeding of energy due to horizontal shears of the mean vertical component of velocity (term $(\textcircled{6})$) attains relatively large magnitudes only at a few isolated points along the track (i. e., near 1021, 1025, and 1026.5 MST). With respect to the

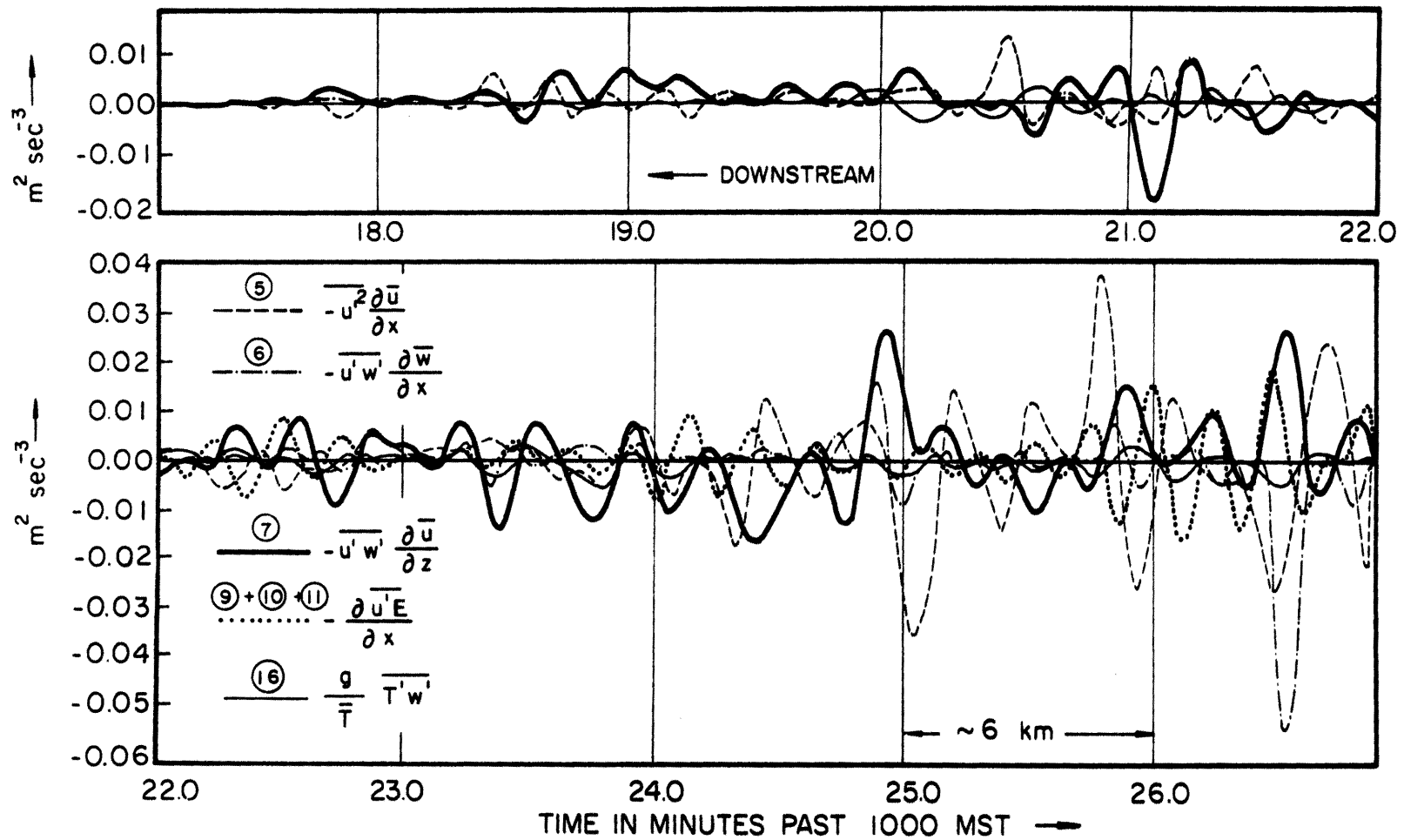


FIGURE 31. Distributions of several terms of equation (51) for Case 3. See inset for identification of curves.

discussions of Cases 1 and 2, such behavior may be indicative of the presence of strong turbulence in a wave of large amplitude. The buoyancy term, (16), displays small positive and negative oscillations throughout the entire record, suggesting that the environmental stability is close to neutral (also see figure 23 and 24).

A parameter which has been applied frequently in the study of CAT is the gradient Richardson number (Ri) which is a ratio between the buoyant damping forces and the shear production of energy. The Richardson number has been shown to have a critical value of 0.25; That is, when $Ri < 0.25$, the turbulence intensity will increase and when $Ri > 0.25$, the turbulence intensity will decrease (Taylor, 1931). Ri is related to R_f , the flux Richardson number (equation (43)), through the exchange coefficients for heat (K_H) and momentum (K_M), i. e., $R_f = \frac{K_H}{K_M} \cdot Ri$. R_f , as a function of distance along the aircraft track, is presented in figure 32. For plotting purposes, values of R_f greater than 5 were set equal to 5 and values less than -5 were set equal to -5. The sensitivity of R_f to zero crossings of $\overline{u'w'}$, which appears as a factor in the denominator of equation (53), is apparent in the many spikes which appear in the diagram. A major part (~ 75%) of the record, however, displays values of R_f between ± 1 .

The general behavior of the flux Richardson number is physically reasonable. As noted earlier, the CAT records (figure 25) are non-homogeneous. The existence of bursts of turbulence and relatively quiet regions suggests that the turbulence patches are in various stages of growth and decay. Thus, it would be expected that local

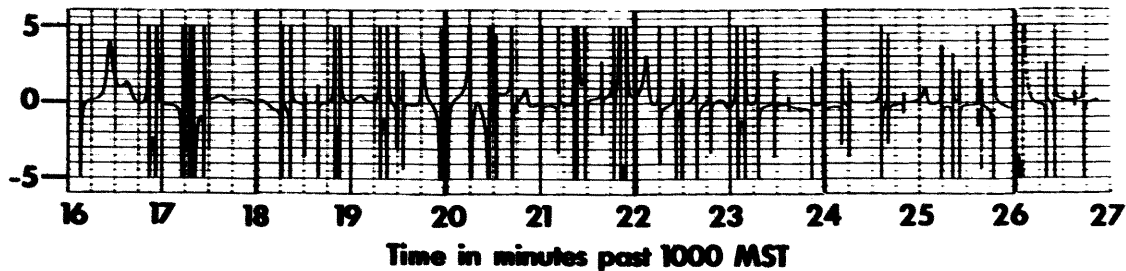


FIGURE 32. Distribution of the flux Richardson number (R_f) along the aircraft track for Case 3.

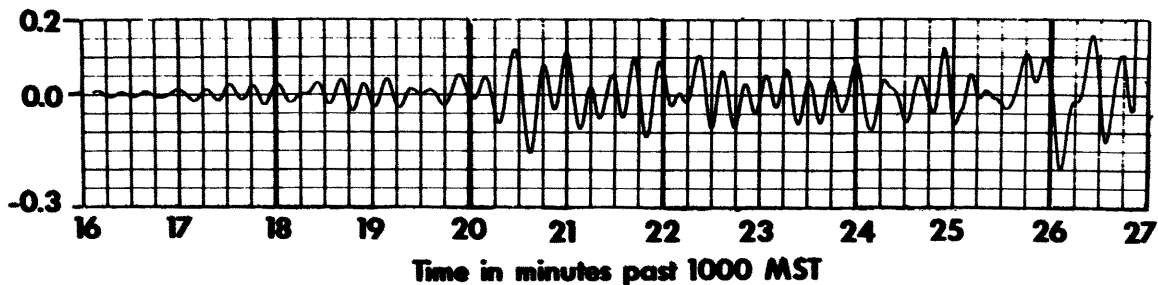


FIGURE 33. Distribution of the residual of computed terms of the energy budget not including interaction terms for Case 3.

Richardson numbers would reflect such small scale differences in the structure of the flow field. The use of the instantaneous Richardson number as a turbulence indicator is not valid since R_f was derived under the assumptions of stationary, horizontal homogeneity and with neglect of dissipation effects.

The summation of the energy budget terms presented thus far is shown in Figure 33. It is noted that the instantaneous budget is out of balance, primarily due to the large magnitude of the advection term, (1) + (2) + (3). The distribution of the residual roughly parallels the horizontal advection term (figure 30) and is of nearly equal magnitude.

Three interaction terms (18), (19), and (20) (equation (52)) were computed to determine the relative importance of the interactions

between the mean flow and the turbulent flow. All three terms behaved similarly in that magnitudes increased gradually with the intensity of the turbulence reaching maximum absolute values of the order of .02 to .03 $m^2 \text{ sec}^{-3}$ near 1025 and 1026.5 MST. The sum of the three interaction terms is given in figure 34.

The total residual of all nine terms appears in figure 35. Also, the computed energy budget terms were integrated in time to yield a budget over the entire flight track. The results are presented in Table 6. Dissipation for the integrated budget has been estimated by assuming that the $-5/3$ slope of the average spectrum of the u-component (figure 26) extends into the inertial subrange (Kolmogorov, 1941; Obukhov, 1941). It is observed in figure 31 and Table 6 that both the instantaneous budget and the total budget are in large imbalance. The reasons for this are found in the neglect of important terms, either

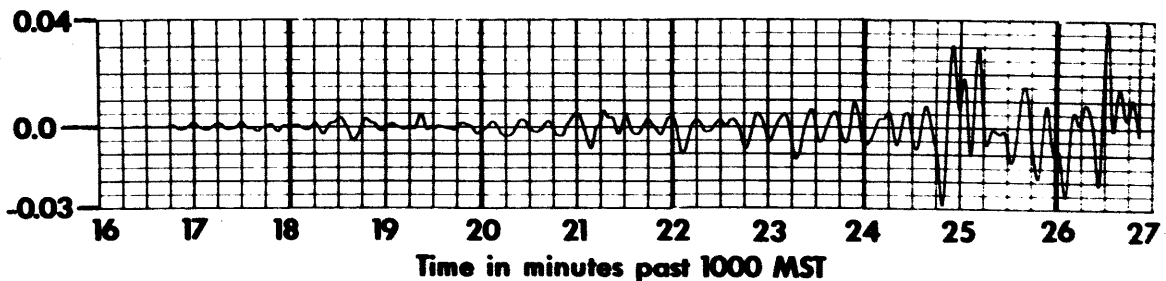


FIGURE 34. Distribution of the sum of the interaction terms, (18), (19) and (20) for Case 3.

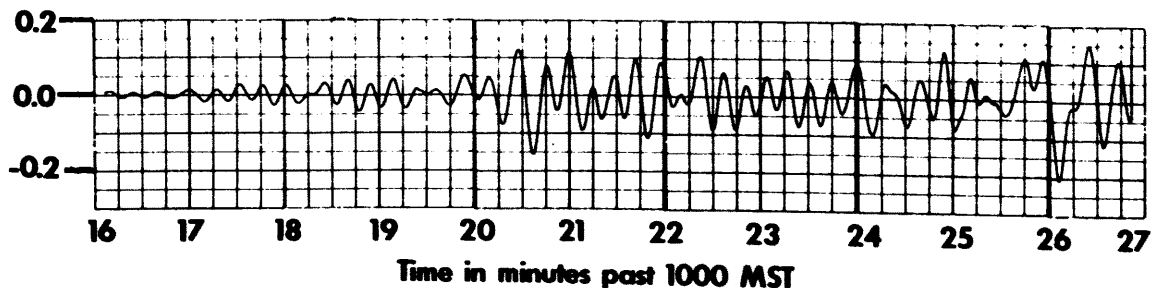


FIGURE 35. Distribution of the residual of computed terms of the energy budget including interaction terms, for Case 3.

TERM			TERM		
⑦	$-\overline{u'w'} \frac{\partial \bar{u}}{\partial z}$	+0.61	⑮	$-\overline{u' \bar{u}} \frac{\partial \bar{u}}{\partial x}$	+0.33
⑯	$-\frac{g}{T} \overline{w'T'}$	-0.43	⑰	$-\overline{\bar{u} w'} \frac{\partial \bar{u}}{\partial z}$	+0.16
⑰	$-\epsilon$	-4.85	⑳	$-\overline{u' \bar{w}} \frac{\partial \bar{w}}{\partial x}$	-0.08
FIRST RESIDUAL		-4.67	FINAL RESIDUAL		-3.13
① + ② + ③	$-\overline{u' \frac{\partial \bar{\epsilon}}{\partial x}}$	+1.70	$R_i = \frac{\frac{g}{\theta} \frac{\partial \theta}{\partial z}}{\left(\frac{\partial \bar{u}}{\partial z}\right)^2}$		0.72
⑤	$-\overline{u'^2} \frac{\partial \bar{u}}{\partial x}$	-0.35	$R_f = \frac{\frac{g}{T} \overline{w'T'}}{\overline{u'w'} \frac{\partial \bar{u}}{\partial z}}$		0.70
⑥	$-\overline{u'w'} \frac{\partial \bar{w}}{\partial x}$	-0.29			
⑨ + ⑩ + ⑪		+0.07			
SECOND RESIDUAL		-3.54			

TABLE 6. Integrated terms of partial energy budget for Case 3. Units are $10^{-3} \text{m}^2 \text{sec}^{-3} (10^{-3} \text{watts kg}^{-1})$. Circled numbers correspond with numbered terms in equation (51). See text for elaboration.

by assumption or simply because they could not be computed. A re-examination of the aircraft data indicate that the assumption, $\bar{v} = 0$, is not valid, especially toward the western end of the track. The mean wind component shifts from a direction approximately parallel to the aircraft path, at the start, to an angle of about 45° (southwest) at the end. This behavior indicates that the energy change due to advection by the mean wind is probably in error in the region of maximum turbulence. Furthermore, the vertical shear of \bar{v} increases by an order of magnitude (10^{-3} to 10^{-2} sec^{-1}) over the length of the track. Thus, again in the region of maximum turbulence, the energy production due to vertical shears is probably underestimated. The vertical flux terms may also be very important, since the lee waves are included in the mean flow and the aircraft is penetrating the turbulence region from above. Two data problems may also have contributed to the budget imbalance. Specifically, the mean vertical shears of \bar{u} were estimated over 1 km layers and at 1 minute (~ 6 km) intervals. This procedure obviously resulted in a severe smoothing of the actual shears along the flight path and casts some doubt on the reliability of the computations of the shear production term in the instantaneous budget. Although all the computed shears are positive, one would expect that the shear would be close to zero in strongly mixed regions, while in other areas it may be larger than computed and possibly of opposite sign. Also, the loss of a portion of the total energy in the v' and w' components due to previously-discussed problems has caused a reduction of approximately 20 per cent in the actual magnitude of the total energy. If the energy depletion is confined to scales of less than 500 m and affects only the amplitudes the v and w components, (i. e., the signs are preserved)

then it would be expected that one of the terms that is severely affected by the loss is the shear production term, (7).

Despite the imbalance, several important aspects of the nature of the turbulence are revealed when one considers individual terms of the energy budget. For example, the advection term ((1) + (2) + (3)) is relatively important, both locally (the instantaneous budget) and overall (the integrated budget). The latter behavior is explained by the large gradient in turbulent kinetic energy in the presence of a strong down-gradient, mean wind, along the flight path. The energy gains due to production by horizontal shears \bar{w} (term (6)) and the convergence of the mean wind along the aircraft path (term (5)) are of the same order of magnitude as the buoyant damping term. Although important at times locally, the flux divergence of turbulent kinetic energy term ((9) + (10) + (11)) appears to be relatively unimportant overall. The interaction terms may also be locally important (instantaneous budget). But only term (18), which may be interpreted as the horizontal advection of the mean flow kinetic energy by the turbulent, u' component, appears to have significant magnitude in the total budget. This is obviously due to the manner in which the budget was obtained and to the fact that u' was occasionally of the same order of magnitude as \bar{u} near the western end of the flight path.

Because of the small regions of large positive and negative flux Richardson numbers, R_f (table 6) was obtained from the ratio of the magnitudes of the integrated values of the buoyancy and (vertical) shear production terms. The value of R_f would have probably been smaller had the term, $-\frac{\overline{v'w'}}{\overline{v}} \frac{\partial \bar{v}}{\partial z}$, been included in the denominator.

The arrangement of terms in Table 6 allows a summary of the important points of the energy budget analysis. The "First Residual" indicates a sum of three of the terms commonly computed in the treatment of the turbulent energy budget near the surface of the earth (e. g. see Lumley and Panofsky, 1964). The "Second Residual" is a sum of the seven terms preceding. The overall importance of terms which arise when horizontal inhomogenities are present, is evident in the comparison of the first two residuals. The "Final Residual" is the sum of the preceding ten terms and is indicative of the role which the interactions play in the total budget.

It is difficult to make a direct comparison of the numerical values of the energy budget terms computed by Dutton (1969) with the terms of the integrated energy budget in Table 6. The filtered turbulence data from the former study include scales of motion which are approximately twice the size of the largest scales considered in Case 3. The effect of the inclusion of larger scales is evident in the magnitudes of total energies. In Dutton's (1969) study, the total energy was of the order of $10.0\text{m}^2 \text{ sec}^{-2}$, while in Case 3 it amounted to only $1.3\text{m}^2 \text{ sec}^{-2}$. Dutton's energy budget (over the entire aircraft track) nearly balances with the computation of only the shear production, buoyancy, and dissipation terms, whereas the same terms in the present case yield a large residual (First Residual in Table 6). Even with the inclusion of seven more terms, four of which are of the same magnitude as the buoyancy and shear production terms, the imbalance persists (Final Residual, Table 6). The major cause of the large residual, as mentioned earlier, is probably the inability to compute important energy production and redistribution terms in an environment which is disturbed

by mesoscale waves. Since Dutton was not able to specify mean flow parameters as a function of distance along the aircraft track, as in the present study, nothing is known about the details of the mesoscale structure in his investigation.

In Cases 1 and 2, the causes of the intermittency of the records were known before the analyses were accomplished (i. e., the CAT records were collected during flights through rotors). Knowledge of the primary turbulence mechanism allowed an interpretation of some of the more obvious aspects of the physics of the situation from the computation of a few terms of the energy budget. Similar information is not available for Case 3. However, the details of the filtered data (means and deviations) and of the partial energy budget have revealed some of the small scale features of the intermittent CAT which may be related to its causes. As an example, the turbulent burst indicated by the vertical arrow near 1021.1 MST in Figure 30 will be considered. The records of pertinent variables are given in figure 36 for the period 1020 - 1022 MST.

The \bar{w} record ((a) in figure 36) indicates that a large amplitude, short wave is present in the vicinity of a turbulent burst (figure 36 (d)). The wave length of the perturbation appears to be 4-5 km. However, this estimate must be interpreted with some caution since the aircraft may be intersecting the short wave at an angle. A schematic sketch of the wave is shown at the bottom of diagram (a). A longer wave ($\lambda \approx 12$ km) is evident in the mean temperature record, (b). Noting that the adiabatic expansions and contractions of the air, as it undulates through the lee waves, leads to cool crests and warm troughs, it is apparent that the mean streamline through the lee wave is 180

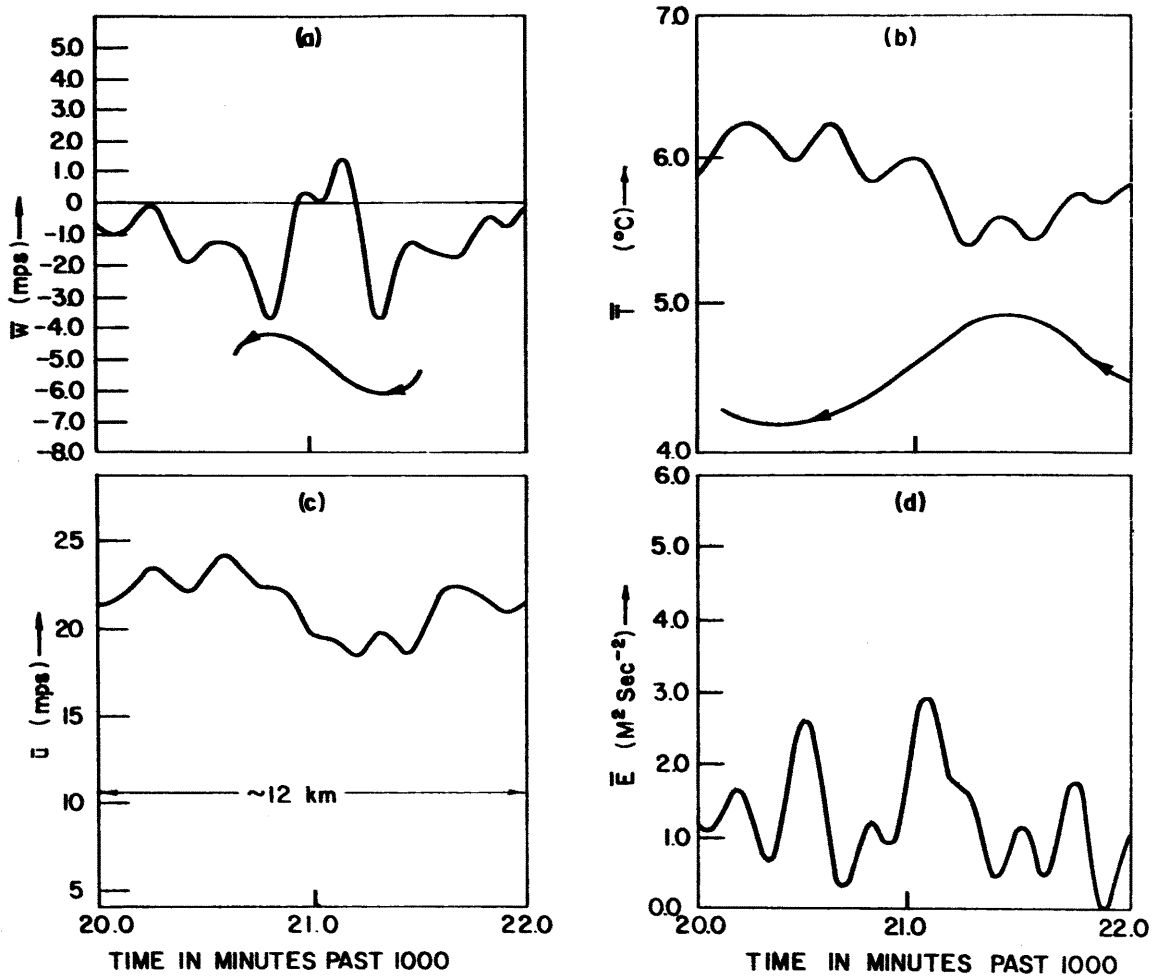


FIGURE 36. Distributions of \bar{w} (a), \bar{T} (b), \bar{u} (c) and \bar{E} (d) for the period 1020 to 1022 MST for Case 3. Schematic sketches of deduced wave forms are shown at the bottom of diagrams (a) and (b). See text for further elaboration.

degrees out of phase with the temperature trace. A sketch of the waveform is found at the bottom of diagram (b) in figure 36.

The picture which evolves from an inspection of the mean flow parameters is one of a short, unstable wave just downwind of the crest of a longer, lee wave. It is suspected that the wave is in the early stages of breaking since it is well-defined in the mean flow and there is a significant amount of turbulent energy present. Energy budget calculations (figure 31) support this hypothesis. Energy production due to horizontal shears in the \bar{w} field (term (6)) and the energy redistribution due to convergence of the mean wind along the flight path (term (5)) show relatively large contributions near 1021.25 MST. It is of interest to note that terms (5) and (6) coincide at 1021.25 MST. Such behavior was conjectured in Case 1 in connection with the rotor (equation (54)).

Immediately downstream of the energy spike at 1021 MST, a second spike of nearly equal magnitude is found at 1020.5 MST (diagram (d) in figure (36)). Inspection of the mean flow characteristics in figure 36 and the energy terms in figure 31 suggests that the instability which has lead to the second burst may be in the final, or dissipation stages. No well-defined perturbation is found near 1020.5 MST in \bar{w} record, despite the magnitude of the turbulent kinetic energy of the burst. The instability has possibly broken down completely and energy has cascaded down the spectrum to the smaller scales.

Although evidence appears to be sufficient to verify the existence of a large amplitude, short wave near 1021.1 MST ((a) in figure (36)), the conclusions with respect to the stage of development of that disturbance and of the one near 1020.5 MST are subject to conjecture.

Only a series of flights along the same track can reveal the time changes. Also, cross wind flights are necessary to define the three dimensional aspects of the shorter waves, such data were not available for Case 3. It has become obvious, however, that the analysis of aircraft data in the prescribed manner takes full advantage of details of the data by revealing the small scale characteristics of individual turbulent bursts. With sufficient planning and facilities, more information with respect to CAT mechanisms can be obtained. Recommendations with respect to the design of CAT experiments to accomplish this aim are presented in Chapter VI.

VI. SUMMARY, CONCLUSIONS AND RECOMMENDATIONS

Summary and Conclusions

An effort has been made to develop a methodology for treating CAT as an intermittent phenomenon. Since intermittency may best be interpreted as a statistical property which describes the variation of the intensity of fluctuations of a given variable within a record, it has been suggested that the probabilistic structure of CAT should be examined for quantitative indications of the degree of intermittency.

A statistical model proposed by Dutton (1968) has been generalized in the present study to provide several useful indicators of statistical intermittency in the amplitude domain. These include the probability density functions, the flatness factor, and the ratio of the mean deviation to the standard deviation. Computations of frequency distributions and statistical moments for actual CAT data have verified the predictions of the model with respect to the shape of the frequency distribution (leptokurtic) and the kurtosis (≥ 3), however, the model did not account for significant skewness which was observed in some cases.

The behavior of the intermittency indicators and the energy spectra are very sensitive to the manner in which samples are selected. Although the definition of a CAT threshold in terms of some minimum vertical acceleration resulted in CAT data records with a certain degree of statistical intermittency, the intermittency could be markedly increased or decreased by changing the threshold slightly or by selecting larger or smaller samples. The physical interpretation of spectra derived from

long, highly intermittent records are subject to conjecture due to the intermittency. The $-5/3$ slope in the double-logarithmic plots of the spectra often extended to scales of a few hundred meters for the largest CAT sample. However, by computing spectra over smaller, more homogeneous subsamples, it was shown that the slope of the spectra of the larger sample was the result of averaging. One must conclude from these findings that the spectrum analyses of non-homogeneous CAT records or the averaging of spectra obtained from subsamples of such records (Otnes et al, 1968) may be very misleading from a physical point of view. It is the opinion of the writer that a certain compromise should be established for a given case between the need for statistical reliability and the need for physically representative analyses.

With the realization that most CAT records are statistically intermittent, it has been proposed that the physical causes of the intermittency be investigated by separating the flow field into a mean and deviation, not by the usual Reynolds averaging scheme, but by applying a set of numerical filters to the data. In this way the mean and turbulent flow parameters become functions of distance along the aircraft track. Also, the use of numerical filters allows one to take advantage of the ability of well-instrumented aircraft to sense important changes over small distances. Thus, the CAT investigator may examine both the meso- and microscale aspects of the turbulence encounter.

The application of the concept of an instantaneous mean to the computation of the turbulent kinetic energy budget has also been suggested for the purpose of determining some of the physical aspects of individual turbulent bursts. A test of the technique on a limited series of case studies has shown that the location, intensity and dimensions

of individual turbulent bursts can be specified in terms of the spatial distribution of turbulent kinetic energy. Furthermore, the relation of a given turbulent burst to its environment can be deduced from the local behavior of the terms of the energy budget. In Case 3, for example, there appeared to be two primary causes of the intermittency: the aircraft gradually penetrated a sloping layer of strong shear and, within the shear layer, the aircraft intercepted a group of short waves in various stages of growth and decay.

The importance of taking the intermittent structure of CAT into consideration in the study of its energetics was revealed in the large relative magnitudes of energy budget terms such as the horizontal advection of turbulent energy by the mean wind and energy production by horizontal shears of the mean vertical velocity. Contributions to the local energy change by these processes were found to be of the same order of magnitude as, for example, losses by buoyant damping and production by vertical shears.

The proposed analytic technique is not without problems. For example, the finite band width over which the cutoff occurs in practical numerical filter applications does not allow the exact satisfaction of the Reynolds averaging rules. However, it appears from the present study, that most of the rules can be approximately satisfied by requiring that the high pass and low pass filters do not overlap and that the filters have as sharp a cutoff as possible.

Unless a gap of a specific width exists in the spectrum of the filtered variables at the scale at which the mean is separated from the turbulent flow, interactions between the mean flow and turbulence arise and are manifested in added terms in the turbulent energy equation. A

few of these were calculated in the present study and have been shown to be of the same order of magnitude as some of the more familiar terms of the energy budget (e.g., the buoyancy term).

In the absence of some sort of a spectral gap, the selection of the scale at which separation should occur is arbitrary. Considering the speeds of modern aircraft and the scales of the phenomenon responsible for CAT, a separation scale of 1 km seems appropriate. However, it must be kept in mind that the analytic technique is perfectly general and may be applied in the study of other time or space dependent phenomena (e.g., boundary layer turbulence). In these cases, a smaller separation scale may be desirable.

The difficulties encountered in the proposed analysis have been outweighed by the success of the technique in illuminating some of the small scale, physical mechanisms which are operating in regions of intermittent CAT. The computation of an instantaneous mean and deviation is a logical approach to a phenomenon which varies radically in space. It is concluded that a great amount of information may be derived from a series of well-planned and well-executed investigations of CAT, if the data are analyzed as in the present study. Furthermore, the procedure of selecting samples for statistical analysis on the basis of the physical characteristics of each CAT occurrence makes the results of such analyses more meaningful.

Recommendations

The following recommendations are made, based on the results of the present study:

Data Collection

(a) In future CAT studies, special efforts should be made to define the mesoscale CAT environment in detail. Such knowledge yields a physical basis upon which certain important assumptions can be made and evaluated, particularly when multiple aircraft observations are not possible, or when aircraft instrumentation is limited.

(b) The sampling of CAT data by a single aircraft should consist of a number of up- and downwind flights along the mean wind vector. This procedure facilitates the analysis of the energetics of the phenomenon.

(c) CAT penetrations by multiple aircraft are strongly recommended to allow the determination of time changes and lateral and vertical derivatives over small scales. The safety and time coordination factors are critical in such an experiment. Staggered formations consisting of one extensively-equipped aircraft (to sense the three velocity components) and two lesser-equipped aircraft (e.g., with the capability of measuring u , or u and w components) are recommended.

(d) Further advantage should be taken of the lee wave environment to study CAT. Mountain lee waves are conducive to CAT generation and offer an opportunity for the researcher to increase the economically-critical ratio of flying hours with CAT to total flying hours. Also, the frequent occurrence of CAT over a given geographical area allows the installation of surface-based equipment (e.g., radar) which, ordinarily, cannot be used extensively in CAT experiments because of a lack of mobility.

Data Reduction

(a) An effort should be made to standardize the definition of a CAT threshold for the selection of CAT samples. Such a convention would allow the intercomparison of intermittency statistics from different studies. The procedure used by Crooks et al. (1968), and in the present study seems applicable. MacReady (1964) has also proposed a standardization procedure based on an estimation of ϵ .

(b) In order to study the physics of a single turbulent patch, it is important that the aircraft data extend into the quiescent region beyond the turbulence. This will allow the examination of the environment in juxtaposition with the CAT and prohibit the loss of important turbulence information in the successive application of high and low pass filters.

(c) Extreme caution should be exercised in utilizing data selection or averaging procedures which apparently make data "statistically reliable" at the expense of the true physics of the CAT occurrence. Repeated flights by aircraft along the same path and at the same level should be conducted to obtain data for the desired ensemble averages.

(d) Objective smoothing (filtering) techniques, such as those utilized in the present investigation should be applied to determine the mesoscale aspects of CAT data collected by aircraft. This procedure would facilitate machine plotting and analyses of the data. Future applications of the proposed filtering technique can be made faster and more efficient through the use of the Fast Fourier Transform (FFT) technique (Cochran et al, 1967, Brigham and Morrow, 1967).

Data Analysis

(a) Spectral techniques such as those utilized by Dutton (1969), should be applied to CAT data to determine some of the more subtle aspects of that phenomenon in frequency space. For example, the determination of scales at which laminar wave motion and random turbulence are occurring may be accomplished by cross-spectrum analysis of the vertical motions and the temperature records (e.g., Busch, 1969). This knowledge may aid in scale separation in the absence of a spectral gap. It must be reemphasized, however, that the behavior of spectra are very sensitive to the manner in which CAT samples are chosen.

(b) A special effort should be made to subject CAT data collected under a variety of mesoscale conditions to the analytic technique presented on the preceding pages in order to verify and expand upon the results found in this study.

The general recommendation which results from the present study is that efforts should be directed toward deriving information with respect to the physics of CAT by examining the results of individual, well-planned and well-executed experiments in much greater detail. Although past programs for the collection and statistical analysis of large masses of aircraft data have been an aid to the aircraft design engineer, those programs have not provided information with respect to the physics of CAT in proportion to the efforts expended in acquiring the data.

LITERATURE CITED

- Axford, D. N., 1968: On the accuracy of wind measurements using an inertial platform in an aircraft, and an example of a measurement of the vertical mesostructure of the atmosphere. Journal of Applied Meteorology, 7, 645-666.
- Batchelor, G. K., 1953: The Theory of Homogeneous Turbulence. Cambridge University Press, Cambridge, England, 173 pp.
- _____, 1961: The dynamics of homogeneous turbulence: introductory remarks. The Mechanics of Turbulence. Gordon and Breach Science Publishers, New York, 85-97.
- Bolgiano, R., Jr., 1959: Turbulent spectra in a stably stratified atmosphere. Journal of Geophysical Research, 64, 2226-2229.
- _____, 1962: Structure of turbulence in stratified media. Journal of Geophysical Research, 67, 3015-3023.
- Bretherton, F. P., (ed.), 1969: The spectral gap. Radio Science, 4, 1361-1363.
- Brigham, E. O., and R. E. Morrow, 1967: The fast Fourier transform. IEEE Spectrum, December, 63-70.
- Brooks, C., and N. Carruthers, 1953: Handbook of Statistical Methods in Meteorology. HMSO, London, 412 pp.
- Busch, N. E., (ed.), 1969: Waves and turbulence. Radio Science, 4, 1377-1379.
- Businger, J. A., 1969: On the energy supply of clear air turbulence. Clear Air Turbulence and Its Detection, Y.-H. Pao, and A. Goldberg, editors, Plenum Press, New York, 100-108.
- Charnock, H., 1957: Notes on the specification of atmospheric turbulence. Royal Statistical Society Proceedings, A120, 398-408.
- Clodman, J., G. M. Morgan, Jr., and J. T. Ball, 1960: High level turbulence. Final Report, Contract AF19(604)-5208. New York University, Research Division, 84 pp.
- Cochran, W. T., J. W. Cooley, D. L. Favin, H. D. Helms, R. A. Kaenal, W. W. Lang, G. C. Maling, Jr., D. E. Nelson, C. M. Rader, and P. D. Welch, 1967: What is the fast Fourier transform? Proceedings of the IEEE, 55, 1664-1677.
- Coles, D., 1961: Interfaces and intermittency in turbulent shear flow. The Mechanics of Turbulence, Gordon and Breach Science Publishers, New York, 229-250.

- Colson, D., 1963: Analysis of clear air turbulence data for March 1962. Monthly Weather Review, 91, 73-82.
- _____, 1969: Clear air turbulence and upper level meteorological patterns. Clear Air Turbulence and Its Detection, Y.-H. Pao, and A. Goldberg, editors, Plenum Press, New York, 337-359.
- Corrsin, S., 1943: Investigation of flow in an axially-symmetric heated jet of air. NACA W-94.
- _____, and A. Kistler, 1955: Free stream boundaries of turbulent flows. NACA Report 1244.
- Courant, R., 1937: Differential and Integral Calculus, Volume I. Interscience Publishers, John Wiley and Sons, Inc., New York, 616 pp.
- Crooks, W. M., F. M. Hoblit, D. T. Prophet, et al, 1967: Project HICAT: an investigation of high altitude clear air turbulence. Volume I. Technical Report AFFDL-TR-67-123. Lockheed-California Co., 255 pp.
- Crooks, W. M., F. M. Hoblit, F. A. Mitchell, et al, 1968: Project HICAT: high altitude clear air turbulence measurements and meteorological correlations. Volumes I and II. Technical Report AFFDL-TR-68-127, Lockheed-California Co., 960 pp.
- DeMandel, R. E., and S. J. Krivo, 1968: Capability of the FPS-16 Radar/Jimspere System for direct measurement of vertical motions. Report CR. 61232, Lockheed Missles and Space Company, Huntsville Research and Engineering Center, 33 pp.
- Dutton, J. A., 1968: Broadening horizons in prediction of the effects of atmospheric turbulence on aeronautical systems. AIAA Paper No. 68-1065, presented at the 5th annual meeting of the American Institute of Aeronautics and Astronautics, Philadelphia.
- _____, 1969: The scientific objectives, philosophy, and management of the MOCAT project. Technical Report AFFDL-TR-69-96, Air Force Flight Dynamics Laboratory, Air Force Systems Command, 136 pp.
- _____, 1970: Personal communication.
- _____, and D. G. Deaven, 1969: A self-similar view of atmospheric turbulence. Radio Science, 4, 1341-1349.
- _____, and J. A. Lane, (eds.), 1969: Intermittency of small scale structure. Radio Science, 4, 1357-1359.
- _____, and H. A. Panofsky, 1970: Clear air turbulence: a mystery may be unfolding. Science, 167, 937-944.
- _____, G. J. Thompson, and D. G. Deaven, 1969: The probabilistic structure of clear air turbulence - some observational results and implications. Clear Air Turbulence and Its Detection, Y.-H. Pao, and A. Goldberg, editors, Plenum Press, New York, 183-206.

- Enochson, L. D., and R. K. Otnes, 1968: Programming and Analysis for Digital Time Series Data. Shock and Vibration Information Center Navy Printing and Publishing Office, Naval District, Washington, 277 pp.
- Essenwanger, O. M., 1970: Elements of Statistical Analysis in Atmospheric Science. Manuscript to be published.
- Endlich, R. M., R. L. Mancuso, J. W. Davies, 1966: Techniques for determining a world wide climatology of turbulence through the use of meteorological data. Scientific Report 1, AFCRL-66-355, Contract AF 19(628)-5173, Stanford Research Institute, Aerophysics Laboratory, 62 pp.
- Etkin, B., 1959: Dynamics of Flight, Stability and Control, John Wiley and Sons, Inc., New York, 519 pp.
- Finn, C. L., and V. A. Sandborn, 1964: Instrument for measuring the intermittency of quasi-steady signals. Fluid Mechanics Paper No. 3, Colorado State University, 16 pp.
- Fleagle, R. G., 1969: The significance of clear air turbulence in large scale meteorology. Clear Air Turbulence and Its Detection, Y.-H. Pao, and A. Goldburg, editors, Plenum Press, New York, 1-3.
- Fujita, T., 1966: Accurate calibration of doppler winds for their use in computation of mesoscale wind fields. Monthly Weather Review, 94, 19-35.
- Gibson, C., G. Stegen, and R. Williams, 1970: Statistics of the fine structure of turbulent velocity and temperature fields measured at high Reynolds numbers, Journal of Fluid Mechanics, 41, Part 1, 153-167.
- Graham, R. J., 1963: Determination and analysis of numerical smoothing weights. NASA Technical Report R-179, 28 pp.
- Gurvitch, A., and A. M. Yaglom, 1967: Breakdown of eddies and probability distributions for small-scale turbulence. Physics of Fluids, Supplement, 10, S59-S65.
- _____, and S. Zubkovski, 1963: On the experimental evaluation of the fluctuations of dissipation of turbulent energy. Izvestia, Geophysics Series, 12, 1856-1858.
- _____, and _____, 1965: Measurement of fourth and sixth correlation moments of a velocity gradient. Izvestia, Atmospheric and Oceanic Physics Series, 1, 797-802.
- Harrison, H. T., 1957: Forecasting the mountain wave at Denver, Colorado. UAL Meteorology Circular No. 42, United Air Lines, Inc., 17 pp.
- Holloway, J. L., Jr., 1958: Smoothing and filtering of time series and space fields. Advances in Geophysics, 4, 351-389.

Holmboe, J., and H. Klieforth, 1954: Sierra wave project. Final Report. Contract AF 19(122)-263, University of California at Los Angeles,

Kibens, G., and L. S. G. Kovasznay, 1969: The intermittent region of a turbulent boundary layer. Interim Technical Report No. 1. Contract DA-31-124-ARO-D-313, Department of Mechanics, the Johns Hopkins University, Baltimore, Maryland, 78 pp.

Kolmogorov, A., 1941: The local structure of turbulence in an incompressible viscous fluid for very large Reynolds numbers. Izvestia, Geophysics Series, 30, p. 309.

_____, 1962: A refinement of previous hypotheses concerning the local structure of turbulence in a viscous, incompressible fluid at high Reynolds numbers. Journal of Fluid Mechanics, 13, 82-85.

Kuettner, J., 1939a: Moazagotl und fohnwelle, Beiträge zur Physik der freien Atmosphäre, 25, 79-114.

_____, 1939b: Zur entstehung der fohnwelle, Beiträge zur Physik der freien Atmosphäre, 25, 251-299.

_____, 1959: The rotor flow in the lee of mountains. Geophysics Research Directorate Research Notes No. 6, Air Force Cambridge Research Center, 20 pp.

_____, and D. K. Lilly, 1968: Lee waves in the Colorado Rockies. Weatherwise, 21, p. 180.

Kung, E. C., 1966a: Kinetic energy generation and dissipation in the large-scale atmospheric circulation. Monthly Weather Review, 94, 67-82.

_____, 1966b: Large scale balance of kinetic energy in the atmosphere. Monthly Weather Review, 94, 627-640.

_____, 1967: Diurnal and long term variations of kinetic energy generation and dissipation for a five-year period. Monthly Weather Review, 95, 593-606.

Lenschow, D. H., 1967: An analysis of airborne systems for measuring air velocity. NCAR Manuscript No. 488, National Center for Atmospheric Research, 31 pp.

_____, 1970: Airplane measurements of planetary boundary layer structure. NCAR Manuscript 70-10, National Center for Atmospheric Research. (Submitted for publication to the Journal of Atmospheric Research.) 41 pp.

Lester, P. F., 1970: The application of shear functions in the study of the meso- and microstructure of the atmosphere. Atmospheric Science Paper No. 159, Colorado State University, 49 pp.

- Lilly, D. K., and W. Toutenhoofd, 1969: The Colorado lee wave program. Clear Air Turbulence and Its Detection, Y.-H. Pao, and A. Goldberg, editors, Plenum Press, New York, 232-245.
- Loving, N. V., 1969: Planning to meet the ALLCAT program objectives. Clear Air Turbulence and Its Detection, Y.-H. Pao, and A. Goldberg, editors, Plenum Press, New York, 127-143.
- Lumley, J. L., 1965: Theoretical aspects of research on turbulence in stratified flows. Proceedings of the International Colloquium on Atmospheric Turbulence and Radio Wave Propagation, Moscow, 105-110.
- _____, and H. A. Panofsky, 1964: The Structure of Atmospheric Turbulence. Interscience Publishers, John Wiley and Sons, Inc., New York, 239 pp.
- MacReady, P. B., Jr., 1964: Standardization of gustiness values from aircraft. Journal of Applied Meteorology, 3, 439-449.
- Mather, G. K., 1969: Clear air turbulence research activities at the National Aeronautical Establishment. Clear Air Turbulence and Its Detection, Y.-H. Pao, and A. Goldberg, editors, Plenum Press, New York, 271-287.
- Martin, M. A., 1963: Digital filters for data processing. G. E. Technical Information Series, 625D484.
- Myrup, L. O., 1969: Turbulence spectra in stable and convective layers in the free atmosphere. Tellus, 21, 341-354.
- National Committee for Clear Air Turbulence, 1966: Report of the National Committee for Clear Air Turbulence, U. S. Department of Commerce, 51 pp.
- Novikov, E. A., and R. W. Stewart, 1964: The intermittency of turbulence and the spectrum of energy dissipation fluctuations. Izvestia, Geophysical Series, 3, 408-413.
- Obukhov, A., 1941: On the distribution of energy in the spectrum of turbulent flow. Doklady Akad. Nauk SSSR, 32.
- _____, 1962: Some specific features of atmospheric turbulence. Journal of Geophysical Research, 67, 3011-3014.
- Otnes, R. K., H. A. Nathans, and L. D. Enochson, 1968: The MAC procedure for computing power spectral densities of gust data (MACS). Final Report, Contract F3365-67-C-1423, Measurement Analysis Corporation, 88 pp.
- Oseen, C. W., (ed.), 1930: Das turbulenzproblem. Proceedings of the Third International Conference on Applied Mechanics, P 1.
- Panofsky, H. A., 1969: Spectra of atmospheric variables in the boundary layer. Radio Science, 4, 1101-1109.

- Pao, Y.-H., and A. Goldberg, (eds.), 1969: Clear Air Turbulence and Its Detection. Plenum Press, New York, 542 pp.
- Phillips, O. M., 1965: On the generation of clear air turbulence by the degradation of internal gravity waves. Proceedings of the International Colloquium on Atmospheric Turbulence and Radio Wave Propagation, Moscow, 130-138.
- Pinus, N. Z., 1963: Statistical characteristics of the horizontal component of the wind velocity at heights of 6-12 km. Izvestia, Geophysical Series, 1, 177-182.
- _____, E. R. Reiter, G. N. Shur, and N. K. Vinnechenko, 1967: Power spectra of turbulence in the free atmosphere, Tellus, 19, 206-213.
- Reed, R. J., 1969: A study of the relation of clear air turbulence to the mesoscale structure of the jet stream region. Clear Air Turbulence and Its Detection, Y.-H. Pao, and A. Goldberg, editors, Plenum Press, New York, 288-307.
- Reiter, E. R., 1962: On the nature of clear air turbulence (CAT). Aerospace Engineering, 21, 39-46.
- _____, 1963: Nature and observation of high-level turbulence, especially in clear air. Report, NWRP 15-1262-071, U. S. Navy Weather Research Facility, Norfolk, Virginia, 28 pp.
- _____, 1968: Recent advances in the study of clear-air turbulence (CAT). Report, NWRP 15-0468-136, U. S. Navy Weather Research Facility, Norfolk, Virginia, 24 pp.
- _____, 1969: The nature of clear air turbulence: A review. Clear Air Turbulence and Its Detection, Y.-H. Pao, and A. Goldberg, editors, Plenum Press, New York, 7-33.
- _____, and A. Burns, 1966: The structure of clear-air turbulence derived from "TOPCAT" aircraft measurements. Journal of Atmospheric Science, 23, 206-212.
- Sandborn, V. A., 1959: Measurements of intermittency of turbulent motion in a boundary layer. Journal of Fluid Mechanics, 6, Part 2, 221-240.
- Scorer, R. S., and H. Klieforth, 1959: Theory of mountain waves of large amplitude. Quarterly Journal of the Royal Meteorological Society, 85, 131-143.
- Sheih, C. M., 1969: Airborne hot-wire measurements of the small-scale structure of atmospheric turbulence. Ph.D. Dissertation, Pennsylvania State University, 159 pp.
- Simons, T. J., 1967: Separation of scales of motion in the atmosphere. Unpublished Manuscript, 16 pp.

- Stewart, R. W., 1959: The natural occurrence of turbulence. Journal of Geophysical Research, 64, 2112-2115.
- _____, J. R. Wilson, and R. W. Burling, 1970: Some statistical properties of small scale turbulence in an atmospheric boundary layer. Journal of Fluid Mechanics, 41, Part 1, 141-152.
- Sutton, O. G., 1949: Atmospheric Turbulence, Methuen & Co., Ltd., London, 107 pp.
- Taylor, G. I., 1931: Effect of the variation of density on the stability of superposed streams of fluid. Proceedings of the Royal Society, A132, 499-523.
- Townsend, A. A., 1948: Local isotropy in the turbulent wake of a cylinder. Australian Journal of Scientific Research, Ser. A, 2, 451-468.
- Trout, D., and H. A. Panofsky, 1969: Energy dissipation near the tropopause. Tellus, 21, 355-358.
- Vergeiner, I., and D. K. Lilly, 1970: The dynamic structure of lee wave flow as obtained from balloon and airplane observations. Monthly Weather Review, 98, 44-58.
- Vinnechenko, N. K., 1969: Recent investigations of clear air turbulence in the U.S.S.R. Clear Air Turbulence and Its Detection, Y.-H. Pao, and A. Goldberg, editors, Plenum Press, New York, 246-270.
- _____, and J. A. Dutton, 1969: Empirical studies of atmospheric structure and spectra in the free atmosphere. Radio Science, 4, 1115-1126.
- _____, N. Z. Pinus, S. M. Shmeter, and G. Shur, 1968: Turbulence in the Free Atmosphere. Hydrometeorological Publishing House, Leningrad, 301 pp.

APPENDIX A
COMPUTATIONAL PROCEDURES

General

All computer calculations were carried out on the CDC 6400 located at Colorado State University and the CDC 6600 located at the National Center for Atmospheric Research (NCAR). In the computational formulae listed below, the following notation is employed:

- x_i An arbitrary, unfiltered variable which occupies the i^{th} position in the data array (aircraft data were equally-spaced in time at 0.125 second intervals).
- N The total number of data points in a record, sample, or subsample.
- $[x_i]_{LP}$ The i^{th} value of an arbitrary variable which has been subjected to low pass filtering.
- $[x_i]_{HP}$ The i^{th} value of an arbitrary variable which has been subjected to high pass filtering.
- $[w_{di}]_{LP}$ The i^{th} value of the vertical velocity component which has been subjected to a low pass filter after detrending by the least squares fit of a straight line.
- Δt The data interval, i.e., $\Delta t = 0.125$ seconds.
- $[GS_i]_{LP}$ The i^{th} value of the aircraft ground speed (GS) after being subjected to low pass filtering.
- $[TAS_i]_{LP}$ The i^{th} value of the true air speed (TAS) of the aircraft after being subjected to low pass filtering.
- \hat{x} The arithmetic average of an arbitrary variable.

In the following equations, the operation symbols used on the left hand side of the equality sign correspond with those used in the main text. Those used on the right hand side are defined above.

Statistical Analysis

$$\mu_1 = \frac{1}{N} \sum_{i=1}^N [x_i]_{HP} \quad (A-1)$$

$$\mu_1 = \frac{1}{N} \sum_{i=1}^N ([x_i]_{HP} - \widehat{[x_i]_{HP}})^2 \quad (A-2)$$

$$\gamma_1 = \frac{1}{N\mu_2^{3/2}} \sum_{i=1}^N ([x_i]_{HP} - \widehat{[x_i]_{HP}})^3 \quad (A-3)$$

$$\beta_2 = \frac{1}{N(\mu_2)^2} \sum_{i=1}^N ([x_i]_{HP} - \widehat{[x_i]_{HP}})^4 \quad (A-4)$$

$$C_{ol} = \frac{1}{N\mu_2^{1/2}} \sum_{i=1}^{N-l} |[x_i]_{HP} - [x_{i+l}]_{HP}| \quad (A-5),$$

where l is the lag and the vertical lines denote absolute value.

Energy Budget Analysis

$$u' = [u_i]_{HP} \quad (A-6)$$

$$v' = [v_i]_{HP} \quad (A-7)$$

$$w' = [w_i]_{HP} \quad (A-8)$$

$$\bar{u} = [GS_i]_{LP} - [TAS_i]_{LP} \quad (A-9),$$

where the drift angle is assumed to be zero.

$$\bar{w} = [w_{di}]_{LP} \quad (A-10)$$

$$E = \frac{1}{2} ([u_i]_{HP}^2 + [v_i]_{HP}^2 + [w_i]_{HP}^2) = E_i \quad (A-11)$$

$$\bar{E} = [E_i]_{LP} \quad (A-12)$$

$$\left(-\bar{u} \frac{\partial \bar{E}}{\partial x} \right) = \frac{-[u_i]_{LP} [E_{i+1}]_{LP} - [E_{i-1}]_{LP}}{2\Delta t [GS_i]_{LP}} \quad (A-13)$$

$$\left(-\bar{u}'^2 \frac{\partial \bar{u}}{\partial x} \right) = -[u_i]_{HP}^2 \frac{[u_{i+1}]_{LP} - [u_{i-1}]_{LP}}{2\Delta t [GS_i]_{LP}} \quad (A-14)$$

$$\left(-\bar{u}'w' \frac{\partial \bar{w}}{\partial x} \right) = -[u_i]_{HP} [w_i]_{HP} \left(\frac{[w_{di+1}]_{LP} - [w_{di-1}]_{LP}}{2\Delta t [GS_i]_{LP}} \right) \quad (A-15)$$

$$\left(-\bar{u}'w' \frac{\partial \bar{u}}{\partial z} \right) = -[u_i]_{HP} [w_i]_{HP} \left(\frac{u_U - u_L}{z_U - z_L} \right)_i \quad (A-16),$$

where u_U is the wind speed at z_U (500 m above flight level) and u_L is the wind speed at z_L (500 m below flight level).

$$\left(-\frac{\partial \bar{u}'E}{\partial x} \right) = -\frac{[u_{i+1}]_{HP} E_{i+1}]_{LP} - [u_{i-1}]_{HP} E_{i-1}]_{LP}}{2\Delta t [GS_i]_{LP}} \quad (A-17)$$

$$\left(-\frac{g}{T} \overline{T'w'} \right) = -\frac{g}{[T_r]_{LP}} [[T_{fi}]_{HP} [w_i]_{HP}]_{LP} \quad (A-18),$$

where g is the acceleration due to gravity and where T_{fi} ($^{\circ}C$) is determined from the record of a fast response temperature sensor and T_r ($^{\circ}K$) is determined from a slow response temperature sensor (see Lenschow, 1970, for details of instrumentation).

$$\left(-\overline{uu'} \frac{\partial \bar{u}}{\partial x} \right) = -[[u_i]_{LP} [u_i]_{HP}]_{LP} \frac{[u_{i+1}]_{LP} - [u_{i-1}]_{LP}}{2\Delta t [GS_i]_{LP}} \quad (A-19)$$

$$\left(-\overline{u'w'} \frac{\partial \bar{u}}{\partial z} \right) = -[[u_i]_{HP} [w_{di}]_{LP}]_{LP} \left(\frac{u_U - u_L}{z_U - z_L} \right)_i \quad (A-20)$$

$$\left(-\overline{uw'} \frac{\partial \bar{w}}{\partial x} \right) = -[[u_i]_{LP} [w_i]_{HP}]_{LP} \cdot \left(\frac{[w_{di+1}]_{LP} - [w_{di-1}]_{LP}}{2\Delta t [GS_i]_{LP}} \right) \quad (A-21)$$

$$(R_f) = \frac{\frac{g}{[T_r]_{LP}} [[T_{fi}]_{HP} [w_i]_{HP}]_{LP}}{[[u_i]_{HP} [w_i]_{HP}]_{LP} \left(\frac{u_U - u_L}{z_U - z_L} \right)} \quad (A-22)$$

APPENDIX B
ANALOGUE AND DIGITAL FILTERS

General

The manner in which electronic and digital filters are applied to the data is critical to the success of the analysis techniques proposed and demonstrated in the main text. In the following paragraphs, the filters utilized in the present study are described and discussed. Except for preliminary processing of the data, the Martin-Graham filter has been used throughout the entire study for numerical filtering. It is described briefly in the main text and details of the derivation of the filter are given by Graham (1963). Other examples of its applications are found in studies by Crooks et al. (1968) and DeMandel and Krivo (1968).

Averaging Effects in Case 1 and 2 Data

Prior to the acquisition of the Queen Air 80 data from NCAR, the data had been processed for mesoscale analysis. Since the high frequencies are not critical in such analyses, the data (32 samples sec^{-1}) were smoothed by arithmetically averaging four adjacent values at a time, subsequently recovering data at a sample rate of 8 samples sec^{-1} . Although the unweighted averages were not overlapping, the procedure used is essentially equivalent to taking four point, unweighted, running averages over the data sample and then selecting every fourth point. Holloway (1958) gives an approximate expression for the response function, $R(f)$, for such filtering, i.e.,

$$R(f) \approx \frac{\sin(\pi f T)}{\pi f T} \quad (B-1),$$

where T is the averaging interval. Equation (B-1) is plotted for Case 1 and Case 2 data ($T = 1/8$ sec) in figure B-1.

Since the filter shown in figure B-1 is not sharp, significant damping of amplitudes occurs beyond about 2 Hz. In fact, by 4 Hz ($= f_n$, the Nyquist frequency, for data sampled at $f_s = 8 \text{ sec}^{-1}$), $R(f) < 0.7$. Although the spectra can be corrected for known filtering effects, there is an additional problem of aliasing, because the response function does not reach zero until 8 Hz. An estimate of the combined effects of aliasing and data averaging can be made in the following manner. It is assumed that the true spectrum has a slope of $-5/3$ in the high frequency range (logarithmic coordinates), i.e.,

$$E(f) = A f^{-5/3} \quad (B-2),$$

where A is set equal to unity for convenience. The averaging effects are estimated by

$$E_o(f) = R^2(f)E(f) \quad (B-3),$$

where $E_o(f)$ is the spectrum which will be observed and $R(f)$ is given in figure B-1. Aliasing effects are estimated by folding the portion of the spectrum in the range f_n to $2f_n$ ($f < f_n$) into the low frequency range. The aliased spectral density at f is then $[E_o(f) + E(2f_n - f)]$. The result of this procedure is shown in figure B-2. It is seen that the aliasing effect partially compensates for averaging, and that the contamination occurs mainly at frequencies below 1 Hz (scales ~ 85 m). For the purpose of the present study, the averaged data (8 samples sec^{-1}) were not adjusted for the effects which have been illustrated

since the correction of one error (averaging) would emphasize the other (aliasing). It should be noted, however, that the slight tendency for the spectra from Cases 1 and 2 to steepen in the frequencies above 1 Hz and subsequently flatten near 4 Hz, may be due to averaging and aliasing effects.

Analogue and Preliminary Numerical Filtering of Case 3 Data

All aircraft data for Case 3 were subjected to analogue filtering during the original sampling and recording. The gain and phase lag for the filter is shown in figures B-3 and B-4, respectively. The data were originally sampled at varying rates up to 128 samples sec^{-1} . For the purposes of the present investigation the four original aircraft data tapes were merged, yielding a single tape with all pertinent data at intervals of 0.0625 second (i.e., 16 samples sec^{-1}). No averaging was done in the process and aliasing was kept to a minimum because of the effects of the analogue filtering.

For the purpose of eliminating the damped frequencies and to put the data in a form similar to the first two cases, the data were subjected to low pass filtering with a cutoff frequency of 4 Hz. A schematic diagram of the response function is indicated with a dashed line in figure B-3. The return of the response function to a value of 1 at 12 Hz is due to the fact that the filter is symmetric with respect to the Nyquist frequency (8 Hz). However (again assuming an arbitrary spectrum with a $-5/3$ slope in logarithmic coordinates), the energy density is approximately an order of magnitude lower at 13 Hz as compared with $E(f)$ at 4 Hz. Multiplying this value by the square of the gain of the analogue filter ($< (0.3)^2$ at 12 Hz) results in

negligible aliasing when every other data piece was selected for a final sampling rate of 8 samples sec^{-1} .

Filters Utilized in the Energy Budget and Statistical Analyses

In order to define the mean and turbulent flow, a set of high and low pass filters was applied in each case study. Since, in final form, all data were at sample rates of 8 sec^{-1} , ($\Delta t = 0.125$ second) and had identical separation frequencies (~ 0.1 Hz), the same filter set was applied in each case. Response functions and pertinent information are given in figures B-5 and B-6. Because the error in the response functions must be kept small in order to avoid errors in the subsequent application of the filter set, a large number of weights (NW) is required. The number of weights chosen in the present study is based on the results of experiments by Crooks et al. (1968) and a number of tests conducted by this investigator. In all filters used in the present study, the maximum error allowed was approximately 3 per cent. Despite this small value, it was noted in the presentation of Case 1 that the low-pass filtered turbulent kinetic energy contained three small negative regions. Since negative values are physically impossible, one must conclude that they are due to the allowed filter errors and the method of computing the average kinetic energy.

Parameters of the filters applied in the Reynolds averaging tests (Appendix C) and in the check of the effects of cutoff frequency on the statistical and energy budget analyses (Appendix D) are presented in table B-1.

Reynolds Averaging Tests	Filters					
	Low Pass			High Pass		
	f_c	f_t	NW	f_c	f_t	NW
1	0.067	0.100	501	0.067	0.100	501
2	0.070	0.085	1001	0.085	0.100	1001
3	0.185	0.200	1001	0.200	0.215	1001
Tests of the Effect of Cutoff Frequency						
1	0.070	0.085	1001	0.085	0.100	1001
2	0.185	0.200	1001	0.200	0.215	1001
3	-	-	-	0.085	0.100	1001
4	-	-	-	0.032	0.060	1001

TABLE B-1. Characteristic parameters of Martin-Graham filters. See text for elaboration.

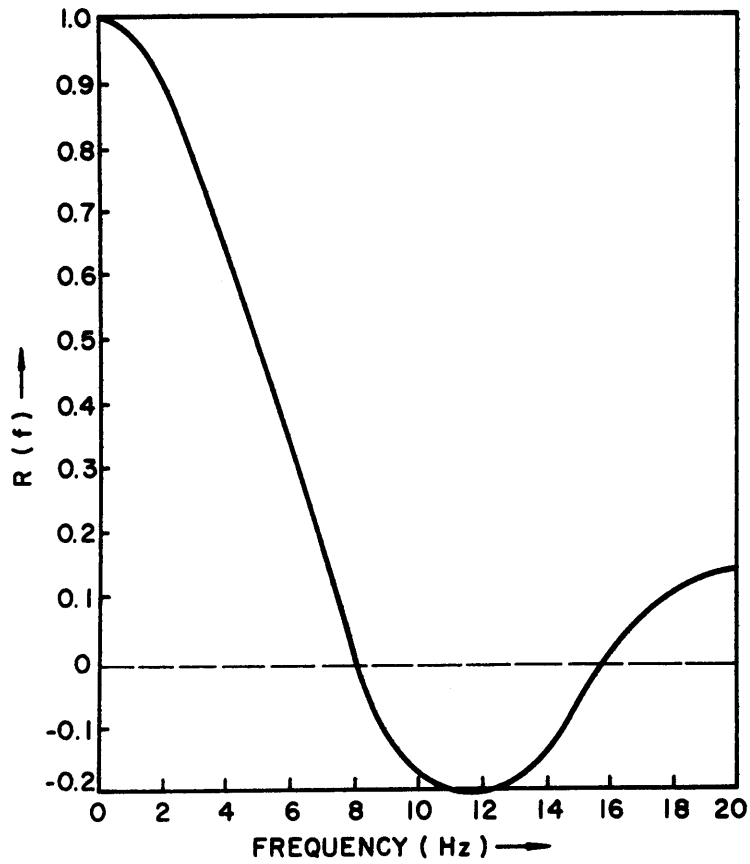


FIGURE B-1. Response function for four-point, equally weighted, running averages. Averaging period is 0.125 sec.

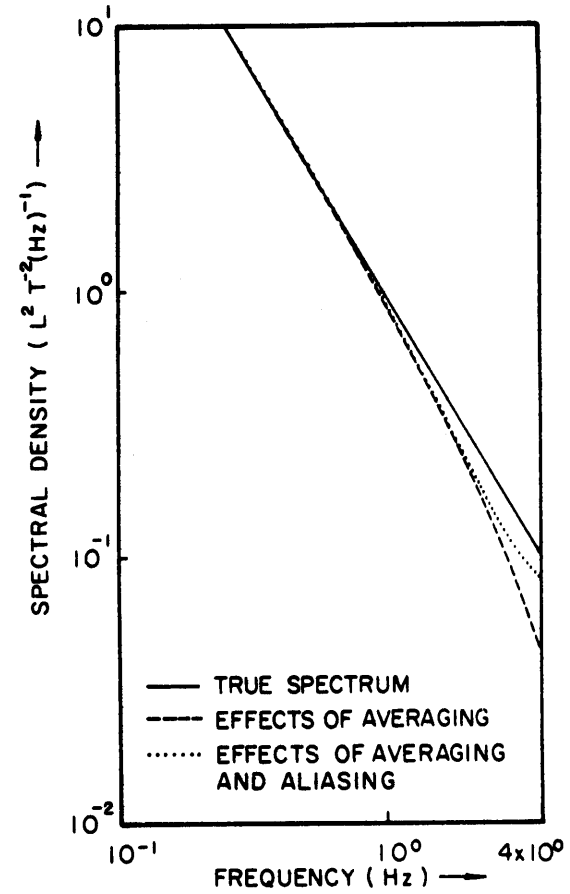


FIGURE B-2. Effects of averaging and aliasing on an idealized spectrum with a $-5/3$ slope in double logarithmic coordinates. See text for discussion.

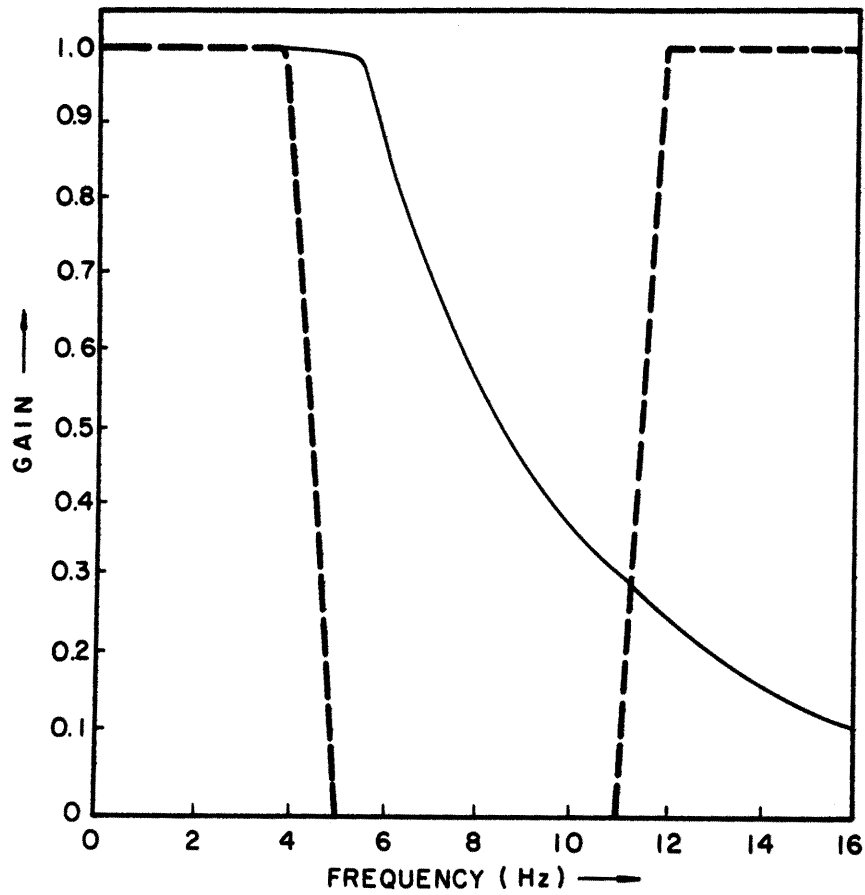


FIGURE B-3. Analogue filter gain (solid line) and Martin-Graham filter response (dashed) for Case 3.

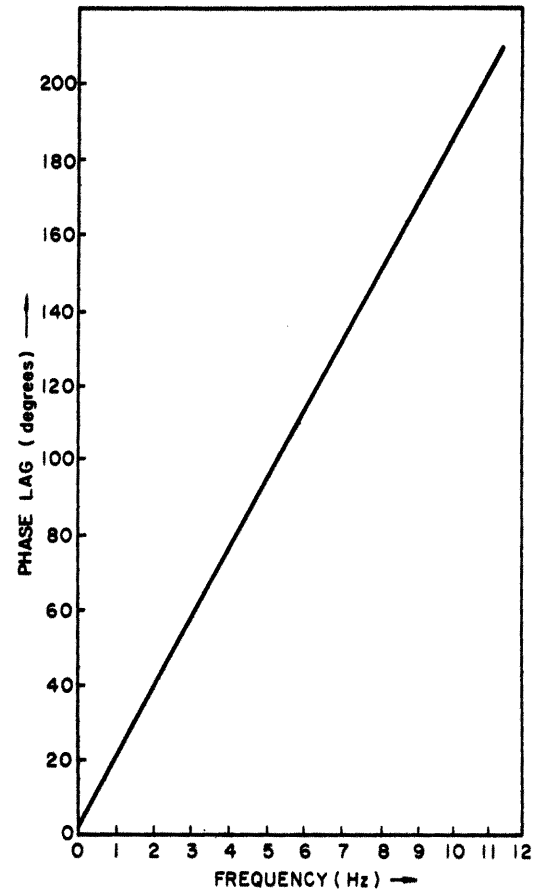


FIGURE B-4. Analogue filter phase lag as a function of frequency for Case 3.

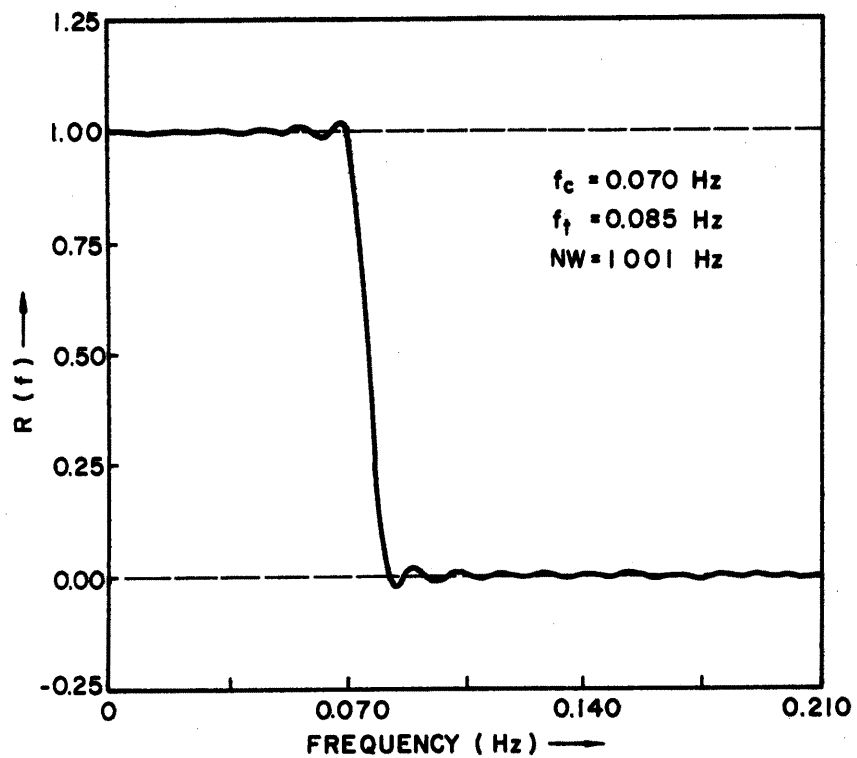


FIGURE B-5. Response function for Martin-Graham low pass filter which was utilized in the analysis of Cases 1, 2 and 3. f_c is the cutoff frequency, f_t is the termination frequency and NW is the total number of weights.

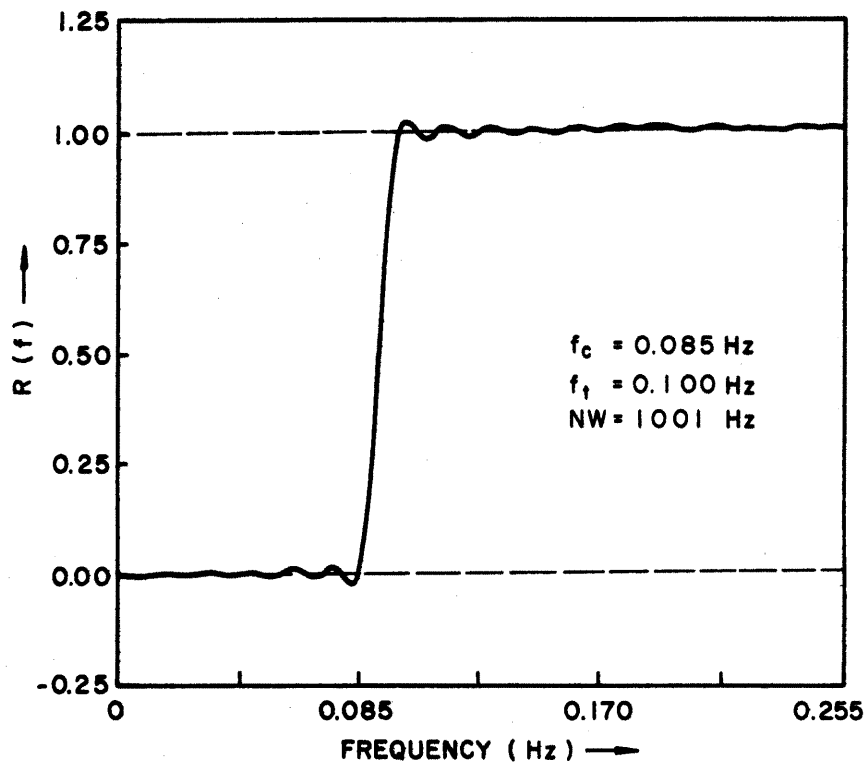


FIGURE B-6. Same as figure B-5, but for high pass filter.

APPENDIX C

FILTERING AND THE REYNOLDS AVERAGING RULES

A series of tests were conducted to determine the validity of the Reynolds averaging rules when the instantaneous turbulent kinetic energy budget is computed. These tests were deemed necessary because (a) the usual arithmetic averaging is replaced by numerical low pass filtering and (b) sharp filter cutoffs are not possible in the practical application of numerical filters.

The basic assumptions which are made in the derivation of the energy equation are the following:

$$\begin{aligned}\overline{\overline{u}} &= \overline{u}, & \overline{u'} &= 0 \\ \overline{\overline{u^2}} &= \overline{u^2}, & \overline{2\overline{uu'}} &= 0\end{aligned}\tag{C-1}.$$

Three tests were carried out to check equation (C-1), utilizing the Doppler wind component along the aircraft path and the true air speed fluctuations from the February 20, 1968 case, presented in Chapter V.

Test 1

A schematic of the response function of the low and high pass filters utilized in test 1 is shown in figure C-1. In this case the filters are complements of one another, that is, the high pass filter is the difference between the all pass and low pass filters and clearly, $u = \overline{u} + u'$. The results of the tests are presented in figures C-2 through C-4. Figure C-2 indicates that $\overline{u} = \overline{\overline{u}}$ and $\overline{u^2} = \overline{\overline{u^2}}$ may be considered valid with a very small error. This result was found in the other tests and therefore similar figures will not be presented.

Figure C-3 illustrates the behavior of $\overline{u'}$. It is noted that in the region of maximum turbulence, the magnitude of $\overline{u'}$ approaches ± 0.3 mps and throughout the record there is a predominant mode with a period of 12-13 seconds. Reinspection of figure C-1 shows that an operation with the high pass filter and the low pass filter results in non-zero amplitudes in a narrow frequency range near f (shaded area). Since $1/f = 12$ seconds, it is obvious that the non-zero $\overline{u'}$ in figure C-3 is due to the filter overlap.

Figure C-4 illustrates the behavior of the term $\overline{uu'}$ in the vicinity of maximum turbulence. The plot of $\overline{u'^2/2}$ is given for comparison. The fact that $\overline{uu'}$ is frequently of equal or greater magnitude than $\overline{u'^2/2}$ indicates that the interactions between the mean and turbulence components may not be neglected in the computation of the instantaneous energy budget.

Test 2

In order to eliminate the problem of $\overline{u'} \neq 0$, high and low pass filters which are not complementary were selected. Response functions are shown in figure C-5. This procedure does not allow $u = \overline{u} + u'$ to be exactly true, however, the discrepancy was kept small by requiring a sharper cutoff than in test 1. Note that $(f_3 - f_1)$ in figure C-5 is less than $(f_t - f_c)$ in figure C-1 and also the number of weights (NW) has been doubled. The success of this approach is shown in figure C-6. The magnitude of $\overline{u'}$ does not exceed $|0.03|$ mps at any point in the record.

Figure C-7 shows the effect of the new filter arrangement (figure C-5) on the interaction term, $\overline{uu'}$. Although it has been

reduced in magnitude due to the elimination of the filter overlap and due to the loss of information near frequency f_2 , $\overline{uu'}$ is still of the same order of magnitude as $\overline{u'^2/2}$ near the maximum turbulent burst.

Test 3

A final test was applied to the data of Case 2 to determine the effect of placing the filter in a spectral gap. The premise is that if the atmosphere shows a natural tendency to separate mean and turbulent flows, the interaction term should be small in the region of the gap. The existence of such a phenomena near 0.2 Hz was indicated in figure 17 of Chapter V, in the discussion of Case 2. The filter arrangement in figure C-5 was utilized, but with $f_1 = 0.185$ Hz, $f_2 = 0.200$ Hz, and $f_3 = 0.215$ Hz (NW = 1001). Figure C-8 shows the variation of $\overline{u'u}$ and $\overline{u'^2/2}$ in the region of maximum turbulence. It is seen that despite efforts to locate the filter in some sort of spectral gap, the magnitude of $\overline{uu'}$ equals or exceeds the magnitude of $\overline{u'^2/2}$ at many points throughout the record. It should be noted that this behavior occurs even with the loss of information due to an induced gap in the filter arrangement (figure C-5).

On the basis of tests 1 through 3, one must conclude that interactions between the mean and turbulent flows cannot be neglected in the computation of terms of the energy equation in the proposed manner.

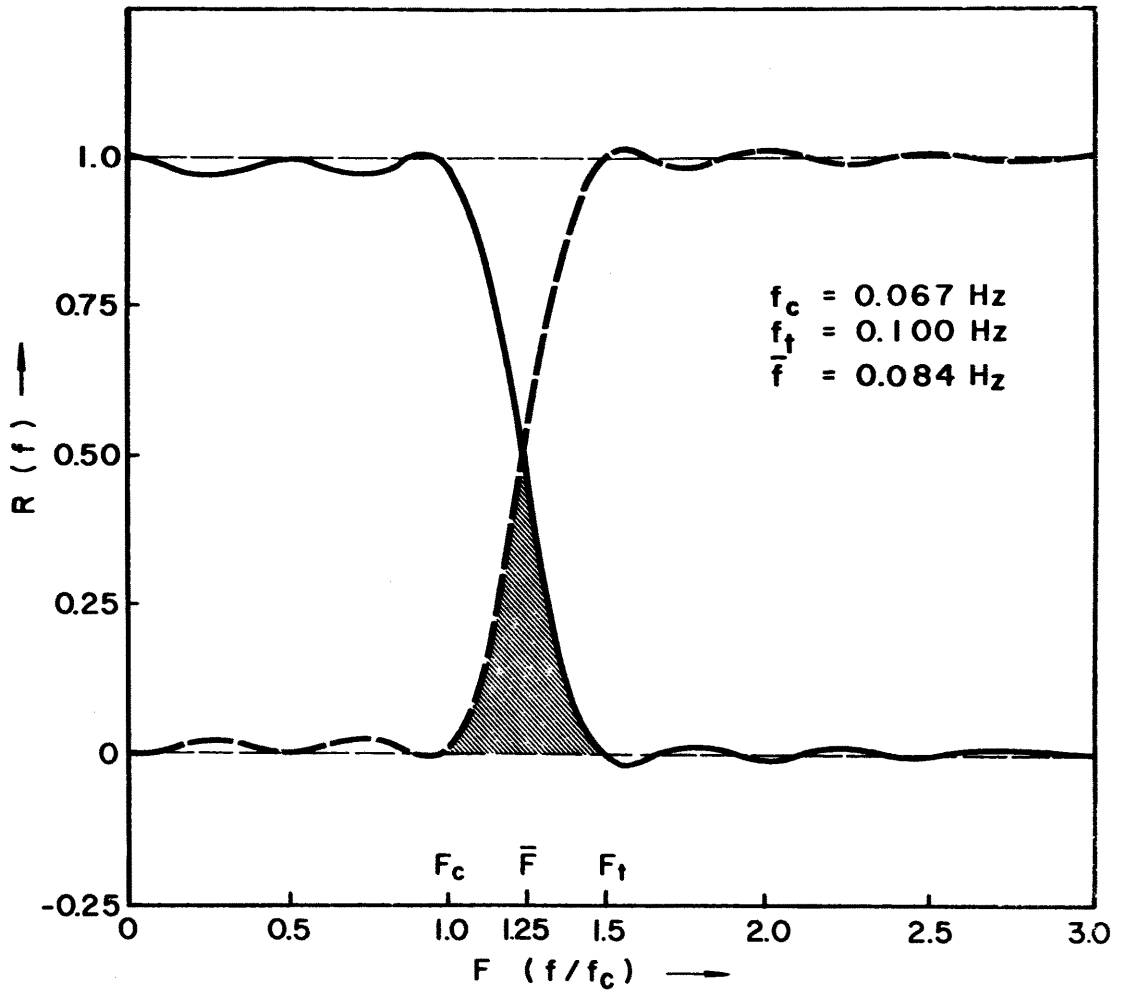


FIGURE C-1. Response functions of Martin-Graham high pass (dashed line) and low pass (solid line) filters utilized for Test 1. F is a non-dimensional frequency given by f/f_c where f is an arbitrary frequency (HZ) and f_c is the cutoff frequency. f_t is the termination frequency. \bar{f} is given by $(f_c + f_t)/2$. Note that the high pass filter is the complement of the low pass filter.

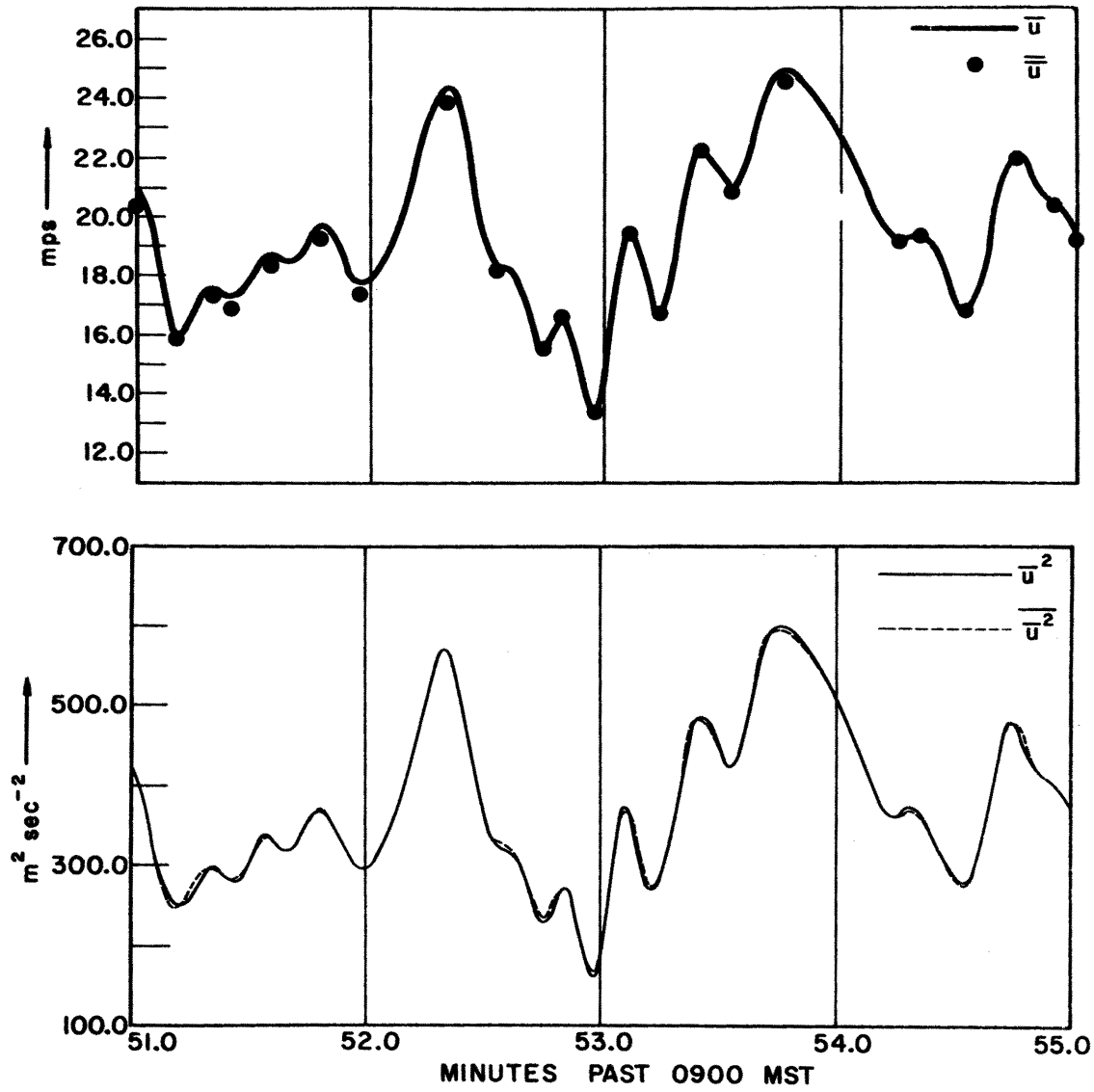


FIGURE C-2. Test 1 results for \bar{u} and $\overline{u^2}$ (top) and \bar{u}^2 and $\overline{u^2}$ (bottom). See text for discussion. Time axes on diagrams are identical.

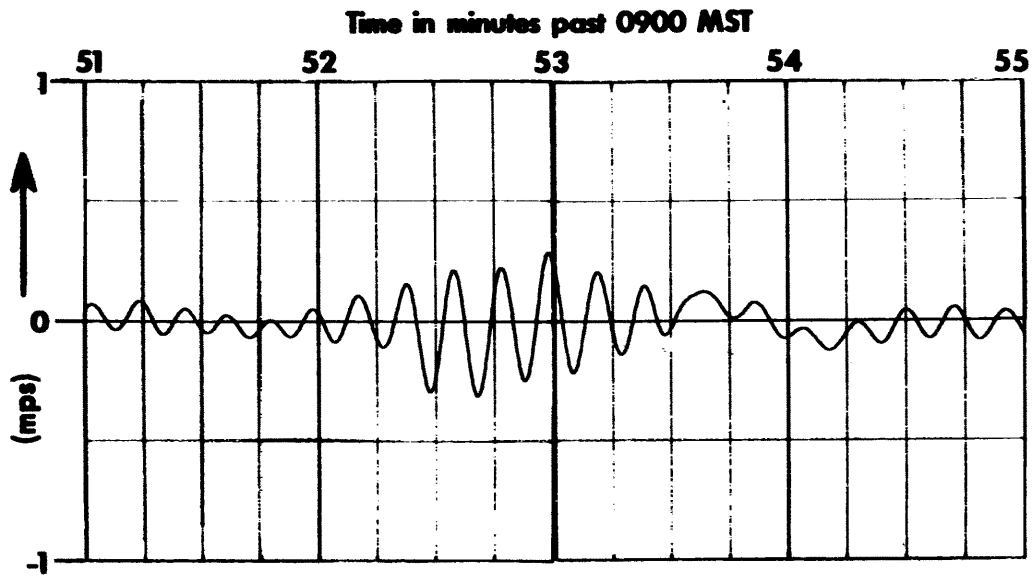


FIGURE C-3. Test 1 results for $\overline{u'}$. See text for discussion.

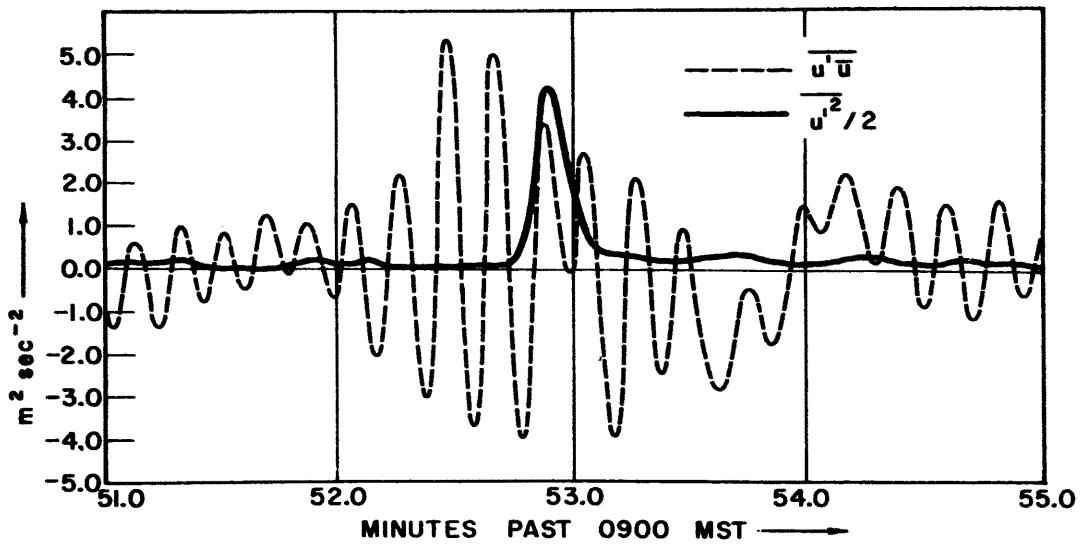


FIGURE C-4. Test 1 results for $\overline{u'u}$ (dashed line) and $\overline{u'^2}/2$ (solid line). See text for discussion.

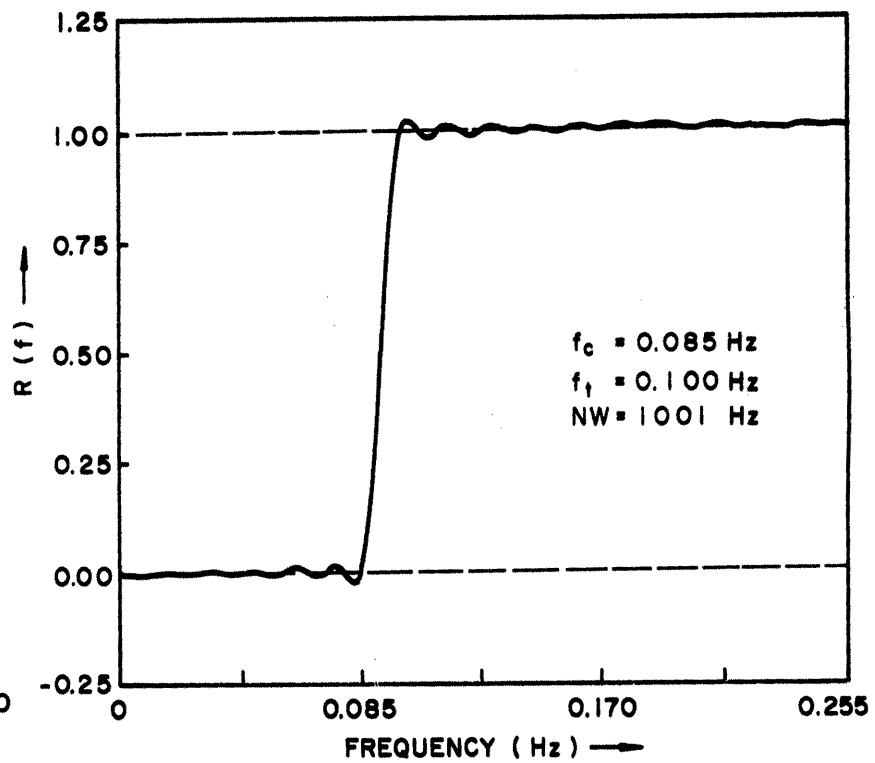
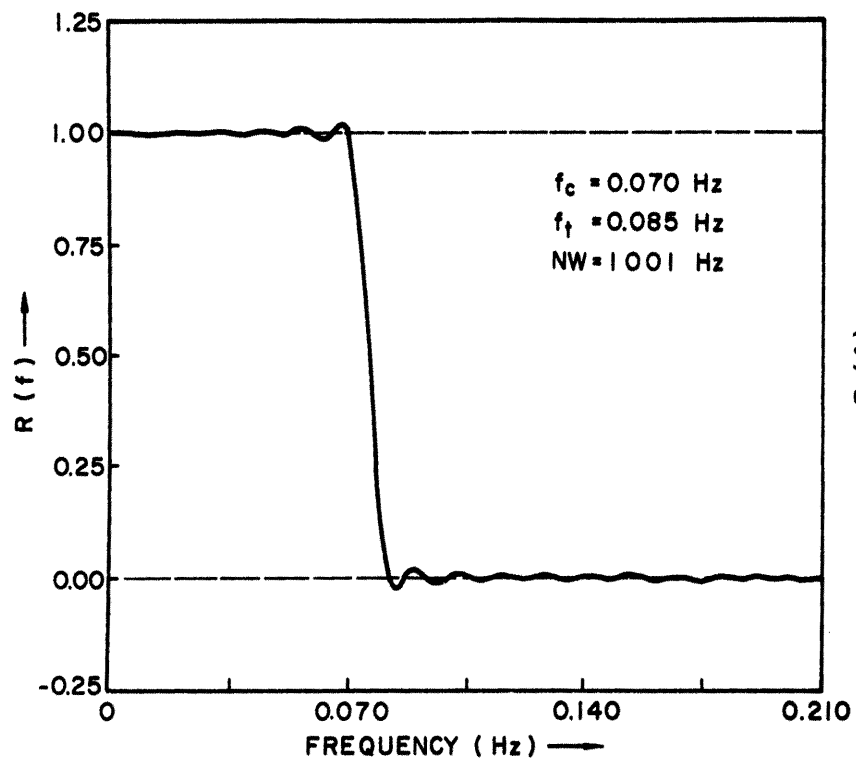


FIGURE C-5. Response functions of Martin-Graham low pass filter (left) and high pass filter (right), utilized in Test 2. See text for discussion.

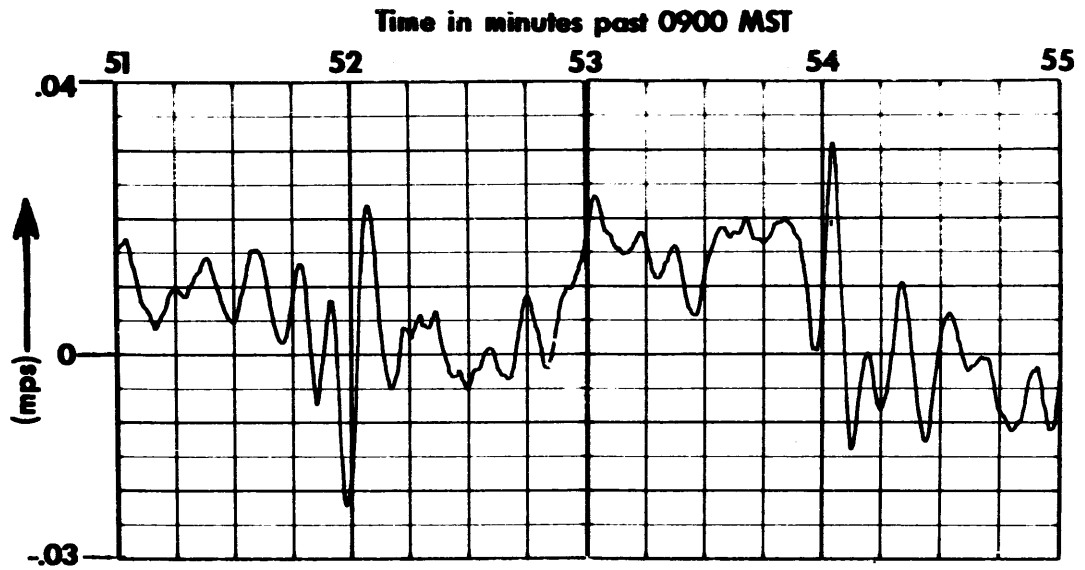


FIGURE C-6. Test 2 results for $\overline{u'}$.

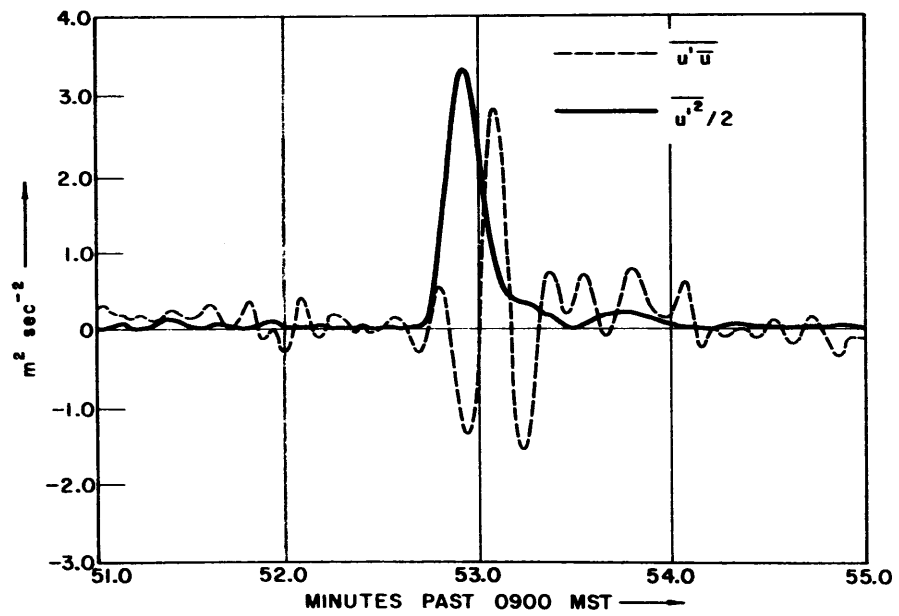


FIGURE C-7. Test 2 results for $\overline{u'u}$ (dashed line) and $\overline{u'^2}/2$ (solid line).

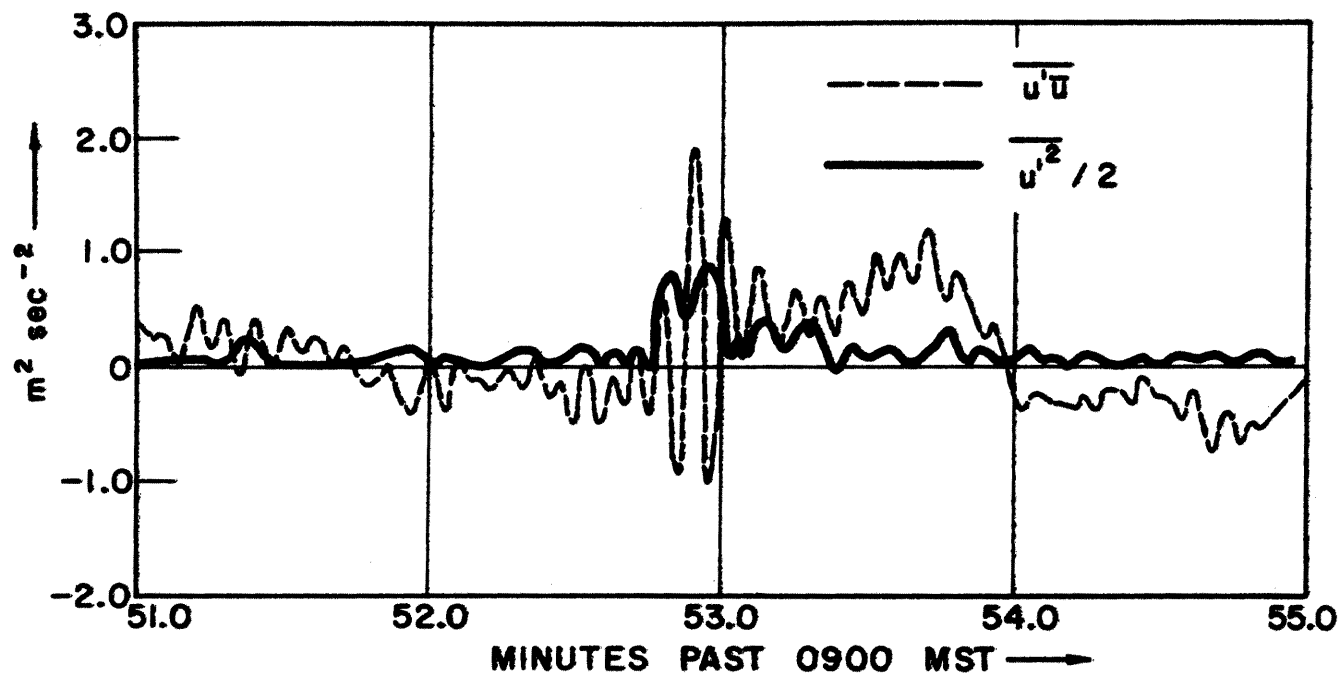


FIGURE C-8. Test 3 results for $\overline{u'u}$ (dashed line) and $\overline{u'^2}/2$ (solid line).

APPENDIX D

THE EFFECTS OF FILTERING ON STATISTICAL
ANALYSES AND ENERGY BUDGET COMPUTATIONS

General

It was noted in the main text that the selection of the scale at which the flow should be separated into a mean and a deviation is arbitrary when a spectral gap does not exist. The problem is analogous to the one which has been faced by meteorologists in the study of boundary layer turbulence; i.e., an averaging time must be defined for the computation of means, covariances, etc. Although there is no clear solution to the problem, data from two cases which were considered in the present study were reanalyzed to demonstrate the effects of a variation in the separation scale.

Statistical Effects

Longitudinal gust data from cases 2 and 3 (Chapter V) were subjected to the high pass filters described in table D-1. Cumulative frequency

Case		f_c (Hz)	f_t (Hz)
2	Original filter	0.085	0.100 (850 m)
	New filter	0.200	0.215 (395 m)
3	Original filter	0.085	0.100 (1000 m)
	New filter	0.042	0.060 (1670 m)

Table D-1. Cutoff frequencies (f_c) and termination frequencies (f_t) for Martin-Graham high pass filters. "Original filter" denotes the filter used in the analyses presented in the main text. The "New filter" was applied in the reanalysis of the data.

distributions and statistical moments were determined for the entire sample and the most turbulent sample of each case. For the purpose of comparing the original analyses with the new analyses, the cumulative frequency distributions (figures D-1 through D-4) were standardized by dividing the central class values by the appropriate standard deviation.

Figures D-1 and D-2 show, respectively, the results of the computations for the entire sample and the most turbulent sample of Case 2. The distributions of the longitudinal gusts, after being subjected to reanalysis, remains significantly different from normal at the 99% level according to the Kolmogorov-Smirnov test (Essenwanger, 1970). Although the effect of filtering with a higher cutoff frequency has reduced both the skewness (γ_1) and the Kurtosis (β_2), the reduction is only significant for the entire sample (figure D-1).

The results of utilizing a lower frequency cutoff for Case 3 are shown in figures D-3 and D-4. Little change is found in the entire sample (figure D-3). Both original distribution ($f_t = 0.100$) and the new distribution ($f_t = 0.06$), by the Kolmogorov-Smirnov test, are significantly different from normal at the 99% level, however, the difference between the former distributions is not significant by the same test. This is also the case for the most turbulent subsample (figure D-4), although significant skewness (γ_1) has arisen due to filtering at a lower frequency.

No conclusions may be drawn from the data presented above since only two cases were considered and the statistical testing was incomplete. However the analyses have served to show some of the effects of the variation of cutoff frequency. This problem should be subjected to further study.

Effects of Filtering on Energy Budget Computations

An abbreviated energy budget computation was performed on Case 2. The longitudinal component of the wind was separated into a mean and a deviation at a frequency of 0.2 Hz (a scale of ~ 425 m). The distribution of u' and $\overline{u'^2}/2$ is shown in figure D-5.

The elimination of energies at scales between 0.1 Hz and 0.2 Hz is evidenced in the overall decrease in the gust magnitudes. The decrease, being frequency dependent, does not occur equally in all bursts. For example, the maximum kinetic energy in the rotor (near 1053 MST in figure D-5) is about 75% less than the maximum which was found for the lower cutoff frequency of 0.1 Hz (~ 850 m). However, the energy of many of the secondary bursts (e.g., near 1051.3 MST) has suffered little, if any, loss due to filtering. Since the rotor is known to be a quasi-steady turbulence source of relatively large dimensions, much of its energy is found in the frequencies which have been eliminated by filtering at 0.2 Hz. On the other hand, the secondary turbulent bursts are either smaller scale instabilities or the remnants of larger scale turbulence phenomena which are in a stage of decay.

The compact nature of the turbulent bursts is especially evident in the behavior of the two terms of the energy equation which are shown in figure D-6. Maxima and minima of the terms are of the same order of magnitude as in the original analysis of Case 2. This is primarily due to the large fluctuations of the turbulence intensity (figure D-5) and of the mean wind over short distances, especially in the vicinity of the rotor.

The brief reanalysis of some of the physical aspects of the turbulence occurrence in Case 2 have emphasized the important influence of

the cutoff frequency on the results of the analysis. When a spectral gap does not exist, the selection of the cutoff frequency must be based on the aims of the investigator. Since, by definition, CAT is a function of the speed and design of the aircraft which encounters it, the "turbulence," which the CAT researcher is concerned with, lies in a variable frequency range. Thus, the proper cutoff frequency cannot be specified exactly. However, from the results discussed above, and the analyses presented in the main text, a separation scale of about 1 km seems appropriate for the investigation of CAT.

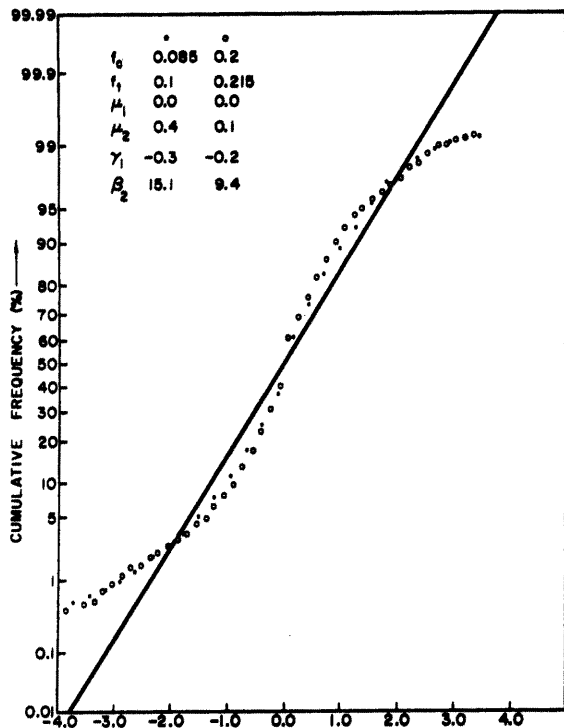


FIGURE D-1. Cumulative frequency distributions of longitudinal gusts which have been defined by two different filters. Data are the entire CAT sample (N = 3760 points) for Case 2. Filter characteristics and statistical parameters are given in the upper left hand corner of the diagram. The units of f_c , μ_1 and μ_2 are HZ, mps and $m^2 \text{sec}^{-2}$, respectively. The abscissa is labeled in standardized units, u'/σ . The class interval is 0.1 mps.

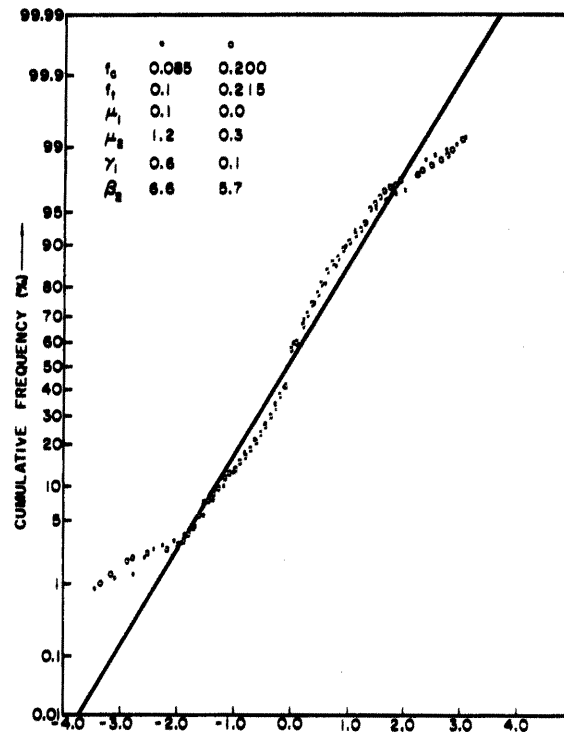


FIGURE D-2. Same as figure D-1, but for the most turbulent subsample of Case 2 (N = 601).

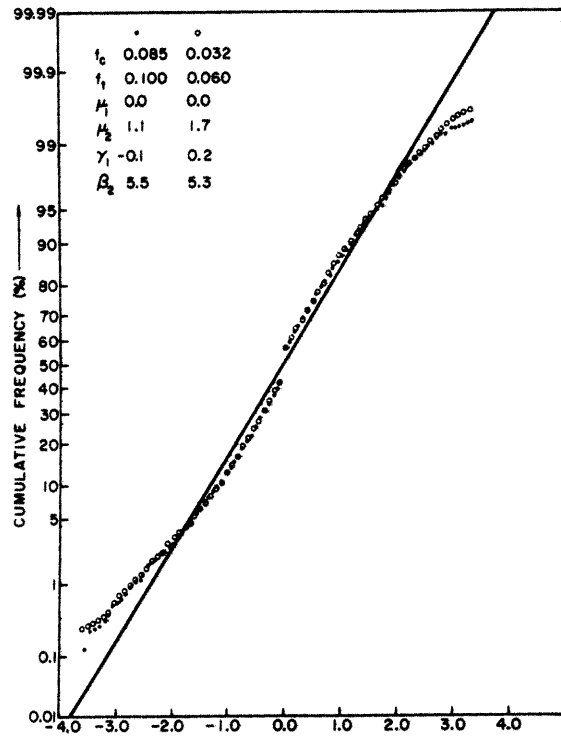


FIGURE D-3. Same as figure D-1, but for the entire sample of Case 3 (N = 5760).

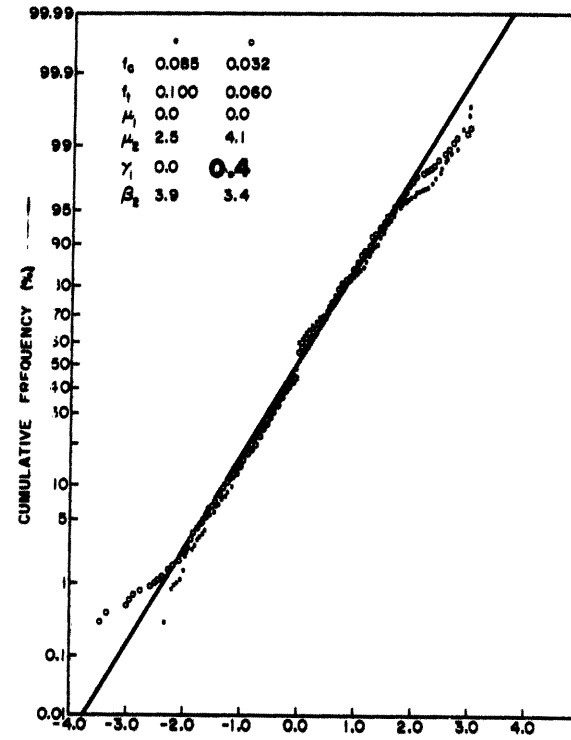


FIGURE D-4. Same as figure D-1, but for the most turbulent sample of Case 3 (N = 960).

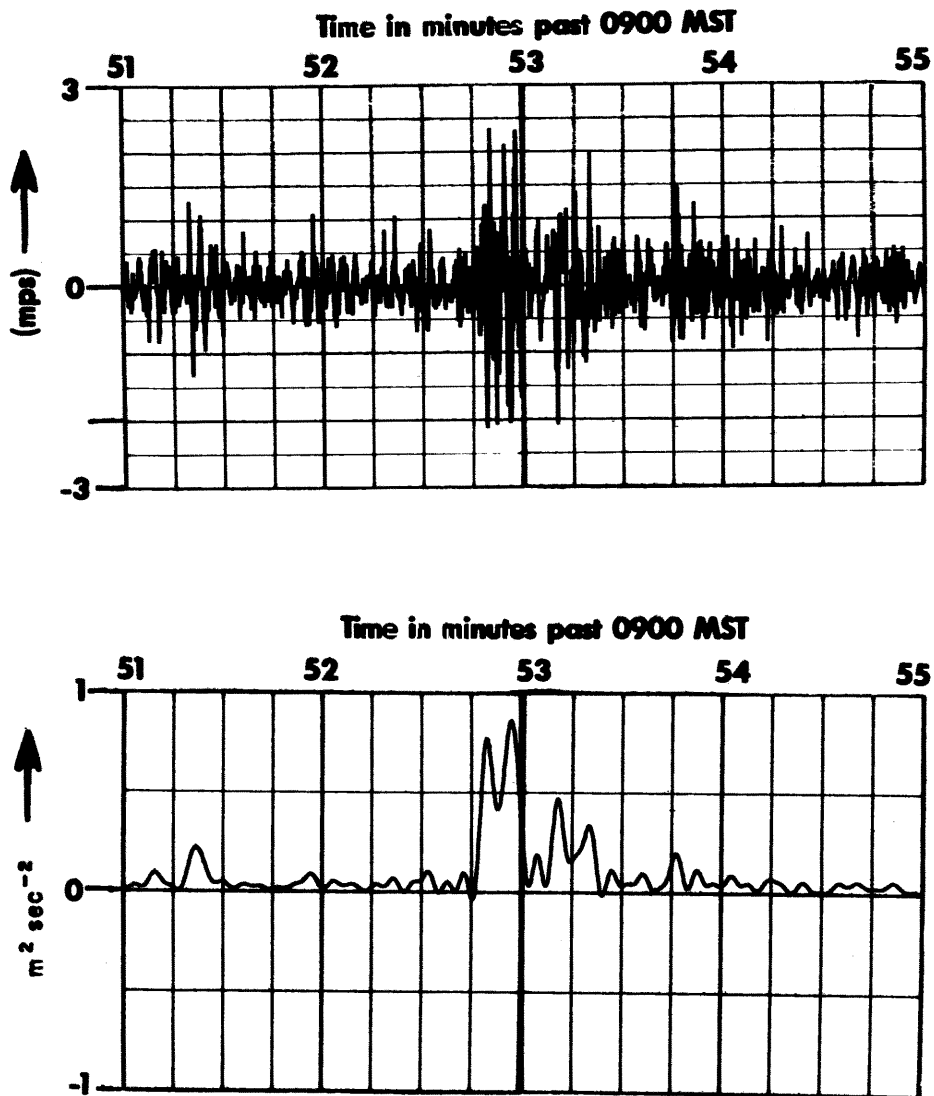


FIGURE D-5. Distributions of u' (top) and $\overline{u'^2}/2$ (bottom) along a portion of the aircraft track for Case 2 after filtering the data with a higher cutoff frequency ($f_c = 0.215$ HZ). See text for further elaboration.

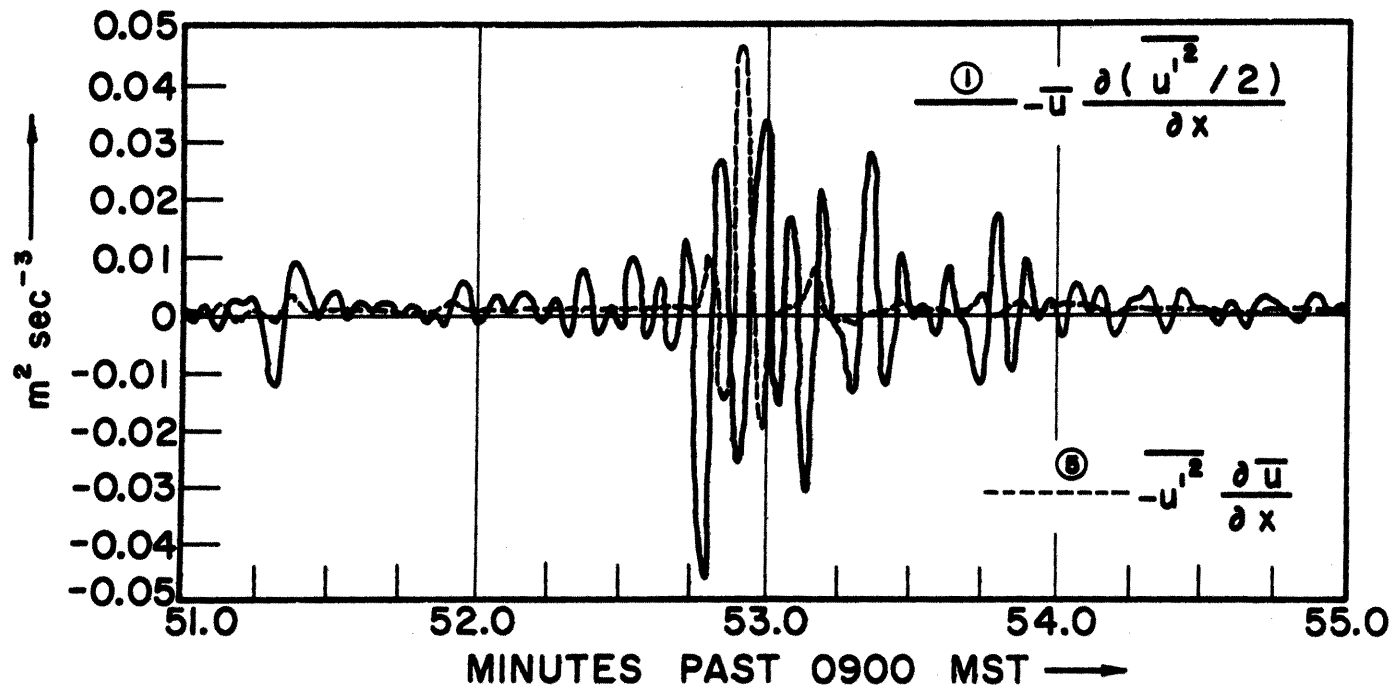


FIGURE D-6. Terms $\textcircled{1}$ and $\textcircled{5}$ of equation (51) from Case 2 data after filtering with a higher cutoff frequency ($f_c = 0.215$ Hz). See text for discussion.